

N 9 2 - 1 5 4 3 4

HALOCARBON OZONE DEPLETION AND GLOBAL WARMING POTENTIALS

Coordinators

R. A. Cox (UK) and D. Wuebbles (USA)

Principal Authors and Contributors

R. Atkinson (Australia)
P. Connell (USA)
R. A. Cox (UK)
H. P. Dorn (FRG)
A. De Rudder (Belgium)
R. G. Derwent (UK)
F. C. Fehsenfeld (USA)
D. Fisher (USA)
I. Isaksen (Norway)

M. Ko (USA)
R. Lesclaux (France)
S. C. Liu (USA)
S. A. Penkett (UK)
V. Ramaswamy (USA)
J. Rudolph (FRG)
H. B. Singh (USA)
W.-C. Wang (USA)
D. Wuebbles (USA)

CHAPTER 4

HALOCARBON OZONE DEPLETION AND GLOBAL WARMING POTENTIALS

TABLE OF CONTENTS

4.1	INTRODUCTION	401
4.2	HALOCARBON OXIDATION IN THE ATMOSPHERE	401
4.2.1	Background	401
4.2.2	Tropospheric Chemistry of Halocarbons	402
4.2.3	Hydroxyl Radical Chemistry in the Troposphere	410
4.2.4	Tropospheric Chemistry Influencing OH and Ozone	417
4.2.5	Model Evaluation of Trends in Tropospheric Ozone and OH	422
4.3	OZONE DEPLETION POTENTIALS	424
4.3.1	Background	424
4.3.2	Definition of ODP	424
4.3.3	Model-Calculated ODPs	427
4.3.4	Uncertainties and Sensitivity Studies	431
4.3.5	Summary	450
4.4	HALOCARBON GLOBAL WARMING POTENTIALS	451
4.4.1	Background	451
4.4.2	Definition of Halocarbon GWP	453
4.4.3	Model-Calculated Halocarbon GWPs	455
4.4.4	Uncertainties	459
4.4.5	Summary	461
	REFERENCES	462

4.1 INTRODUCTION

Concern over the global environmental consequences of fully halogenated chlorofluorocarbons (CFCs) has created a need to determine the potential impacts of other halogenated organic compounds on stratospheric ozone and climate. The CFCs, which do not contain an H atom, are not oxidized or photolyzed in the troposphere. These compounds are transported into the stratosphere where they decompose and can lead to chlorine-catalyzed ozone depletion. The hydrochlorofluorocarbons or hydrofluorocarbons (HCFCs or HFCs), in particular those proposed as substitutes for CFCs, contain at least one hydrogen atom in the molecule, which confers on these compounds a much greater sensitivity toward oxidation by hydroxyl radicals in the troposphere, resulting in much shorter atmospheric lifetimes than CFCs, and consequently lower potential for depleting ozone.

The main objective of this chapter is to review the available information relating to the lifetime of those compounds (HCFCs and HFCs) in the troposphere, and to report on up-to-date assessments of the potential relative effects of CFCs, HCFCs, HFCs, and halons on stratospheric ozone and global climate (through "greenhouse" global warming).

The lifetimes of the HCFCs and HFCs are determined by their rate of oxidation by hydroxyl (OH) radicals in the troposphere. Therefore it was necessary to consider the components of tropospheric chemistry affecting the OH radical concentration (i.e., tropospheric ozone, hydrocarbons, and nitrogen oxides) as well as the kinetics and degradation mechanism of the halocarbons. Special attention is also given to the nature of the products of the degradation of the HCFCs and HFCs being considered as possible replacements for CFCs. In parallel with this assessment, an initiative with similar objectives—the Alternative Fluorocarbon Environment Acceptability Study (AFEAS)—was carried out. AFEAS was an in-depth examination by over 50 scientists. The present evaluation has benefited from the availability of this material and the conclusions drawn from it. The AFEAS report, Vol. II, is an Appendix to this report.

The chapter is divided into three main sections. The first section concerns the oxidation of halocarbons in the troposphere. The kinetics and degradation mechanisms of the halocarbons are reviewed and the nature and fate of the degradation products are identified. Estimates of current global OH abundances in the troposphere are discussed and consequent halocarbon lifetimes are provided. The current picture concerning tropospheric ozone and its precursors, as they affect OH, is presented together with a summary of recent model predictions of future changes in tropospheric ozone and OH. The second section concerns the evaluation of potential effects on stratospheric ozone through the determination of relative (to CFC-11) Ozone Depletion Potentials (ODPs), while the third section relates their effects to climate through evaluation of relative halocarbon Global Warming Potentials (GWPs) for these compounds. Discussion in these sections also emphasizes the uncertainties pertinent to calculations of ODPs and halocarbon GWPs.

4.2 HALOCARBON OXIDATION IN THE ATMOSPHERE

4.2.1 Background

The oxidation of atmospheric trace gases containing carbon, hydrogen, nitrogen, sulphur and halogens, emitted by a variety of natural and man-made sources, occurs by chemical reactions initiated directly or indirectly by solar radiation. These chemical processes yield either non-reactive long-lived products such as CO₂ or water vapor, or acidic species such as HNO₃, H₂SO₄, HF, or HCl which are removed from

OZONE DEPLETION POTENTIALS

the atmosphere by physical processes. The oxidation processes occur mainly in the troposphere, and they prevent the build-up of excessive concentrations of these trace substances in the atmosphere. Moreover, in the context of the topic of stratospheric ozone depletion, tropospheric oxidation acts as a filter preventing the injection into the stratosphere of the source gases for radicals in the NO_x , ClO_x , and BrO_x families, which can catalytically destroy ozone.

The chemical oxidation processes generally, but not exclusively, take place in the gas phase. For volatile organic compounds including halogenated hydrocarbons, the major oxidizing species is the hydroxyl radical OH, which reacts to abstract hydrogen atoms or adds to unsaturated linkages, thus initiating a free radical degradation mechanism. The fully halogenated chlorofluoroalkanes do not contain these reactive sites and consequently cannot be degraded in this way.

The OH radicals are generated photochemically and are maintained at a steady-state concentration in the sunlit atmosphere. The average concentration of OH, together with its rate coefficient for reaction with a particular compound, determines the atmospheric lifetime of that compound. For a given emission rate, the amount of any compound that can build up in the troposphere will be in proportion to its lifetime, and it follows that the amount that reaches the stratosphere by transport from the troposphere will be heavily influenced by its rate of tropospheric oxidation. Current and future changes in the oxidizing efficiency of the troposphere, as measured by the average OH concentration, are clearly of high importance in assessing the suitability of hydrochlorofluorocarbons as substitutes for the CFCs.

The oxidation mechanisms in the troposphere are caused by the presence of ozone, since photolysis of ozone in the ultraviolet region leads to the formation of the hydroxyl radical. Moreover, approximately 10% of the total ozone column is present in the troposphere, and therefore, changes in ozone concentration in this altitude range need to be considered as part of the assessment of overall column changes. Tropospheric ozone also adds significantly to the total greenhouse warming by virtue of its pressure-broadened infrared absorption in the atmospheric window, and also by its influence through chemistry on other radiative active trace gases (e.g., CH_4).

In recent years there has been a major initiative to understand the budgets and life cycle of tropospheric ozone. It is now clear that earlier theories, advocating a purely dynamical description with injection of ozone from the stratosphere and removal by surface deposition, are inadequate. *In situ* chemical production and loss of ozone, first suggested in the mid 1970s, clearly plays a role in determining the global tropospheric ozone budget and has probably led to increases in O_3 over large parts of the Northern Hemisphere. The reactions controlling ozone production and loss in the troposphere are photochemically initiated and involve a variety of trace species including nitrogen oxides, volatile organics, and free radicals in the HO_x family (OH and HO_2).

There are other oxidizing species present in the troposphere which help to maintain stable composition in the atmosphere. These include peroxy radicals, nitrate radicals (NO_3), halogen atoms, and ozone. These species are generally much less important than OH for tropospheric oxidation. Other oxidizing reactions can occur in the aqueous phase in cloud and rain, where hydrogen peroxide (H_2O_2) plays an important role. These are not important for oxidation of halocarbons.

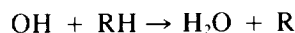
4.2.2 Tropospheric Chemistry of Halocarbons

As discussed in Section 4.2.1 above, most organic compounds including halocarbons are degraded in the troposphere primarily by reaction with the OH radical. The chemical reactivity of halocarbons is

reviewed in this section, considering the dominant atmospheric removal pathways, i.e. gas phase reaction with the OH radical and photolysis. Reactions with O₃ and with the NO₃ radical are of negligible importance as an atmospheric removal pathway. In addition, the specific reaction pathways of the halocarbon degradation processes prevailing in the troposphere are examined and the principal halogenated degradation products are identified. The final fate of these degradation products in the troposphere is discussed by considering both their homogeneous gas phase chemistry and their physical removal pathways. The reactions of HCFCs and HFCs with O(¹D) atoms are unimportant in the troposphere but may be important in producing active chlorine or OH in the stratosphere.

4.2.2.1 OH Radical Reactions

The reaction of OH with HFCs and HCFCs involves abstraction of a hydrogen atom to form water and a haloalkyl radical (R):



The rate constants for the reactions of OH with many HFCs and HCFCs have been evaluated as part of the AFEAS assessment (see Vol. II, Appendix). Recommendations are given for the five HCFCs and three HFCs specified by AFEAS as primary alternatives as well as for all other isomers of C₁ and C₂ HCFCs and HFCs where rate data exist. In addition, recommendations are included for CH₃CCl₃, CH₂Cl₂, and CH₄. The recommended rate constants from this evaluation are given in Table 4.2-1.

The format used for the presentation of the recommended rate constant data is the same as that used by the NASA Panel for Data Evaluation (see DeMore et al., 1987). The rate constant tabulation is given in Arrhenius form $k(T) = A \exp(-E/RT)$, and contains the following information:

1. Reaction stoichiometry.
2. Arrhenius A factor (in units of cm³ molecule⁻¹ s⁻¹).
3. Temperature dependence ("activation temperature," E/R) and associated uncertainty (ΔE/R).
4. Rate constant at 298 K (in units of cm³ molecule⁻¹ s⁻¹).
5. Uncertainty factor at 298 K.

All of the uncertainties are one standard deviation, 1σ. Hence, 95% confidence limits are given by 2σ. The uncertainty (1σ) at any temperature can be calculated from the expression:

$$f(T) = f(298) \exp\{\Delta E/R(1/T - 1/298)\}$$

The rate constants are well defined and significant uncertainties only appear when the Arrhenius expressions in Table 4.2.1 are used for extrapolations over a wide temperature range. In particular, at temperatures around 277 K, which corresponds to the region of the troposphere where most of the degradation of these molecules occurs, the rate coefficients are accurate to within ~20%.

4.2.2.2 Photolysis

Photolysis is a potential atmospheric loss process for those haloalkanes containing multiple Cl and/or Br atoms. The absorption spectra are unstructured and continuous, and may extend out to 300 nm,

OZONE DEPLETION POTENTIALS

Table 4.2-1. Recommended rate constants and uncertainties for reactions of OH with selected HFCs and HCFCs

Reaction	Fluorocarbon Number	A ^a	E/R ± E/R ^b	k ₂₉₈ ^a	f(298)
OH + CHFCl ₂	HCFC-21	1.2(-12)	1100 ± 150	3.0(-14)	1.1
OH + CHF ₂ Cl	HCFC-22	1.2(-12)	1650 ± 150	4.7(-15)	1.1
OH + CHF ₃	HFC-23	7.4(-13)	2350 ± 400	2.1(-16)	1.5
OH + CH ₂ Cl ₂	30	5.8(-12)	1100 ± 150	1.4(-13)	1.2
OH + CH ₂ FCI	HCFC-31	3.0(-12)	1250 ± 150	4.5(-14)	1.15
OH + CH ₂ F ₂	HFC-32	2.5(-12)	1650 ± 200	1.0(-14)	1.2
OH + CH ₃ F	HFC-41	5.4(-12)	1700 ± 300	1.8(-14)	1.2
OH + CH ₄	50	2.3(-12)	1700 ± 200	7.7(-15)	1.2
OH + CHCl ₂ CF ₃	HCFC-123	6.4(-13)	850 ± 150	3.7(-14)	1.2
OH + CHFClCF ₃	HCFC-124	6.6(-13)	1250 ± 300	1.0(-14)	1.2
OH + CHF ₂ CF ₃	HFC-125	3.8(-13)	1500 ± 500	2.5(-15)	2.0
OH + CH ₂ ClCF ₂ Cl	HCFC-132b	3.6(-12)	1600 ± 400	1.7(-14)	2.0
OH + CH ₂ ClCF ₃	HCFC-133a	5.2(-13)	1100 ± 300	1.3(-14)	1.3
OH + CHF ₂ CHF ₂	HFC-134	8.7(-13)	1500 ± 500	5.7(-15)	2.0
OH + CH ₂ FCF ₃	HFC-134a	1.7(-12)	1750 ± 300	4.8(-15)	1.2
OH + CH ₃ CCl ₃	140a	5.0(-12)	1800 ± 300	1.2(-14)	1.3
OH + CH ₃ CFCl ₂	HCFC-141b	2.7(-13)	1050 ± 200	7.5(-15)	1.3
OH + CH ₃ CF ₂ Cl	HCFC-142b	9.6(-13)	1650 ± 150	3.8(-15)	1.2
OH + CH ₂ FCHF ₂	HFC-143	2.8(-12)	1500 ± 500	1.8(-14)	2.0
OH + CH ₃ CF ₃	HFC-143a	2.6(-13)	1500 ± 500	1.7(-15)	2.0
OH + CH ₂ FCH ₂ F	HFC-152	1.7(-11)	1500 ± 500	1.1(-13)	2.0
OH + CH ₃ CHF ₂	HFC-152a	1.5(-12)	1100 ± 200	3.7(-14)	1.1
OH + CH ₃ CH ₂ F	HFC-161	1.3(-11)	1200 ± 300	2.3(-13)	2.0

^aUnits are cm³ molecule⁻¹s⁻¹.

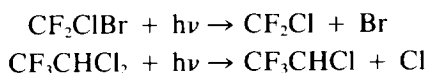
^bUnits are K.

which could result in photodissociation in the troposphere. However, the cross sections are very low in the long wavelength region, resulting in very low photolysis rates in the troposphere for fluorochloroalkanes and brominated compounds such as CF₃Br. Only for haloalkanes containing one Br and one or more Cl atoms (CF₂ClBr, CHCl₂Br, and CH₂ClBr) or two or more Br atoms (CF₂Br₂, CH₂Br₂, CHClBr₂, and CHBr₂) does photolysis in the troposphere become significant.

Solar photolysis is likely to contribute significantly to the stratospheric destruction of the alternative fluorocarbons which have two or more chlorine atoms bonded to the same carbon atom.

The absorption cross sections for several HFCs and HCFCs have been reviewed as part of the AFEAS assessment. Two of the eight HCFCs considered in the review, namely HCFC-123 and HCFC-141b, have significant stratospheric photolysis. For these two species there is good agreement among the various measurements of the ultraviolet cross sections in the wavelength region which is important for atmospheric photodissociation, that is, around 200 nm. There is also good agreement for HCFC-124, HCFC-22, and HCFC-142b; these three species contain only one chlorine atom per molecule and OH reaction is the dominant loss process in both the stratosphere and the troposphere.

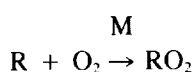
Photodissociation occurs with quantum yields which are expected to be unity, and results in the detachment of a Br atom for bromine-containing haloalkanes, or a chlorine atom from HCFCs, e.g.,



The subsequent reactions of the haloalkyl radicals formed are discussed below.

4.2.2.3 Reactions of the Haloalkyl (R) Radicals

Under tropospheric conditions, the only reaction of the haloalkyl radicals, R, is with O₂.



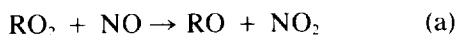
For the halomethyl radicals CF₃, CFCl₂, and CCl₃, these additional reactions are in the fall-off region between second- and third-order kinetics at the temperatures and pressures encountered in the troposphere. However, the bimolecular rate constants are estimated to be within a factor of ~2 of the limiting high pressure rate constants throughout the troposphere, with

$$k(\text{R} + \text{O}_2) \cong 10^{-12} \text{ cm}^3 \text{ molecule}^{-1} \text{ s}^{-1}$$

leading to a lifetime of the haloalkyl radicals in the troposphere of <10⁻⁶s.

4.2.2.4 Reactions of the Haloalkyl Peroxy (RO₂) Radicals

At the expected tropospheric concentrations of NO, NO₂, the HO₂ radical, and other organic peroxy radicals, the dominant reactions of the haloalkyl peroxy radicals will be with NO, NO₂, and the HO₂ radical, i.e., these reactions proceed by



M



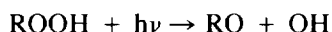
leading to the formation of haloalkoxy radicals, RO, halogenated peroxy nitrates (ROONO₂) and hydroperoxides (ROOH). Based upon kinetic data reported for reactions (a) and (b) of the chlorofluoromethyl peroxy radicals (NASA, 1987; IUPAC, 1989), it appears that $k_a \sim 1.6 \times 10^{-11} (\text{T}/300)^{-1.2} \text{ cm}^3 \text{ molecule}^{-1} \text{ s}^{-1}$ and $k_b \sim 1 \times 10^{-11} \text{ cm}^3 \text{ molecule}^{-1} \text{ s}^{-1}$ for tropospheric conditions.

No data are available for the reactions of haloalkyl peroxy radicals with the HO₂ radical. Based upon the absolute rate constant data for the reactions of the HO₂ radical with CH₃O₂ and C₂H₅O₂, the rate constant for the reactions of alkyl peroxy radicals with HO₂ is $\sim 3.4 \times 10^{-13} e^{800/T} \text{ cm}^3 \text{ molecule}^{-1} \text{ s}^{-1}$, and in the absence of experimental data for the haloalkyl peroxy radicals this expression may be assumed to apply for reaction (c) above.

OZONE DEPLETION POTENTIALS

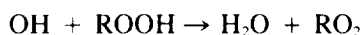
4.2.2.5 Reactions of the Hydroperoxides (ROOH)

The gas-phase loss processes of the hydroperoxides are expected to be photolysis and reaction with the OH radical. The absorption cross sections for CH₃OOH have been measured, and photolysis



is estimated to lead to a lifetime of CH₃OOH and other ROOH species of a few days in the lower troposphere.

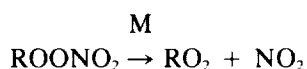
Reaction of the haloalkyl hydroperoxides, ROOH, with the OH radical will proceed by H atom abstraction to reform the RO₂ radical



Abstraction of an H atom from the haloalkyl (R) group, even if possible, is estimated to be of minor or negligible importance. Based upon the available kinetic data for (CH₃)₃COOH and CH₃OOH, the rate constant for the reaction of the OH radical with ROOH to form RO₂ + HO₂ is $1.7 \times 10^{-12} e^{220/T} \text{ cm}^3 \text{ molecule}^{-1} \text{ s}^{-1}$. This OH radical reaction is then of comparable importance to the photolysis of the ROOH species. However, since the estimated lifetime of the ROOH species due to photolysis and reaction with the OH radical is ~2–3 days in the lower troposphere, wet deposition and/or incorporation of ROOH into cloud, rain and fog water must also be expected to be of importance as a tropospheric sink for these hydroperoxides.

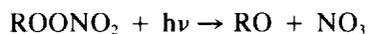
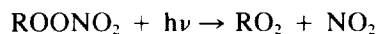
4.2.2.6 Reactions of the Haloalkyl Peroxynitrates (ROONO₂)

The peroxynitrates undergo thermal decomposition and photolysis. Thermal decomposition



is expected to be the dominant loss process for these compounds in the lower troposphere. Consistent with the reverse formation reaction, the decomposition rate constants for the halomethyl peroxynitrates are in the fall-off region at the temperatures and pressures of the troposphere, but are within a factor of ~2 of the high-pressure rate constants (IUPAC, 1989). For the peroxynitrates CF₂ClOONO₂, CFC₂OONO₂, and CCl₃OONO₂, the limiting high-pressure decomposition rate constant is $\sim 1 \times 10^{15} e^{-11000/T} \text{ s}^{-1}$.

The absorption cross sections of CFC₂OONO₂ and CCl₃OONO₂ have been measured over the wavelength range 210–280 nm (Morel et al., 1980) and the cross sections for these ROONO₂ species are generally similar to those for HOONO₂ and CH₃OONO₂. Photolysis is expected to proceed by



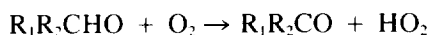
with an overall quantum yield of unity. The individual quantum yields for these photolysis pathways are not known.

The tropospheric reactions of the haloalkyl peroxy radicals lead ultimately to the corresponding alkoxy radicals, RO.

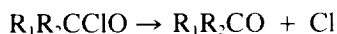
4.2.2.7 Reactions of the Haloalkoxy (RO) Radicals

Haloalkoxy radicals undergo three types of reactions under the conditions of the troposphere:

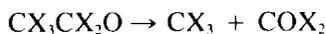
- (1) reaction with O₂ for those radicals containing an α-H atom



- (2) Cl atom elimination for those radicals containing an α-chlorine atom



- (3) C-C bond dissociation for ≥ C₂ radicals,



where X is an H or halogen atom.

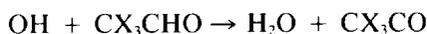
All of these RO radical reactions yield carbonyl compounds. Experimental studies of haloalkane oxidation mechanisms and thermochemical considerations allow the preferred reaction pathway(s) to be predicted with a reasonable degree of confidence for each particular RO radical. The tropospheric reactions of CF₃O are not well understood, since F atom elimination is too slow to be of any significance. However, it is assumed that CF₃O will form COF₂ under tropospheric conditions.

The principal carbonyl compounds expected to be formed during the tropospheric degradation reactions of the haloalkanes are HCOF, HCOCl, HCOBr, COF₂, COFCl, COCl₂, CF₃COF, CF₃COCl, and other CX₃COY compounds (X being H and/or halogen and Y a halogen atom). A complete list of the products expected from the degradation of the HCFCs and HFCs selected for the AFEAS assessment are summarized in Table 4.2-2.

4.2.2.8 Reactions of Carbonyl Halides, Acetyl Halides, and Halogen-Substituted Acetaldehyde

Reactions of the carbonyl halides COX₂ and acetyl halides CX₃C(O)Y (X = H and/or halogen; Y = halogen) with OH radicals and other reactive tropospheric species are expected to be too slow to be of any significance. Furthermore, photolysis is expected to be very slow for these species.

The halogen-substituted acetaldehydes, CX₃CHO (X = F, H, Cl), can, however, react with the OH radical

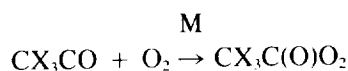


to form an acyl radical. As for the acetyl radical (IUPAC, 1989), these CX₃CO radicals will rapidly add O₂ (with a rate constant of ~10⁻¹² cm³ molecule⁻¹ s⁻¹ under tropospheric conditions)

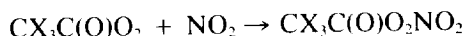
OZONE DEPLETION POTENTIALS

Table 4.2-2. Fluorine-containing products in the atmospheric degradation of selected fluorocarbons

Compound	Formula	Atom & Radical	Carbonyl	Acid	Hydroxide	Nitrate
HCFC-123	HCCl ₂ CF ₃	CF ₃ CCl ₂ OO CF ₃ CCl ₂ O CF ₃ OO CF ₃ O	CF ₃ CClO		CF ₃ CCl ₂ OOH CF ₃ OOH CF ₃ OH	CF ₃ CCl ₂ OONO ₂ CF ₃ OONO ₂ CF ₃ ONO ₂
HCFC-141b	CCl ₂ FCH ₃	CCl ₂ FCH ₂ OO CCl ₂ FCH ₂ O CCl ₂ FOO CCl ₂ FO CCl ₂ FC(O)OO	CCl ₂ FCHO CClFO	CCl ₂ FC(O)OOH CCl ₂ FC(O)OH	CCl ₂ FCH ₂ OOH CCl ₂ FOOH	CCl ₂ FCH ₂ OONO ₂ CCl ₂ FOONO ₂ CCl ₂ FC(O)OONO ₂
HCFC-142b	CClF ₂ CH ₃	CClF ₂ CH ₂ OO CClF ₂ CH ₂ O CClF ₂ OO CClF ₂ O CClF ₂ C(O)OO CClF ₂ C(O)OH	CClF ₂ CHO CF ₂ O	CClF ₂ C(O)OOH	CClF ₂ CH ₂ OOH CClF ₂ OOH	CClF ₂ CH ₂ OONO ₂ CClF ₂ OONO ₂ CClF ₂ C(O)OONO ₂
HCFC-22	CHClF ₂	CClF ₂ OO CClF ₂ O	CF ₂ O		CClF ₂ OOH	CClF ₂ OONO ₂
HCFC-124	CHCl- FCF ₃	CF ₃ CClFOO CF ₃ CClFO CF ₃ OO CF ₃ O	CF ₃ CFO		CF ₃ CClFOOH CF ₃ OOH CF ₃ OH	CF ₃ CClFOONO ₂ CF ₃ OONO ₂ CF ₃ ONO ₂
HFC-134a	CH ₂ FCF ₃	CF ₃ CHFOO CF ₃ CHFO CF ₃ OO CF ₃ O CFO	CHFO CF ₃ CFO		CF ₃ CHFOOH CF ₃ OOH CF ₃ OH CF(O)OOH	CF ₃ CHFOONO ₂ CF ₃ OONO ₂ CF ₃ ONO ₂ CF(O)OONO ₂
HFC-152a	CHF ₂ CH ₃	CH ₃ CF ₂ OO CH ₃ CF ₂ O CHF ₂ CH ₂ OO CHF ₂ CH ₂ O CHF ₂ OO CHF ₂ O CHF ₂ C(O)OO CFO	CF ₂ O CHF ₂ CHO CHFO	CHF ₂ C(O)OOH CHF ₂ C(O)OH CF(O)OOH	CH ₃ CF ₂ OOH CHF ₂ CH ₂ OOH CHF ₂ OOH	CH ₃ CF ₂ OONO ₂ CHF ₂ CH ₂ OONO ₂ CHF ₂ OONO ₂ CHF ₂ C(O)OONO ₂ CF(O)OONO ₂
HFC-125	CHF ₂ CF ₃	CF ₃ CF ₂ OO CF ₃ CF ₂ O CF ₃ OO CF ₃ O	CF ₂ O CF ₃ CFO		CF ₃ CF ₂ OOH CF ₃ OOH CF ₃ OH	CF ₃ CF ₂ OONO ₂ CF ₃ OONO ₂ CF ₃ ONO ₂



to form acyl peroxy radicals. These radicals are expected to degrade ultimately to the carbonyl halides and carbon dioxide. However, the $\text{CX}_3\text{C(O)O}_2$ radicals are expected to form peroxy nitrates by reaction with NO_2 :



The peroxy nitrate products are similar to the well-known peroxyacetyl nitrate (PAN) and are expected to be thermally stable in the troposphere. In addition, photolysis of these halogenated peroxy nitrates is expected to be very slow and their residence time due to gas phase degradation could be long.

4.2.2.9 Physical Loss Processes

The low gas phase reactivity of many of the halogenated carbonyl compounds produced in the degradation of HCFCs and HFCs leads to a potentially important role for physical loss process from the atmosphere, i.e., incorporation into rain or clouds, or sea water, with subsequent hydrolysis. Although handicapped by the total absence of Henry's law solubility data for any of the compounds of interest and the limited availability of relevant kinetic data, an assessment of the rates and mechanisms of aqueous phase removal of the gas phase degradation products has been carried out, as part of the AFEAS assessment.

The species X_2CO , HXCO , CH_3CXO , CF_3OH , CX_3OONO_2 , and ROOH ($\text{X} = \text{F}$ or Cl , $\text{R} =$ halo-substituted methyl or acetyl) are all expected to be removed from the atmosphere on time scales limited by transport to cloudy regions or the marine boundary layer (i.e., about 1 month). Some support for this comes from the recent measurements of COCl_2 by Wilson et al. (1988) in the troposphere and lower stratosphere, which are consistent with a tropospheric physical loss process. Aqueous phase reactions of these species result in the formation of chloride, fluoride, and carbon dioxide, as well as formic, acetic, and oxalic acids. The species CX_3CXO , $\text{CX}_3\text{CX}_2\text{OOH}$, $\text{CX}_3\text{CX}_2\text{OONO}_2$, $\text{CX}_3\text{C(O)OONO}_2$, and $\text{CX}_3\text{C(O)OOH}$ are also expected to be removed from the atmosphere rapidly, and their aqueous phase reactions result in the formation of halo-substituted acetates, $\text{CX}_3\text{C(O)O}$.

The species $\text{CX}_3\text{C(O)OH}$ are very acidic and, as a result, are highly soluble in cloud water. These acids are expected to be rapidly removed from the atmosphere by rainout. However, the aqueous phase species $\text{CX}_3\text{C(O)O}^-$ are expected to be resistant to chemical degradation. Trichloroacetate can thermally decompose on a time scale of 2–10 years to yield carbon dioxide and chloroform. In freshwater, the reaction of $\text{CCl}_3\text{C(O)O}^-$, $\text{CF}_2\text{ClC(O)O}^-$ may have very long aqueous phase lifetimes. The longest-lived species, $\text{CF}_3\text{C(O)O}^-$, could have a lifetime in natural waters as long as several hundred years. Processes which could possibly degrade $\text{CF}_n\text{Cl}_{3-n}\text{C(O)O}^-$ on shorter time scales than suggested above, but whose rates cannot be estimated with any degree of confidence at this time, include oxidation by photochemically generated valence band holes in semiconductor particles and hydrolysis catalyzed by enzymes in microorganisms and plants; further research aimed at characterizing these processes is needed.

One possible gas phase degradation product about which very little is known is CF_3ONO_2 . This compound has never been observed, and may be thermally unstable. If CF_3ONO_2 is thermally stable, then it may have a long lifetime toward aqueous phase removal. Henry's law solubility data and hydrolysis kinetics data for CF_3ONO_2 are needed before its aqueous phase removal rate can be assessed with any degree of confidence.

OZONE DEPLETION POTENTIALS

4.2.2.10 Summary of Halocarbon Oxidation Chemistry

The following main conclusions concerning possible CFC substitutes can be drawn from the discussion of halocarbon processes contained in this chapter and in the more detailed AFEAS assessment contained in the Appendix to this report.

Tropospheric reaction with the OH radical is the major and rate determining loss process for the HFCs and HCFCs in the atmosphere. The rate coefficients for the OH reactions are well defined at the temperatures appropriate for tropospheric reaction. There are virtually no experimental data available concerning the subsequent reactions occurring in the atmospheric degradation of these molecules. By consideration of data for degradation of alkanes and chloroalkanes, it is possible to postulate the reaction mechanism and products formed in the troposphere from HCFCs and HFCs. However, the results are subject to large qualitative and quantitative uncertainty, and may even be incorrect.

A large variety of chlorine- and fluorine-containing intermediate products such as hydroperoxides, peroxy nitrates, carbonyl halides, aldehydes, and acids can be expected from the degradation of the proposed CFC substitutes. Based on the available knowledge of gas phase chemistry, only four of these products appear to be potentially significant carriers of chlorine to the stratosphere. These are CClFO , CF_3CClO , $\text{CClF}_2\text{CO}_2\text{NO}_2$, and $\text{CCl}_2\text{FCO}_2\text{NO}_2$. However, physical removal processes may reduce this potential. In addition, the possibility of pathways and products not predicted by the arguments-by-analogy are a cause for concern.

A large part of the uncertainty of the mechanistic details of the HCFC oxidation arises from an insufficient knowledge of the thermal stability and reactivity of halogenated alkoxy radicals. In particular, the mechanism of oxidation of the CF_3O radical, which is assumed to produce CF_2O , is not known for atmospheric conditions and needs further study. Particular attention should also be paid to obtaining data on the photochemistry, gas phase reactivity, and solubility of the carbonyl, acetyl, and formyl halides in order to assess their removal rates and mechanisms.

Based on current knowledge, the products identified are unlikely to cause significant changes to the effective greenhouse warming potential of the proposed CFC substitutes. This conclusion would be modified if long-lived products such as CF_3H were formed by unidentified pathways.

It would be prudent to carry out comprehensive laboratory tests and atmospheric measurements to ascertain the validity of the proposed degradation mechanisms for HCFCs and HFCs, before large amounts of these substances are released to the environment.

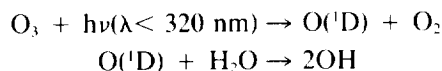
4.2.3 Hydroxyl Radical Chemistry in the Troposphere

4.2.3.1 Processes Governing OH Concentration in the Troposphere

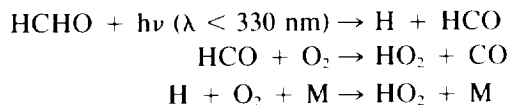
Following Weinstock's (1969) suggestion that reaction with OH radicals provides a major sink for atmospheric CO and CH_4 , Levy (1971) was the first to propose that relatively high steady-state concentrations of OH and other radicals might be present in the troposphere, as a result of photochemical reactions involving ozone and other trace gases. Since that time, a comprehensive and relatively consistent theory has been developed concerning the sources, chemical cycles, and sinks which control the OH concentration in the troposphere.

OZONE DEPLETION POTENTIALS

The essential chemistry in the theory of tropospheric OH is illustrated in Figure 4.2-1. The steady-state concentration of OH is determined by a balance between production and loss processes for free radicals, and the fast interconversion reactions coupling OH with the hydroperoxy radical (HO_2). The main production route results from the photolysis of ozone at $\lambda < 320 \text{ nm}$ to produce excited $\text{O}(^1\text{D})$ atoms. The $\text{O}(^1\text{D})$ atoms are mainly quenched to the ground state, but a significant fraction reacts with water vapor to produce OH:



It follows that the rate of OH production is proportional to the water vapor mixing ratio. In addition, the photolysis of H_2O_2 organic hydroperoxides provide minor secondary sources of OH in the troposphere. Because the hydroperoxyl radical, HO_2 , is rapidly converted to OH by reacting with NO and O_3 , photochemical reactions leading to formation of HO_2 provide a further, indirect source of OH. The most important contribution of this type comes from the UV photolysis of formaldehyde, HCHO, which is present in the troposphere as a result of the oxidation of CH_4 and other volatile organic compounds:



Because CH_4 oxidation is a chain reaction initiated by OH attack (see Figure 4.2-1), the organic oxidation chemistry provides an amplification of the primary OH production resulting from ozone photolysis, as emphasized by Warneck (1975).

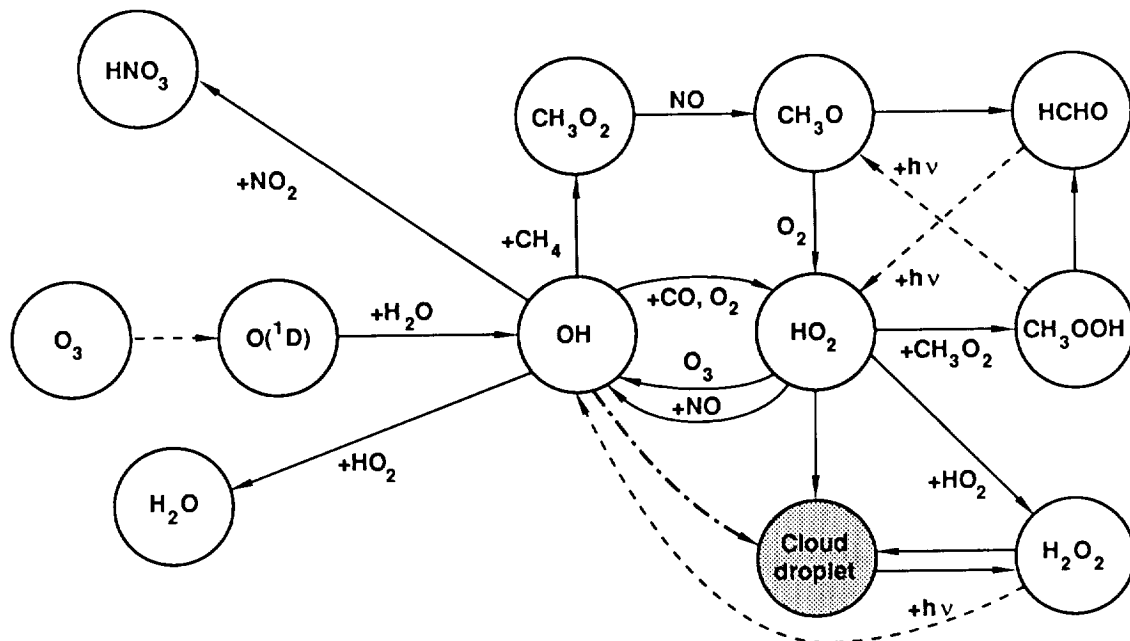


Figure 4.2-1. Reactions governing concentrations of OH and HO_2 .

OZONE DEPLETION POTENTIALS

The loss processes involve combination reactions of the OH and HO₂ radicals with each other and also with NO₂ to form stable, non-radical products, e.g., H₂O, H₂O₂, HNO₃, and HO₂NO₂. The more rapid reactions of OH with CO and CH₄ do not lead to overall loss of radicals since HO₂ is formed, which is cycled back to OH. Nevertheless, the steady-state concentration of OH is influenced by the concentrations of reactive trace gases such as CH₄, CO, O₃, and NO since these determine, through the fast interconversion reactions, the partitioning of the total radical pool between OH and HO₂.

The possible influence of cloud droplets and aerosol particles in providing heterogeneous loss mechanisms for HO_x free radicals has been considered by Warneck (1974). Aerosol loadings in the clean troposphere are too low to provide significant sinks; but in the polluted boundary layer and in fogs and clouds, heterogeneous loss of HO₂, which has a longer chemical lifetime than OH, can be an important factor in reducing the radical concentration. These factors combined with the dependence of OH on local trace gas concentration lead to an expected large local variability in the concentrations of OH.

Since the dominant primary source of OH is the UV photolysis of ozone, a large seasonal, diurnal, and latitudinal variation in the production rate is implied. Moreover, water vapor mixing ratio and cloudiness will also influence OH production. These factors were discussed by Warneck (1975) and have subsequently been investigated in detail in photochemical models of the troposphere, used to calculate globally averaged tropospheric OH concentration (Crutzen and Fishman, 1977; Derwent and Curtis, 1977; Logan et al., 1981). The models predict highest OH concentrations in the lower tropical troposphere with very low values in polar regions.

At nighttime, there are no photochemical sources of OH. Nighttime free radical chemistry does occur, however, as a result of initiation by attack of nitrate radicals on organic molecules, but OH steady-state concentrations are much lower than in the sunlit atmosphere.

4.2.3.2 Validation of OH Photochemistry

In contrast to the well-developed theory of tropospheric OH, experimental measurements of OH concentrations and verification of the theory have provided a challenge which has not yet been satisfactorily overcome.

Three techniques for the time-resolved measurement of local OH concentrations have been developed over a number of years, these being the ¹⁴C-tracer method, laser-induced fluorescence (LIF), and long-path absorption spectroscopy (LPAS). Both the ¹⁴C-tracer method and the LIF technique are subject to a number of potentially severe interferences, and the results of even the most recent measurements using these techniques must be treated with caution. To date the UV LPAS technique appears to give the most reliable measurements. The most recently developed high resolution instrument (Dorn et al., 1988; Platt et al., 1988) overcomes interference problems by detecting a spectral range covering several OH absorption features. This method gives absolute OH concentrations and does not require calibration. The only information needed for data analysis is the oscillator strength for OH which is known to be better than 5%.

The daytime OH measurements published over the last four years using all three techniques vary between approximately 0.4 and 9×10^6 OH radicals per cm³, which is broadly consistent with current model predictions. Validation of a time-dependent model, however, requires not only the measurement of OH itself, but also the simultaneous determination of all input parameters that control the local OH chemistry. In the recent LPAS measurements, sufficient supporting data were obtained to allow full model

calculation of the expected local OH concentrations (Perner et al., 1987). Comparison of these recent experimental results with the model calculations leads to the following conclusions:

1. In the presence of high NO_2 concentrations (>2 ppbv), the steady-state OH concentration is controlled only by the primary source term (ozone photolysis and subsequent reaction of $\text{O}(^1\text{D})$ atoms with water vapor) and one main loss reaction ($\text{OH} + \text{NO}_2$ forming nitric acid). Thus the calculation of OH concentrations needs only measurements of O_3 , $J(\text{O}^1\text{D})$, H_2O , and NO_2 , with the most critical being the correct determination of $J(\text{O}^1\text{D})$. In this case the measurements agree with the calculated OH concentrations to within $\sim 50\%$.
2. In relatively clean air ($\text{NO}_2 < 1$ ppbv), the OH concentration calculated using a detailed model with the supporting measurements as input parameters exceeded the measured concentrations by about a factor of two. This implies an inadequate description of the HO_x losses in the model.

Further development of techniques for OH measurements are clearly necessary and confidence in the measurements would be aided by a successful intercomparison of more than one system. Also, there is a need for measurements at different characteristic locations, in particular at high altitudes remote from local terrestrial sources of gases and particles.

4.2.3.3 Indirect Determination of Global Hydroxyl Radical

Indirect methods for determining the OH abundance from trace gas budget considerations have provided the best test for global models of OH distribution. In principle, any molecule can be used provided that the following conditions are satisfied.

- Its removal occurs by reaction with OH alone and the rate of this removal is accurately known both as a function of temperature and pressure.
- Its atmospheric abundance is accurately known.
- The source strength and distribution in time and space is accurately known.

While many chemicals (e.g., CO, non-methane hydrocarbons [NMHC]) are nearly exclusively removed by OH radicals, it has not been possible to use them because their sources are diverse and often unknown. However, in two cases the above conditions are met to varying degrees: man-made halocarbons and naturally occurring ^{14}CO . In recent decades synthetic halogenated chemicals have been injected into the environment in such significant amounts that a measurable global background is present. Because of the exclusive man-made source of halocarbons, the major uncertainties associated with the source term can, in principle, be eliminated. A select group of these halocarbons are also removed from the atmosphere nearly exclusively by reaction with OH. Similarly, ^{14}CO has a well-defined cosmic ray source and its atmospheric abundance can be related to OH. In the following paragraphs previous attempts to evaluate OH abundance in this way are summarized and a recent assessment of the global OH concentrations and resultant halocarbon lifetimes conducted within AFEAS is presented.

Methyl chloroform and the hydroxyl radical

A first demonstration of this technique was presented by Singh (1977a, b) and Lovelock (1977), who selected methyl chloroform (CH_3CCl_3) as the currently most suitable OH-tracer fulfilling the above criteria.

OZONE DEPLETION POTENTIALS

Analysis of CH_3CCl_3 data have been performed by numerous investigators during the last decade. In most cases, box models of various kinds have been used to estimate its lifetime. Table 4.2-3 summarizes the global average lifetime of CH_3CCl_3 derived in a variety of published studies. The first emission inventory reported by Neely and Plonka (1978) has been widely used. Subsequent emissions data have been estimated from production figures assuming that the production-to-emission ratio of Neely and Plonka (1978) has not changed significantly. Only 3 to 4% of the emissions are thought to occur in the Southern Hemisphere. Prinn et al. (1987) estimate that the CH_3CCl_3 global emission data are probably known to be $\sim 5\%$. A recent analysis of methyl chloroform emissions by Midgely (1989) confirms this.

A bulk of the uncertainty in CH_3CCl_3 lifetime reported in Table 4.2-3 comes from the determination of the atmospheric burden of CH_3CCl_3 . Over the years the estimates of the global average CH_3CCl_3 lifetime cover the range 6–12 years. The most recent ALE/GAGE data after correction (see Table 4.2-3) result in a mean CH_3CCl_3 lifetime of 6 to 7 years.

The CH_3CCl_3 mean lifetime estimate can be compared to that predicted by a global model with a well-defined OH field. It is convenient to define an equivalent average OH concentration that is consistent with the CH_3CCl_3 global lifetime. Such an estimate of OH must take into account the fact that $\text{OH} + \text{CH}_3\text{CCl}_3$ reaction rate is a function of temperature and also must assume that other removal processes are negligible. With these assumptions a mean OH concentration of $5\text{--}7 \times 10^5$ molecule cm^{-3} fits the data best. The hemispheric asymmetry in the CH_3CCl_3 lifetime (Table 4.2-3) also implies that the OH levels in the SH are somewhat higher than the NH values.

Table 4.2-3. Atmospheric lifetime of methyl chloroform and estimates of equivalent OH concentrations

Global average CH_3CCl_3 Lifetime (years)	Mean OH (10^5 molecule cm^{-3}) ^a	Comments	Reference
7 ± 1	3–6		Singh (1977a)
5–10	5–10		Lovelock (1977)
8–11	4	$\tau_{\text{NH}} \sim 1.5 \tau_{\text{SH}}$	Singh (1977b)
3	10	$\tau_{\text{NH}} \sim 3 \tau_{\text{SH}}$	Neely and Plonka (1978)
8	6		McConnell and Schiff (1978)
7 ± 1	—		Makide and Rowland (1981)
5 ± 2	7 ± 2		Derwent and Eggleton (1981)
9 ± 2	6 ± 1		Singh et al. (1983)
$10(^{+5}/_{-4})^b$	5 ± 2		Prinn et al. (1983)
6 ± 1.5^c	8		Khalil and Rasmussen (1984)
6 ± 1^c	7 ± 2		Fraser et al. (1986)
12^b	—		Golombek and Prinn (1986)
6 ± 1^c	8 ± 1	$\tau_{\text{NH}} \sim 1.15 \tau_{\text{SH}}$	Prinn et al. (1987)
6.5 ± 1	—	$\tau_{\text{NH}} \sim 1.2 \tau_{\text{SH}}$	Blake and Rowland (1988)

^aUsing model results it is reasonable to assume that the OH abundance between $0\text{--}30^\circ$ latitude is nearly twice as large as between $30\text{--}90^\circ$ latitude. Thus, a global OH average (molecule cm^{-3}) of 7.5×10^5 would correspond to OH values of 10×10^5 and 5×10^5 at $0\text{--}30^\circ$ and $30\text{--}90^\circ$ latitudes, respectively.

^bUncorrected ALE/GAGE CH_3CCl_3 data.

^cCorrected ALE/GAGE CH_3CCl_3 data. All atmospheric measurements multiplied by 0.8. The actual derived lifetime is 6.3 years.

Other halocarbons have been used in a similar manner to estimate OH, for example, dichloromethane, 1,2 dichloroethane and tetrachloroethene (Singh et al., 1983). A two-box model shows that removal rates of these molecules are consistent with average OH concentrations of 4 to 5×10^5 molecules cm^{-3} . Because of their relatively short lifetimes (several months) compared to CH_3CCl_3 , these chemicals could potentially reveal OH latitudinal and seasonal gradients with greater sensitivity. However, their source strengths are not as well defined as that of CH_3CCl_3 . In addition, these analyses are sensitive to the seasonal variations in emissions which are poorly known.

^{14}CO and the hydroxyl radical

The first attempts to calculate the global mean tropospheric hydroxyl concentration from isotopic distribution in atmospheric carbon monoxide were made by Weinstock (1969) and by Weinstock and Niki (1972). They used the three available ^{14}CO measurements by McKay et al. (1963), an estimate of the global source strength for ^{14}CO from the well-known cosmic ray bombardment of atmospheric nitrogen molecules, and the $\text{OH} + \text{CO}$ rate coefficient to derive an estimate for the atmospheric turnover time for ^{12}CO of the order of 1 month. Furthermore, they suggested that OH radicals were responsible for the CO removal and obtained an estimate of the global mean OH abundance.

The ^{14}CO concentrations in the troposphere are extremely small with a winter maximum of 20 molecule cm^{-3} and a summer minimum of about 10 molecule cm^{-3} . Volz et al. (1981) improved the methodology based on four refinements, viz:

- additional measurements of ^{14}CO in the lower troposphere,
- evaluated chemical kinetic data for the $\text{OH} + \text{CO}$ reaction, and
- a global two-dimensional time-dependent model to investigate the coupled $\text{CH}_4\text{-H}_2\text{-CO-NO}_x\text{-O}_3$ life cycles, replacing the box model approach.

These analyses led Volz et al. (1981) to obtain a mean tropospheric OH concentration of $6.5^{+3}_{-2} \times 10^5$ molecule cm^{-3} . No additional data on ^{14}CO have been collected in the intervening years and no Southern Hemispheric data are available. Derwent and Volz-Thomas (1989) in a re-evaluation of this technique conclude that the average OH derived by this method remains unchanged.

4.2.3.4 Recent Assessment of Tropospheric OH Abundance and Halocarbon Lifetimes

The above summary shows that an overall volume-averaged OH concentration of $6 (\pm 2) \times 10^5$ molecule cm^{-3} best represents all of the available information on the CH_3CCl_3 and ^{14}CO budgets. However, the usefulness of a global mean OH concentration for determination of overall reaction rates and lifetimes of HCFCs derived in this fashion is questionable. This arises because of the non-uniformity of the OH abundance and of the distribution of the molecules with which it reacts, and also because of the different temperature dependencies of the reaction rates in the troposphere. In the recent AFEAS assessment these factors were considered at some depth. Prather (1989) used 3-dimensional tropospheric OH fields that were calculated from a climatology of sunlight, temperature, and trace gas mixing ratios. These OH fields were then used to study the methyl chloroform budget by calculating the integrated loss of this molecule in a 3-D chemical transport model of the troposphere and to test the accuracy of scaling the HCFC lifetimes to an assumed methyl chloroform lifetime.

OZONE DEPLETION POTENTIALS

In the AFEAS assessment, the lifetimes of HCFCs and HFCs were determined by three separate approaches:

1. 2-D chemical transport model with semi-empirical fit to ^{14}CO ;
2. Photochemical calculation of 3-D OH fields and integrated loss;
3. Scaling of the inferred CH_3CCl_3 lifetime by rate coefficients.

Resulting lifetimes from all three independent approaches generally agree within 15%, as shown in Table 4.2-4. The integrated losses calculated from the global OH fields in the models (1 and 2) are constrained by modeling of the observations and budgets for ^{14}CO and CH_3CCl_3 , respectively. Method (3) may be expressed simply as

$$\text{lifetime}(\text{HCFC}) = 6.3 \text{ yr} \times k(\text{CH}_3\text{CCl}_3 \text{ at } T = 277 \text{ K}) / k(\text{HCFC at } T = 277 \text{ K}),$$

where the current estimate of the lifetime for methyl chloroform (6.3 yr) is based on the ALE/GAGE analysis (Prinn et al., 1987). Some of the errors associated with this scaling and the choice of the temperature of 277 K for scaling the reaction rates have been tested with the 3-D OH fields from method (2). Based on the sensitivity studies from methods (1) and (2), method (3) should be reliable for calculating HCFC lifetimes in the range 1 to 30 years. Method (2) shows that the middle tropical troposphere (2–6 km) dominates the atmospheric loss and would be an important region in which to make observations of OH.

Table 4.2-4. Atmospheric lifetimes for HCFCs and HFCs, based on Derwent and Volz-Thomas (1989) and Prather (1989)

HCFC	$k(\text{cm}^3 \text{ molec}^{-1} \text{ s}^{-1})$	Lifetime (yr) for method ^a		
		(1)	(2)	(3)
CH_3CCl_3 (range)	$5.0 \times 10^{-12} \exp(-1800/T)$	5.0 (3–7)	5.4 (4–7)	6.3 (5.4–7.5)
CH_3F	$5.4 \times 10^{-12} \exp(-1700/T)$	3.3	3.8	4.1
CH_2F_2	$2.5 \times 10^{-12} \exp(-1650/T)$	6.0	6.8	7.3
CHF_3	$7.4 \times 10^{-13} \exp(-2530/T)$	635.0	289.0	310.0
CH_2FCI	$3.0 \times 10^{-12} \exp(-1250/T)$	1.26	1.33	1.44
CHFCl_2	$1.2 \times 10^{-12} \exp(-1100/T)$	1.80	1.89	2.10
CHF_2C (22)	$1.2 \times 10^{-12} \exp(-1650/T)$	13.0	14.2	15.3
$\text{CH}_3\text{CH}_2\text{F}$	$1.3 \times 10^{-11} \exp(-1200/T)$	0.31	0.25	0.28
$\text{CH}_2\text{FCH}_2\text{F}$	$1.7 \times 10^{-11} \exp(-1500/T)$	0.60	0.58	0.63
CH_3CHF_2 (152a)	$1.5 \times 10^{-12} \exp(-1100/T)$	1.46	1.53	1.68
CH_2FCHF_2	$2.8 \times 10^{-12} \exp(-1500/T)$	3.2	3.5	3.8
CH_3CF_3	$2.6 \times 10^{-13} \exp(-1500/T)$	40.0	38.0	41.0
CHF_2CHF_2	$8.7 \times 10^{-13} \exp(-1500/T)$	10.4	11.4	12.3
CH_2FCF_3 (134a)	$1.7 \times 10^{-12} \exp(-1750/T)$	13.1	14.4	15.5
CHF_2CF_3 (125)	$3.8 \times 10^{-13} \exp(-1500/T)$	25.9	26.1	28.1
CH_2CFCl_2 (141b)	$2.7 \times 10^{-13} \exp(-1050/T)$	6.7	6.7	7.8
$\text{CH}_3\text{CF}_2\text{Cl}$ (142b)	$9.6 \times 10^{-13} \exp(-1650/T)$	16.6	17.8	19.1
$\text{CH}_2\text{CICF}_2\text{Cl}$	$3.6 \times 10^{-12} \exp(-1600/T)$	3.5	4.0	4.2
CH_2CICF_3	$5.2 \times 10^{-13} \exp(-1100/T)$	4.1	4.4	4.8
CHCl_2CF_3 (123)	$6.4 \times 10^{-13} \exp(-850/T)$	1.40	1.42	1.59
CHFClCF_3 (124)	$6.6 \times 10^{-13} \exp(-1250/T)$	5.5	6.0	6.6

^aLifetimes from Method (1) do not include stratospheric loss; those from Method (2) include small additional stratospheric loss. Method (3) is based on scaling the methyl chloroform lifetime of 6.3 yr (Prinn et al. 1987) by the ratio of the rate coefficients at 277 K.

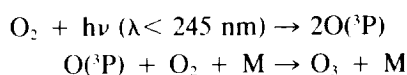
Estimated uncertainties in the HCFC and HFC lifetimes between 1 and 30 years are $\pm 50\%$ for (1) and $\pm 40\%$ for (3) and (2). These ranges include the uncertainty in the rate constants for the OH reactions. Global OH values that give lifetimes outside of these ranges of uncertainty are inconsistent with detailed analyses of the observed distributions for ^{14}CO and CH_3CCl_3 . The expected spatial and seasonal variations in the global distribution of HCFCs with lifetimes of 1 to 30 years have been examined with methods (1) and (2) and found to have insignificant effect on the calculated lifetimes. Larger uncertainties apply to gases with lifetimes shorter than one year; however, for these species our concern is for destruction on a regional scale rather than global accumulation.

Clearly any changes in the concentrations of ozone and other trace gases in the troposphere, which affect OH abundance, will have an impact on HCFC lifetimes and in the following section we review the relevant tropospheric chemistry and current perception of future atmospheric behavior in this context.

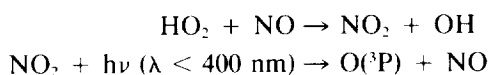
4.2.4 Tropospheric Chemistry Influencing OH and Ozone

4.2.4.1 Processes Controlling Tropospheric Ozone

Tropospheric ozone may be produced by *in situ* chemistry (Crutzen, 1973; Chameides and Walker, 1973; Fishman and Crutzen, 1978) or by transfer from the stratosphere, where O_3 is generated by the photodissociation of molecular oxygen at altitudes above 25 km, followed by combination of the ground state oxygen atoms with O_2 :



The *in situ* source of tropospheric ozone is the reaction of HO_2 or organic peroxy radicals with NO followed by the photodissociation of the nitrogen dioxide produced and the $\text{O}(^1\text{P}) + \text{O}_2$ reaction.



Although NO and NO_2 concentrations are very low throughout most of the troposphere, the effect of this reaction sequence can provide a significant O_3 source.

Ozone is also consumed in the troposphere as a result of photodissociation in the ultraviolet region. Most of the excited $\text{O}(^1\text{D})$ atoms are quenched by N_2 and O_2 to the ground state, $\text{O}(^3\text{P})$, which reform ozone, but that fraction which reacts with other trace molecules (e.g., with water to produce OH), represents a net loss of ozone. Photolysis of ozone in the near UV (Huggins bands) and visible (Chappuis bands) does not lead to net ozone loss. There is also an *in situ* loss of ozone through reaction with NO_2 (to give NO_3), HO_2 and unsaturated hydrocarbons. Model calculations (e.g., Levy et al., 1985) point to an approximate balance between *in situ* sources and sinks for tropospheric ozone, averaged over the globe. This is consistent with estimates of the magnitude of the surface sink for ozone, which averaged over the globe, is approximately equal to the stratospheric injection. However, analysis of observations and regional budgets (Logan, 1985; Bojkov, 1986; Penkett, 1988) show a clear indication that Northern Hemisphere tropospheric ozone is increasing. Changes in the seasonal modulation of ozone concentration, and in the man-made emissions and concentration of trace gases which affect ozone, suggest that the increase is due to a shift in the balance between *in situ* production and loss (Penkett, 1988). This balance essentially depends on the amount of

OZONE DEPLETION POTENTIALS

NO_x present in the background atmosphere together with the concentration of peroxy radicals derived from oxidation of CO, CH₄ and non-methane hydrocarbons, which controls the flux through the reactions in which NO is oxidized to NO₂.



The amount of tropospheric ozone is clearly central to the problem of the oxidizing efficiency of the troposphere, since O₃ photolysis is the primary source of OH radicals as well as being an oxidizing species itself. It follows that the future trends of oxidizing capacity will be tied to the future tropospheric burden of CO, CH₄, non-methane hydrocarbons and other organics, as well as nitrogen oxides. We now summarize the current picture of the distribution of ozone precursors in the troposphere. The distribution of ozone itself in the troposphere is covered in the assessment of global ozone concentrations in Chapter 2.

4.2.4.2 Tropospheric Distribution of Reactive Nitrogen Species

The tropospheric lifetime of NO_x (NO + NO₂) is rather short and consequently it is not possible to define an average, representative NO_x mixing ratio on a hemispheric or global scale.

The NO_x levels in urban and industrial areas are determined largely by anthropogenic sources. This leads to near surface NO_x mixing ratios in rural areas of the eastern United States and Western Europe typically in the range between 1 ppbv and 10 ppbv. In less populated and coastal regions, the NO_x levels depend on the prevailing meteorology and the proximity and distribution of urban sources. In these locations the NO_x mixing ratios typically range between 0.1 and 1 ppbv.

Surface measurements at remote locations reflect the influence of natural sources, such as soil emissions and lightning, which are principally terrestrial sources that are seasonal. These sources may provide surface concentrations of NO_x that typically range between 0.02 ppbv and 0.1 ppbv (Fehsenfeld et al., 1988). It should be noted that at most locations on land, particularly in the mid-latitudes, the NO_x levels in ambient air are influenced by anthropogenic activities. In remote maritime air and in the polar regions that are not influenced by anthropogenic activities, the NO_x concentrations are exceedingly small, typically 0.001 ppbv to 0.01 ppbv, and are associated with the downward mixing of NO_x from NO_x reservoirs in the upper troposphere.

The free tropospheric burden of NO_x is also strongly influenced by anthropogenic NO_x, particularly from combustion sources in the Northern Hemisphere. Variability in the atmospheric transport and photochemical lifetimes, together with the contribution of aircraft emissions of NO_x and natural sources such as lightning and stratospheric subsidence, increases the variability of NO_x concentration in the free troposphere. Here the NO_x mixing ratios may vary from 0.02 ppbv in remote regions to 5 ppbv over populated areas. In general, throughout the free troposphere the NO_x mixing ratio increases with height, as illustrated by the NO distribution shown in Figure 4.2-2.

The distribution of NO_y (NO_y: sum of all oxidized nitrogen species except N₂O = NO + NO₂ + NO₃ + 2 × N₂O₅ + HNO₃ + PAN + HO₂NO₂ + organic nitrates) is very similar to that of the source compound NO_x. Near the sources the majority of NO_y is in the form of NO_x. However, the NO_x will be rapidly converted to PAN, HNO₃, or other NO_y compounds. For example, during periods of maximum insolation the photochemical lifetime of NO_x is less than one day. Thus, in the remote free troposphere NO_x accounts for only a small fraction (approximately 10%) of the NO_y. For this reason, NO_y is a more

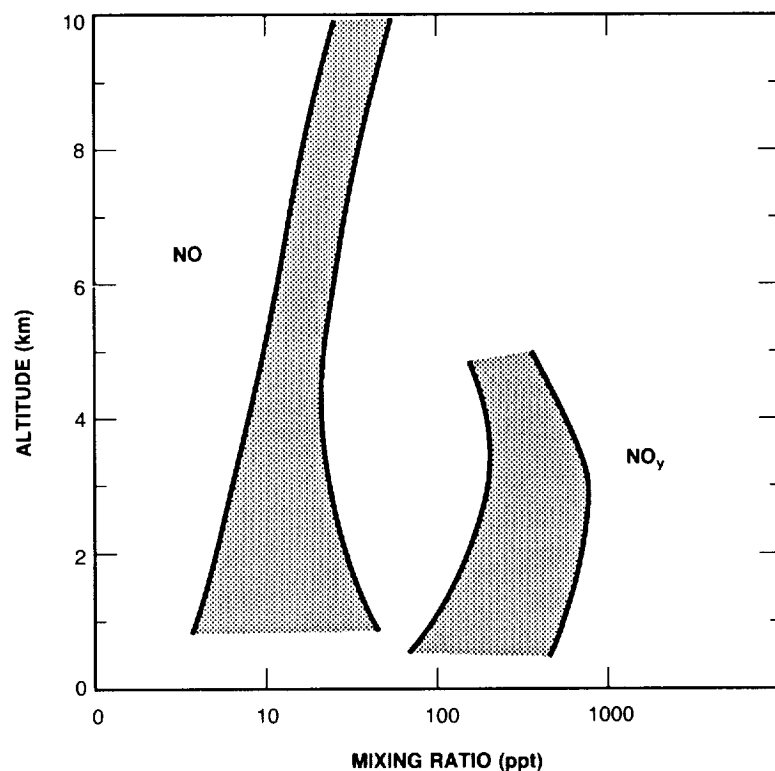


Figure 4.2-2. Schematic presentation of the measured vertical distribution of NO and NO_y over midlatitude oceanic and coastal regions.

conserved compound and the variation in the concentration of NO_y will be less than that of its short-lived precursor, NO_x.

In the remote troposphere the main fraction of the total NO_y often consists of HNO₃ and PAN (Fahey et al., 1986). HNO₃ can be quite effectively removed from the atmosphere by wet and dry deposition, whereas PAN is reasonably quickly thermally decomposed back into peroxyacetyl radicals and NO₂ at temperatures representative of the atmospheric boundary layer at low latitudes and at mid-latitudes in summer. Due to its stability at lower temperature, sometimes PAN levels of several hundred pptv can be observed in the free troposphere at mid- and high northern latitudes (Singh et al., 1986). Thus PAN and possibly other organic nitrates can serve as a potential reservoir and transport medium for the rather short-lived NO_x. However, up to now no quantitative estimate of the possible magnitude of such an effect has been made.

There is evidence from analysis of ice cores from Greenland and the Alps of a substantial increase in the concentration of nitrate ions, formed from NO₂ oxidation, over a similar period (1895–1978) (Neftel et al., 1985). This points to an increasing concentration of NO_x in parts of the Northern Hemisphere troposphere. Because of their short lifetimes, any increases in nitrogen oxides are expected to be confined to the continental source areas and nearby regions. The influence of nitrogen oxides may be spreading, however, due to a widening of source areas associated with increasing economic activity in the developing

OZONE DEPLETION POTENTIALS

world and due to reservoir species such as peroxyacetyl nitrate (PAN), which are formed in NMHC-NO_x interactions and which have relatively long atmospheric lifetimes and can dissociate to produce NO₂ far from source regions.

4.2.4.3 Tropospheric Distribution of Hydrocarbons and CO

The most important and abundant atmospheric hydrocarbon is methane. Its global distribution is well established and it exhibits only a relatively small variability in the background troposphere. The Northern Hemispheric CH₄ mixing ratios are about 1.7 ppm, the Southern Hemispheric levels are slightly lower, about 1.6 ppm.

CO has a considerably lower tropospheric abundance, but due to its higher reactivity towards OH radicals it is very important for the oxidizing efficiency of the atmosphere. The tropospheric distribution of CO is reasonably well known and there is a significant interhemispheric gradient. CO mixing ratios in the Southern Hemisphere are around 50–70 ppbv, and roughly a factor 2–3 higher in the Northern Hemisphere. A distinct seasonal variation in CO levels in both hemispheres has been identified. However, global coverage of CO distribution is still inadequate.

The current picture of the distribution of non-methane hydrocarbons (NMHC) in the troposphere is still far from complete due in part to the limited number of investigations, and there is large variability in the background concentrations. This variability results from the relatively short average atmospheric residence times, which range from a few hours to a few months. Also, the different NMHCs have various sources with different geographical distributions. The most important sources are listed in Table 4.2-5.

Large-scale distributions of NMHC in the remote troposphere have been published by several investigators (Singh and Kasting, 1988; Rudolph, 1988). Most of these studies focused on the latitudinal variability of NMHC, but there are also a few studies which present data on the vertical distribution of NMHC.

Table 4.2-5. Estimates of global hydrocarbon emissions into the atmosphere^a

Source	C ₂ H ₆	C ₃ H ₈	C ₄ H ₁₀	C ₂ H ₂	C ₆ H ₆	C ₂ H ₄	C ₃ H ₆	C ₅ H ₁₂	C ₇ H ₈	C ₈ H ₁₀	C ₅ H ₈	C ₁₀ H ₁₆
Engine exhaust	+	+	+	++	++	++	+	+	++	++		
Evaporation losses			++		+			++	+	+		
Natural gas leakage	++	++	++									
Oil + coal burning												
Chemical industry	+					+			+			
Solvent use									++	+		
Biomass burning	++	++		+	+	++	++		+	+	+++	+++
Foliage emissions	+					+					+++	+++
Microbial production	+					++	+					
Ocean emissions	++	++	++			+++	+++	++				

^aData from Ehhalt and Rudolph, 1984.

Note: + = Moderate source

++ = Strong source

+++ = Very strong source

The distribution of the longer-lived NMHC ($\tau > 1$ week) show some systematic features which can be ascribed to a representative latitudinal profile. On the average the highest mixing ratios are observed at mid- to high northern latitudes, roughly 1–3 ppbv of ethane, 0.2–0.6 ppbv of propane and n-butane, 0.1–0.5 ppbv of acetylene, 0.05–0.25 ppbv of benzene, and 0.02–0.1 ppbv of i-butane. In general, all these species show a considerable decrease towards lower latitudes and this gradient is more pronounced for the shorter-lived of these NMHC. This reflects both the source distribution with high emissions in the industrialized zone of the Northern Hemisphere and the faster removal at low latitudes due to the higher OH radical concentrations at tropical latitudes. Average Southern Hemisphere mixing ratios are roughly 0.15–0.4 ppbv ethane, 0.03–0.1 ppbv propane, 0.01–0.05 ppbv n-butane, 0.01–0.05 ppbv acetylene, 0.01–0.03 ppbv benzene, and 0.005–0.03 ppbv i-butane. There is a clear seasonal cycle in the troposphere mixing ratios of the light aliphatic hydrocarbons, with substantially higher values in the winter months. The cycle is consistent with predominant removal of these hydrocarbons by reaction with OH.

There seems to be a slight but systematic decrease from low southern latitudes towards mid southern latitudes. For ethane and probably the other hydrocarbons, there seems to be a significant and systematic seasonal cycle. In both hemispheres the minima are in the respective late summer, maxima in late winter.

For more reactive NMHC with average atmospheric residence times of less than one week, it is no longer justified to consider their distributions as being systematic with latitude. These atmospheric concentrations are determined by emissions, removal reactions, and transport on a local or regional scale (up to several hundred km). The most important NMHC in this category ($1 \text{ week} > \tau > 0.5 \text{ days}$) are C_2 – C_5 alkenes and, to a lesser extent, $< C_5$ alkanes and alkylbenzenes. Since the sources of C_2 – C_5 alkenes include biomass burning, emissions from vegetation, and emissions from oceans, substantial concentrations in the range from 0.1 to a few ppbv of ethene and propane have been observed over nonindustrialized continental regions and the oceans.

The extremely reactive terpenes and isoprene in general show a very strong decrease with increasing altitude and can generally only be observed near their sources within the atmospheric boundary layer. Over areas with dense vegetation, isoprene mixing ratios around 0.5–2 ppbv and monoterpene mixing ratios approaching 1 ppbv are frequently observed (Rasmussen and Khalil, 1988; Zimmerman et al., 1988). The emissions of many biogenic NMHC strongly depend on temperature, relative humidity, and light intensity. The types of emitted compounds also depend on the type of vegetation, e.g., isoprene is primarily emitted from deciduous plants whereas coniferous trees mainly act as terpene sources. The estimated global emission rate of isoprene is about $480 \times 10^{12} \text{ g yr}^{-1}$ (Rasmussen and Khalil, 1988). Comparable emission rates have been estimated for the other terpenoid compounds.

The global source strength of all NMHCs, but not including isoprene and the terpenes, is estimated to be about 100 – $130 \times 10^{12} \text{ g yr}^{-1}$. Since these NMHC emission estimates are highly uncertain and probably underestimated, we cannot yet make any quantitative estimates on the contribution of NMHC to the tropospheric O_3 and OH concentrations. Also, the atmospheric oxidation of NMHC leads to the *in situ* production of CO, which has a longer residence time than the NMHC and could extend their influence over a wider spatial regime. A comparison with the global CH_4 emission rate of about $400 \times 10^{12} \text{ g yr}^{-1}$ shows that the possible contribution of NMHC (not including isoprene and terpenes) can be quite substantial. The influence of isoprene and the terpenes on O_3 and OH may also be very substantial but, as yet, this effect has not been quantified.

The available measurements of non-methane hydrocarbons in the troposphere do not allow a systematic long-term trend to be recognized. Moreover, the observed variability of NMHC will prevent easy

OZONE DEPLETION POTENTIALS

recognition of any global trend in the near future. It appears more promising to estimate future (and past) changes of atmospheric NMHC concentrations from possible changes in their main sources. The fossil fuel activities have led to large increases in the emissions of non-methane hydrocarbons (NMHCs), but as yet these are on a smaller scale than methane itself and again the magnitude of the sources is in dispute. The question of the influence of the breakdown of halogenated organic molecules such as the HCFCs and HFCs on tropospheric ozone production has been reviewed in the AFEAS assessment (Niki, 1989). It is concluded that these molecules are such a small fraction of the total budget of organic compounds oxidized that their effect will be trivial.

4.2.5 Model Evaluation of Trends in Tropospheric Ozone and OH

As shown in Chapter 2, there is now observational evidence that changes are taking place in the concentration of tropospheric ozone and its precursor gases such as CH₄, CO, and possibly NO_x. The hydroxyl radical concentration is controlled by fast gas phase reactions. Simple model analysis of the photochemistry (Cox and Derwent, 1981; Liu, 1988) shows that increases in CH₄ and CO tend to decrease OH concentration whereas increases in NO_x and O₃ tend to increase OH. Changes in the solar UV due to depletion of stratospheric ozone could potentially lead to an increase in the oxidizing efficiency through direct effects on the ozone and OH photochemistry. Increases in water vapor concentration due to global warming will also lead to an increase in OH production. Observational data are totally inadequate for establishment of any changes in OH concentration and assessment of such changes must rely on model calculations.

There have been a number of model evaluations of the impact of man's activities on tropospheric ozone and OH concentrations through increased emissions of methane, CO, NO_x, and non-methane hydrocarbons. Initially, models with limited spatial resolution were employed, but increasingly one-, two-, and three-dimensional models have been developed to study both the chemical and dynamical aspects of tropospheric ozone (Crutzen, 1974; Fishman and Crutzen, 1978; Derwent and Curtis, 1977; Isaksen, 1981; Levy, Mahlman and Moxim, 1980; Logan et al., 1981; Crutzen and Bruhl, 1989). Attention given to tropospheric modeling in previous ozone layer depletion evaluations has not been as detailed as that given to stratospheric modeling. Nevertheless, considerable progress has been made in theoretical studies towards resolving many of the issues relevant to an understanding of tropospheric sinks for alternative halocarbons and increased tropospheric ozone concentrations.

The major conclusions of these studies can be summarized as follows:

- The increased availability of NO_x due to man's activities can change the Northern Hemisphere photochemistry from a net sink for ozone into a net source.
- The Northern Hemisphere ozone budget is now dominated by man-made sources, particularly in the lower troposphere.
- There may well have been a small decrease in the mean tropospheric OH concentration in the Southern Hemisphere since the pre-industrial era. The magnitude and direction of any change in the Northern Hemisphere is not clear.

The accuracy with which any of these statements based on tropospheric modeling reflect what has actually happened in the real world depends on the adequacy and completeness of the model formulations together with their input assumptions. Significant progress in basic understanding has been achieved

towards the goal of predicting the extent and direction of man's influence on the oxidizing capacity of the troposphere.

However, significant problems still remain. Potential sources of error or uncertainty in current one- and two-dimensional models arise principally through the following inadequacies of formulation:

- the non-linear relationship between ozone production and precursor molecule concentrations, which creates difficulties in spatial averaging;
- the short lifetime of NO_x and its close coupling to a surface wet and dry deposition sink, which creates difficulties with large-scale transport modeling;
- uncertainties in the latitudinal and seasonal distributions of the source strengths of methane, CO, NO_x , and non-methane hydrocarbons;
- uncertainties in the representation of tropospheric chemistry, including the representation of peroxy radical reactions, photodissociation processes (including the representation of clouds and aerosol scattering), nighttime chemistry and heterogeneous chemistry (including the removal of peroxy radicals on clouds, droplets and aerosols); and
- inadequate observational data to test the models.

In particular, the consideration of the first two areas listed above suggests that current models may overestimate tropospheric ozone production from man-made sources. On the other hand, some modeling studies have demonstrated an important role for convective lifting of NO_x from the boundary layer to the free troposphere with increased O_3 production. Despite these considerable uncertainties, current models are able to account for the observed trends in tropospheric ozone concentrations in the Northern Hemisphere from pre-industrial times through to the present day. This requires a simultaneous and consistent treatment of man's influence on the life cycles of methane, CO, NO_x , and the non-methane hydrocarbons. Many of the relevant factors are poorly understood. However, there is no reason to anticipate that man's influence on these trace gas life cycles will diminish over the next decade or so. It is pertinent to extrapolate current trends of these trace gas concentrations into the near future and to explore with the current models the influence of the changes on the oxidizing capacity of the troposphere in terms of OH and ozone.

As worldwide industrial development continues in mid-latitudes and spreads to lower latitudes of the Northern Hemisphere, ozone concentrations are anticipated to grow throughout the Northern Hemisphere as a result of increased emissions of the precursors (Crutzen, 1988). The magnitude of any change in OH or ozone will be strongly scenario dependent and will be related directly to the pattern of change in the methane, CO, NO_x , and non-methane hydrocarbon source terms (Isaksen and Hov, 1987; Thompson et al., 1989). Based on current perceptions of trends in trace gas concentrations, tropospheric ozone could increase by as much as 50% and the tropospheric mean OH concentration could decrease by as much as 25% by the middle of the next century.

The evaluation of future changes in tropospheric ozone and OH with current one- and two-dimensional models are subject to similar errors and uncertainties as those described above in the context of changes from the pre-industrial to the present-day atmosphere. Again, the non-linearities involved in relating OH and ozone to NO_x concentrations give rise to concern. Models incorporating a more realistic description of the transport processes may indicate less sensitivity of tropospheric ozone and OH to changes in trace gas concentrations.

OZONE DEPLETION POTENTIALS

So far attention has been given to the direct influences on the oxidizing capacity of the troposphere and they can only be crudely represented in current one- and two-dimensional models. Several potentially important indirect influences have been proposed. These include:

- increased UV-B penetration due to ozone depletion will increase tropospheric ozone photolysis rates, and consequently increase the mean OH source term (Liu and Trainer, 1987);
- increased tropospheric temperatures may decompose methane clathrates and stimulate tundra methane emissions and biogenic hydrocarbon emissions (Ehhalt, 1988); and
- increased water vapor mixing ratios may increase tropospheric OH concentrations.

Understanding is growing steadily such that it should be possible in the near future to generate some consistent trace gas scenarios to aid in evaluating the influence of mankind on future tropospheric ozone and OH concentrations.

4.3 OZONE DEPLETION POTENTIALS

4.3.1 Background

Recent consideration of international regulatory actions on the production of chlorofluorocarbons (CFCs) and other halogenated species has prompted significant interest in determination of the relative potential from such industrially produced compounds to affect stratospheric ozone and, more recently, global climate. The concept of relative Ozone Depletion Potentials (ODPs), introduced by Wuebbles (1981), has been adopted as a guideline or quick reference for estimating the relative potential for CFCs and other halocarbons to destroy stratospheric ozone. Several past papers have determined ODPs for selected chlorinated constituents (Wuebbles, 1983; Hammitt et al., 1987; Rognerud et al., 1989). This concept plays an important role in the implementation of the regulatory policies for fully halogenated CFCs adopted in the Montreal Protocol (UNEP, 1987).

Several atmospheric modeling groups have recently reevaluated the ODPs for the relevant CFCs, the potential replacements (particularly several HCFCs and HFCs), and other industrially produced chlorinated and brominated compounds of interest being considered. The 1-D and 2-D global atmospheric models used in these evaluations incorporate the most recently available laboratory data on the chemical kinetics and radiative parameters of the species being examined. The discussion that follows primarily focuses on the recent studies by Fisher et al. (1989a, b), Connell and Wuebbles (1989), and Gillotay et al. (1989). Most of the calculations presented here are also contained, generally in greater detail, in the Fisher et al. (1989b) paper published in the AFEAS Report (Vol. II Appendix to this report). The Fisher et al. (1989a, b) papers are the result of a cooperative study among four modeling groups: Atmospheric and Environmental Research, Inc. (AER); E.I. du Pont de Nemours and Company (DuPont); Lawrence Livermore National Laboratory (LLNL); and the University of Oslo. The Belgian Institute for Space Aeronomy (BISA) also contributed some 1-D model results to this report; these results were done separately and have not been as carefully compared as were the results of the other four groups.

4.3.2 Definition of ODP

Ozone Depletion Potential (ODP) has traditionally been defined as the steady-state ozone reduction calculated for each unit mass of a gas emitted per year (as a continuous release) into the atmosphere relative

OZONE DEPLETION POTENTIALS

to that for a unit mass emission of CFC-11. This definition provides a single-valued relative measure of the maximum calculated effect on ozone of a given compound compared to the effect calculated for CFC-11.

Figure 4.3-1, taken from Fisher et al. (1989a), shows the resulting reduction in total ozone from the DuPont 1-D model for 5×10^9 kg of halocarbon emitted into the atmosphere during the first year, with no emission in subsequent years. As seen from the table insert in Figure 4.3-1, the time-integrated effects of the initial 5×10^9 kg emissions agree closely to the normal steady-state determined ODPs. This confirms that ODP is a valid measure of the relative, cumulative effect on stratospheric ozone for each mass unit emitted into the atmosphere.

It is also important to recognize the limitations in the ODP concept as defined above. As an example, ODP is defined in terms of the steady-state ozone change; it is, therefore, not representative of the relative transient effects expected for shorter-lived compounds during the early years of emission. During these early years, shorter-lived compounds may have changes in ozone much closer to the changes in ozone determined for longer-lived gases, such as CFC-11, than would be expected based on their relative ODP values.

Figure 4.3-2 shows the tropospheric concentration of two compounds following the onset of a constant emission level of each. One of the compounds has a 100-year lifetime (comparable to lifetimes of CFCs) and the other compound has a 5-year lifetime (comparable to lifetimes of hydrohalocarbons). We see that the ratio of the relative atmosphere concentration ratio does not approach steady-state until after about

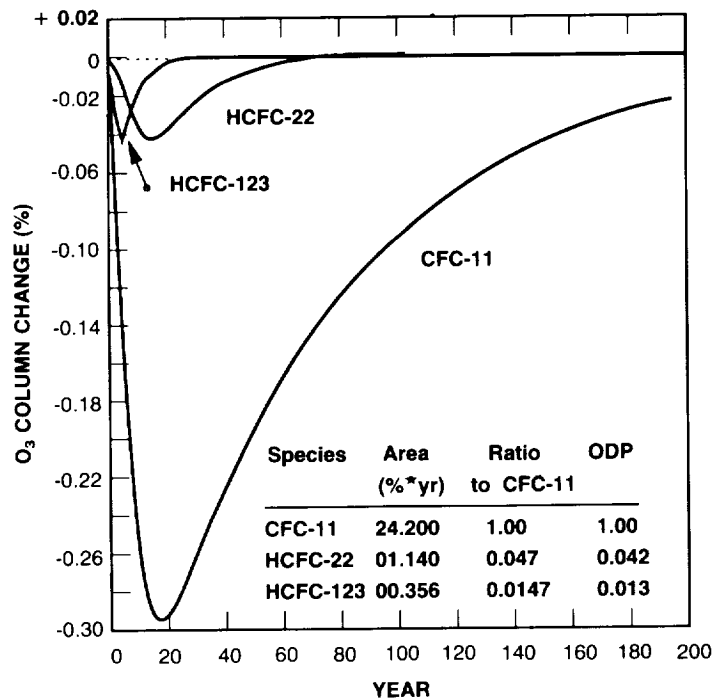


Figure 4.3-1. Calculated column ozone change in the DuPont 1-D model following a pulsed input (for one year) of 5.0×10^9 kg (Fisher et al., 1989 b) of specified gas.

OZONE DEPLETION POTENTIALS

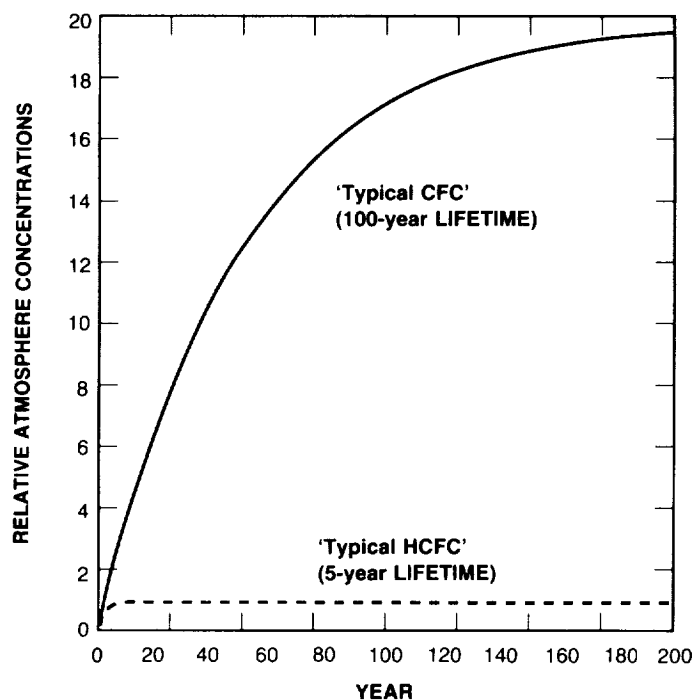


Figure 4.3-2. Atmospheric concentrations of halocarbons with 5- and 100-year lifetimes following onset of a constant emission of each compound.

400 years. Since the ODPs are based on steady-state relative effects which are (nearly) proportional to CFC concentrations, the calculated relative effects for short-lived compounds during the approach to steady-state can be larger than indicated by the ODP value. This is simply because the effect from the short-lived species has reached its full strength, whereas the effect from the long-lived species is still short of its steady-state value.

Other uncertainties and limitations associated with the concept of and determination of Ozone Depletion Potentials will be discussed later. Included is further evaluation of time-dependent relative ozone depletion.

In order to make the ODP definition consistent among models and at the same time have a conservative estimate of relative effects, the following criteria were selected for the model calculations included:

1. Depletion level—the calculations are based on emission rates of each compound required to give a modeled ozone depletion of approximately 1%. This value of depletion was selected in order to yield results large enough to avoid the noise level inherent with numerical models, yet small enough to remain in the linear perturbation region.
2. Trace gas levels—changing concentrations of other trace gases affect calculated tropospheric OH levels (Sze [1977] and Chameides et al. [1977]) and future depletions. However, we chose to base the calculations on current levels of CO₂, CH₄, CO, and N₂O due to the uncertainties in

future concentrations. The constant concentration assumption was chosen for clarity and simplicity.

3. Chlorine levels—since the long-lived CFCs are present in today's atmosphere and will affect chlorine chemistry over the time scales that hydrohalocarbons might be used, background halocarbon concentrations were assumed constant at current levels (yielding an asymptotic chlorine concentration of ~3 ppbv, with the exception of U. Oslo, who used 5.2 ppbv).
4. Bromine chemistry—current levels of bromine compounds were included in the model chemistry where appropriate.

Using the above provisions, the ODP for species x was then calculated as:

$$\text{ODP}(x) = \delta\text{O}_3(x) / \delta\text{O}_3(\text{CFC-11})$$

where $\delta\text{O}_3(x)$ is the change in total ozone at steady-state per unit mass emission rate. CFC-11 is used as the reference gas.

4.3.3 Model-Calculated ODPs

Each compound considered enters the atmosphere at ground level and, in general, is removed by a combination of chemical processes: reaction with hydroxyl (OH) in the troposphere and the stratosphere, reaction with excited-state oxygen in the stratosphere, and photolytic breakdown by ultraviolet light in the stratosphere. Laboratory measurements indicate that CFCs (e.g., CFC-11, -12, -113, -114, and -115) are primarily destroyed by ultraviolet light in the stratosphere and, to a lesser degree, by reaction with excited atomic oxygen; reaction with hydroxyl radical for these gases is unimportant. Hydrohalocarbons are removed by all three processes, but the predominant mechanism is reaction with OH in the troposphere. The reaction of the hydrohalocarbons with hydroxyl radicals leads to appreciably shorter atmospheric lifetimes compared to the CFCs.

Reaction rate constants and photolysis cross sections required as model input were obtained consistently from a number of sources for most of the calculations presented here. Whenever possible, recommendations from the most recent evaluation by the NASA panel (DeMore et al., 1987) were used. Rate data for several key reactions have been reevaluated by Hampson et al. (1989), and Molina (1989); these were used when available. Some reaction rate parameters were obtained from the open literature (Davidson et al. [1978], Hubrich and Stuhl [1980]), while some data were only available from unpublished sources (Magid, private communication, 1988). Finally, for some HFCs, no photolysis measurements could be found; since photolysis is of little importance for these species, neglecting this destruction mechanism has little impact on the derived lifetimes. Table 4.3-1 lists references and, when possible, the assumed reaction rates for destruction of each CFC, HCFC, and HFC. Several halons (namely, halon -1301, -1211, -1202, and -2402) are also considered in this report. The photolysis data needed for the halon species are based primarily on Molina et al. (1982). All models utilize their "best" representations for transport and radiation processes.

Both one- and two-dimensional models have been used for these evaluations. One-dimensional models calculate the global-averaged altitudinal variation of the relevant atmospheric chemical processes. These models all share the advantage that they are easy to operate and evaluate. Two-dimensional (2-D) models allow examination of calculated effects over the full range of latitudes and seasons. As such, their added complexity is offset by better representation of nonlinear characteristics of global stratospheric transport

OZONE DEPLETION POTENTIALS

Table 4.3-1. Chemical rate data used in ODP calculations

Species	Photolysis Ref.	OH Reactions			O('D) Reactions		
		Reaction Rate ^a		Ref.	Reaction Rate ^b	Branching Ratio ^c	Ref.
A	E/R						
CFC-11	a	—	—	—	2.3(-10)	0.75	a
CFC-12	a	—	—	—	1.4(-10)	0.86	a
CFC-113	b	—	—	—	2.0(-10)	0.80	c
CFC-114	b	—	—	—	1.6(-10)	0.80	c
CFC-115	b	—	—	—	8.9(-11)	0.80	c
HCFC-22	a	1.2(-12)	1650	f	1.0(-10)	1.0	f
HCFC-123	d	6.4(-13)	850	f	2.3(-10)	1.0	f
HCFC-124	d	6.6(-13)	1250	f	1.0(-10)	1.0	f
HFC-125	—	3.8(-13)	1500	f	0.5(-10)	1.0	f
HFC-134a	e	1.7(-12)	1750	f	0.5(-10)	1.0	f
HCFC-141b	d	2.7(-13)	1050	f	1.5(-10)	1.0	f
HCFC-142b	d	9.6(-13)	1650	f	1.4(-10)	1.0	f
HFC-143a	—	2.6(-13)	1500	f	0.6(-10)	1.0	f
HFC-152a	e	1.5(-12)	1100	f	1.0(-10)	1.0	f
CCl ₄	a	—	—	—	3.3(-10)	0.86	a
CH ₃ CCl ₃	a	5.0(-12)	1800	a	3.18(-10)	0.80	c

^aReaction rate constant of form: $k = A \exp[-E/(RT)]$, where A and k have the units of $\text{cm}^3/(\text{molecule sec})$.

^bReaction rate constant with units $\text{cm}^3/(\text{molecule sec})$.

^cFraction of O('D) disappearances proceeding through reaction channel, remainder pass through quenching channel to O(³P) and no reaction with the halocarbon.

Reference Key:

- a DeMore et al. (1987)
- b Hubrich and Stuhl (1980)
- c Davidson et al. (1978)
- d Molina (1989)
- e Magid (private communication, 1988)
- f Hampson, Kurylo, and Sander (1989)

and radiative processes. Ozone changes calculated by 2-D models are averaged with respect to both latitude and seasons before calculation of ODPs.

The calculated atmospheric lifetime of each gas species provides a key comparison of modeled results. Table 4.3-2 shows a comparison of lifetime values (of the CFCs, HCFCs, and HFCs) calculated by the models. In general, the calculated lifetimes for CFC-11 and CFC-12 are consistent with the lifetimes determined from the ALE-GAGE observations (Cunnold et al., 1986; Watson et al., 1988). However, the CFC-11 lifetimes from the 2-D models are on the low side of the uncertainty range, while 1-D results for the CFC-12 lifetime tend to be on the high side. The calculated HCFC and HFC lifetimes from all of the models are within the uncertainty range of those reported in section 4.2 as determined by Prather (1989) and Derwent and Volz-Thomas (1989) in the AFEAS Report (see Vol. II, Appendix).

The Ozone Depletion Potentials calculated by eight models (from five research groups) for each of these species is given in Table 4.3-3. For each of the hydrogen-containing compounds, the calculated ODPs have been scaled by the ratio of the inferred lifetime for methyl chloroform (~6.3 years; see section 4.2) to the lifetime derived by each model. This scaling is an attempt to indirectly account for the different global tropospheric amounts of OH between models. The reaction with OH is a primary sink for the

OZONE DEPLETION POTENTIALS

Table 4.3-2. Atmospheric lifetimes (in years) calculated with one-dimensional and two-dimensional models^a

Species	Chemical Formula	1-D Model Results				2-D Model Results			
		LLNL	AER	DuPont	BISA	Oslo	LLNL	AER	DuPont
CFC-11	CFCl ₃	80.0	60.0	71.0	85	60.0	52.0	47.0	46.0
CFC-12	CF ₂ Cl ₂	154.0	125.0	154.0	166	105.0	101.0	95.0	118.0
CFC-113	CFCl ₂ CF ₂ Cl	96.0	96.0	117.0	113	101.0	79.0	—	—
CFC-114	CF ₂ ClCF ₂ Cl	209.0	260.0	319.0	—	236.0	197.0	—	—
CFC-115	CF ₂ ClCF ₃	680.0	690.0	548.0	—	522.0	393.0	399.0	—
HCFC-22	CHClF ₂	20.0	20.0	16.0	—	17.2	15.0	24.0	12.7
HCFC-123	CF ₃ CHCl ₂	1.9	2.1	1.6	—	1.7	1.5	2.4	1.2
HCFC-124	CF ₃ CHClF	8.4	8.8	6.9	—	7.4	6.4	10.0	5.3
HFC-125	CF ₃ CHF ₂	37.0	37.0	25.0	—	—	27.0	43.0	19.0
HFC-134a	CF ₃ CH ₂ F	21.0	21.0	16.0	—	—	15.0	24.0	12.5
HCFC-141b	CCl ₂ FCH ₃	8.9	9.4	7.8	—	8.0	6.9	11.0	5.8
HCFC-142b	CClF ₂ CH ₃	25.0	25.0	19.0	—	20.9	19.0	28.0	18.1
HFC-143a	CF ₃ CH ₃	54.0	52.0	42.0	—	—	40.0	—	—
HFC-152a	CHF ₂ CH ₃	2.1	2.3	1.7	—	—	1.5	2.7	1.3
Carbon Tetrachloride	CCl ₄	73.0	53.0	61.0	64	52.2	47.0	40.0	40.0
Methyl Chloroform	CH ₃ CCl ₃	7.4	7.4	6.0	—	6.3	5.8	7.8	4.7

^aThe results of the LLNL, AER, DuPont, and Oslo groups have been published by Fisher et al. (1989a, b).

Table 4.3-3. Ozone Depletion Potentials (ODP) calculated with one-dimensional and two-dimensional models, assuming scaling for HCFC ODPs by methyl chloroform inferred lifetime^a

Species	Chemical Formula	1-D Model Results				2-D Model Results			
		LLNL	AER	DuPont	BISA	Oslo	LLNL	AER	DuPont
CFC-11	CFCl ₃	1.0	1.0	1.0	1.0	1.0	1.0	1.0	1.0
CFC-12	CF ₂ Cl ₂	1.0	0.9	1.0	0.9	0.9	0.9	0.9	0.9
CFC-113	CFCl ₂ CF ₂ Cl	0.8	0.8	0.9	0.9	0.9	0.8	—	—
CFC-114	CF ₂ ClCF ₂ Cl	0.8	0.6	0.8	0.8	0.6	0.6	—	—
CFC-115	CF ₂ ClCF ₃	0.4	0.4	0.5	0.4	0.4	0.3	0.4	—
HCFC-22	CHClF ₂	0.05	0.05	0.04	0.05	0.04	0.05	0.06	0.04
HCFC-123	CF ₃ CHCl ₂	0.13	0.16	0.13	0.01 ^b	0.013	0.017	0.022	0.017
HCFC-124	CF ₃ CHClF	0.016	0.018	0.017	—	0.018	0.019	0.024	0.017
HFC-125	CF ₃ CHF ₂	0.0	0.0	0.0	0.0	0.0	0.0	0.0	0.0
HFC-134a	CF ₃ CH ₂ F	0.0	0.0	0.0	0.0	0.0	0.0	0.0	0.0
HCFC-141b	CCl ₂ FCH ₃	0.07	0.08	0.07	0.1 ^b	0.09	0.09	0.11	0.09
HCFC-142b	CClF ₂ CH ₃	0.05	0.05	0.05	0.06 ^b	0.06	0.05	0.06	0.05
HFC-143a	CF ₃ CH ₃	0.0	0.0	0.0	0.0	0.0	0.0	0.0	0.0
HFC-152a	CHF ₂ CH ₃	0.0	0.0	0.0	0.0	0.0	0.0	0.0	0.0
Carbon Tetrachloride	CCl ₄	1.1	1.2	1.1	1.0	1.2	1.1	1.0	1.2
Methyl Chloroform	CHCl ₃	0.10	0.12	0.10	—	0.14	0.13	0.16	0.15

^aScaling assumes CH₃CCl₃ lifetime of 6.3 years, based on discussion in Section 4.2.

^bBased on Gillotay et al. (1989).

OZONE DEPLETION POTENTIALS

hydrogen-containing species; differences in calculated tropospheric OH concentrations account for much of the model differences in chemical lifetimes for these gases. Therefore, amounts of OH account for much of the variation in ODPs derived between models. However, as noted by Fisher et al. (1989a, b), using globally averaged OH deduced from CH₃CCl₃ to calculate lifetimes for other HCFCs may not necessarily be accurate, particularly for those HCFCs with lifetimes substantially different from methyl chloroform.

As seen in Table 4.3-3, the ODPs for each hydrogen-containing species, including the suggested replacement compounds, are much smaller than those for the CFCs. This difference largely reflects the reactivity of these species with OH, resulting in shorter chemical lifetime for the HCFCs compared to the CFCs. Several compounds, such as HFC-134a and HCF-152a, have ODPs of zero because they do not contain chlorine.

In general, the ODPs derived using the different models compare extremely well with each other. However, significant differences between modeled ODPs still exist. The variation between models in the ODP for CH₃CCl₃, for example, is likely related to differences in the calculated distribution of OH with altitude and latitude between models. Although the two-dimensional models generally have a sounder physical basis for their formulation than existing one-dimensional models, there are no significant differences between the 1-D and 2-D model results.

Table 4.3-4 gives the ODPs determined by three groups (AER and LLNL 1-D models and U. Oslo 2-D model) for several brominated halocarbons. Although the ODPs for these compounds are shown relative to CFC-11 for historical reasons, the ODPs for bromine-containing compounds should in reality be compared relative to each other because of the strong dependence to background chlorine levels in determining bromine effects on ozone. Therefore, in Table 4.3-4, Bromine Ozone Depletion Potentials (BODPs) are used for relative comparisons with halon-1301, the compound with the longest lifetime and largest ODP, as the reference. The major ozone destruction due to the halons comes from coupled chlorine-bromine chemistry in the lower stratosphere. Because of interactions between chlorine and bromine chemistry, the traditional ODPs are critically dependent on chlorine levels in the background atmosphere. Also, because current models underestimate the ClO concentrations in the lower stratosphere at high latitudes in early spring, the traditional ODP definition (relative to CFC-11) may underestimate the true ozone depletion potential for these compounds.

Table 4.3-4. Ozone depletions (ODPs) for brominated compounds as calculated in the AER and LLNL 1-D models and the U. Oslo 2-D model

Common Name	Atmospheric Lifetime (yrs)			ODP ^a			BODP ^b		
	AER	LLNL	Oslo	AER	LLNL	Oslo	AER	LLNL	Oslo
halon-1301	81	107.0	72	16.0	13.2	7.8	1.0	1.0	1.0
halon-1211	12	15.0	18	3.5	2.2	3.0	0.22	0.17	0.38
halon-1202		1.5			0.3			0.02	
halon-2402		28.0	23		6.2	5.0		0.5	0.64

^aRelative to CFC-11, shown for historical purposes. Values will be underestimates if they account for effects at polar latitudes.

Assumed upper stratospheric Cl, mixing ratio is 3 ppbv in the LLNL and AER models and 4.5 ppbv in the Oslo model.

^bBromine Ozone Depletion Potentials (BODPs) defined relative to halon-1301, the longest brominated gas.

4.3.4 Uncertainties and Sensitivity Studies

The above globally averaged ODP values are derived from model calculations based on present-day atmospheric conditions using current representations of chemical and transport processes. Although the ODPs agree reasonably well among the models, many uncertainties still exist. Establishing a strict criterion for estimating the overall uncertainty in the calculated ODPs is not a straightforward task. There are still many uncertainties associated with the treatment of atmospheric chemical, radiative, and dynamical processes in current models. Perhaps the single largest uncertainty is that none of the models used for calculating ODPs includes the chemical and dynamical processes causing the seasonal ozone losses associated with the ozone hole over Antarctica. The possible impact of this uncertainty is discussed below.

Additional calculations have been carried out to test the sensitivity of the relative ODP effects to (1) levels of other trace gases, (2) seasonal and latitudinal dependencies and (3) assumed stratospheric transport processes. The relative time-dependent effects of different gases on total ozone is also examined.

4.3.4.1 Ozone Hole Effects

None of the ODP calculations consider the potential effect of heterogeneous chemistry in the lower stratosphere, particularly within the circulation vortex occurring at either pole during late winter and early springtime. Currently, inclusion of such effects in ODP calculations is premature since modeling of heterogeneous chemistry in general, and the polar phenomena in particular, are still in the early stages.

Because of the apparent special chlorine processing and dynamics within the winter polar vortex, local Antarctic ODPs are expected to be larger than those shown in Table 4.3-3. Insofar as the observed long-lived tracer distributions, such as those for CFC-11 in the polar vortex, suggest that much of the total chlorine may be available there, then an upper limit on Antarctic ODPs can be determined by calculating the relative amounts of chlorine transported through the tropopause by the different gases. It can be argued, within existing uncertainties, that active chlorine at all altitudes within the stratosphere, and perhaps into the mesosphere, may be available for affecting ozone within the polar vortex.

Values from four 2-D models (AER, LLNL, Oslo, DuPont) for the maximum relative chlorine loading into the stratosphere, termed Chlorine Loading Potentials (CLPs), are given in Table 4.3-5 based on the model calculated lifetimes. CLP, defined as the chlorine transported through the tropopause per mass emitted relative to CFC-11, is proportional to the relative number of chlorine atoms per molecule and the atmospheric lifetime and is inversely proportional to the molecular weight. A set of reference lifetimes, based on the estimates used in scenario development in Chapter 3, section 3.2.1 for the CFCs and from the analysis in Section 4.2 for the HCFCs and HFCs, is given in Table 4.3-6 along with the corresponding CLP values. These values are as much as a factor of two to three larger than the derived ODP values.

The reader may wonder why the values of the chlorine loading potential CLP are often larger than the ODPs for the same species. If all sources of stratospheric chlorine were equivalent in the photochemical reactivity sense once they reached the stratosphere, CLP values would be identical to the ODP values. Two major reasons account for the chlorine loading potential values being larger than the ODPs for many of the species. First, several of the CFCs and HCFCs, such as HCFC-22 and HCFC-142b, are incompletely dissociated within the stratosphere. Second, differences in the dissociation reactivity produce different chlorine distribution for the various gases.

OZONE DEPLETION POTENTIALS

Table 4.3-5. Chlorine Loading Potentials (CLPs) from 2-D models for CFCs, HCFCs, and HFCs, scaled by lifetime of CH₃CCl₃ (= 6.3 yr)

Species	Oslo CLP	LLNL CLP	AER CLP	DuPont CLP
CFC-11	1.0	1.0	1.0	1.0
CFC-12	1.3	1.5	1.5	1.9
CFC-113	1.2	1.1		
CFC-114	2.1	2.0		
CFC-115	2.6	2.2	2.5	
HCFC-22	0.15	0.17	0.22	0.20
HCFC-123	0.017	0.01	0.03	0.02
HCFC-124	0.04	0.04	0.06	0.05
HFC-125	0.0	0.0	0.0	0.0
HFC-134a	0.0	0.0	0.0	0.0
HCFC-141b	0.10	0.11	0.15	0.13
HCFC-142b	0.16	0.18	0.22	0.20
HFC-143a	0.0	0.0	0.0	0.0
HFC-152A	0.0	0.0	0.0	0.0
CCl ₄	1.0	1.1	1.0	1.0
CH ₃ CCl ₃	0.11	0.12	0.14	0.14

Table 4.3-6. Maximum relative Chlorine Loading Potential (CLP) for examined CFCs, HCFCs, HFCs, and other chlorinated halocarbons based on reference species lifetimes chosen to be compatible with available atmospheric measurements and modeling studies

Species	Reference ^a Lifetime (yrs)	Chlorine Loading Potentials ^b
CFC-11	60.0	1.0
CFC-12	120.0	1.5
CFC-113	90.0	1.11
CFC-114	200.0	1.8
CFC-115	400.0	2.0
HCFC-22	15.3	0.14
HCFC-123	1.6	0.016
HCFC-124	6.6	0.04
HFC-125	28.1	0.0
HFC-134a	15.5	0.0
HCFC-141b	7.8	0.10
HCFC-142b	19.1	0.14
HFC-143a	41.0	0.0
HFC-152a	1.7	0.0
CCl ₄	50.0	1.0
CH ₃ CCl ₃	6.3	0.11

^aLifetimes (e-folding time) are on estimates used in scenario development in Chapter 3, section 3.2.1 for the CFCs and from the analysis in Section 4.2 for the HCFCs and HFCs.

^bChlorine Loading Potential is defined as the maximum chlorine transported across the tropopause per mass emitted relative to the same for CFC-11; it is proportional to lifetime and the number of chlorine atoms per molecule, and is inversely proportional to molecular weight.

At this time, until model studies of heterogeneous chemistry and validation of transport parameterization have been completed, it is difficult to put definite limits on the uncertainties of the model-calculated ODP values. The answer to this question depends on the extent of the influence that polar springtime ozone destruction will have on global ozone, and on the extent of the downward transport within the Antarctic and Arctic polar vortex. The preliminary results reported in Fisher et al. (1989b) indicate that comparison of model-simulated trace gas distributions with available observation may be useful to limit the uncertainties. The CLP values (i.e., Table 4.3.6) provide an upper limit on ODP value within the Antarctic (and perhaps, the Arctic) region, while dilution effects, after breakup of the vortex, may extend higher ODP values to other latitudes. At this time, the ramifications of polar ozone depletion on the globally determined concept of ODPs are not clear.

4.3.4.2 Sensitivity of ODPs to Other Trace Gas Levels

ODP values have all been based on calculated ozone changes in a modeled atmosphere, assuming present-day levels of CFCs, CO₂, CH₄, CO, N₂O, Br_x, and other trace gases. Because it is important to quantify the effects of possible changes in the future trace gas concentrations on ODPs, we will present calculations of the sensitivity of the ODPs to trace gas concentrations that may occur within the next century if current concentration trends continue.

Trace gas concentrations were varied from current concentrations as shown in Table 4.3-7. These concentrations were changed both individually and as an ensemble in the sensitivity calculations. Calculated changes in ozone for tested CFCs and HCFCs are relative to an atmosphere including the assumed trace gas perturbation. Two models were used to determine the sensitivity of atmospheric lifetimes and ODPs to trace gas concentrations. Calculations with the AER 1-D model assumed a background stratospheric chlorine content of 3 ppbv. Calculations with the Oslo 2-D model used a background chlorine amount of 5.2 ppbv. Prior calculations with the Oslo model indicate little effect on the derived ODPs from the assumed chlorine background amount.

Table 4.3-8 shows the calculated changes in atmospheric lifetimes of CFC-11, CFC-12, HCFC-22, and HCFC-123 for the various sensitivity calculations. The largest effects are evident for the HCFCs in the cases where CH₄ and CO concentrations are perturbed. Both CH₄ and CO strongly influence tropospheric HO_x chemistry; therefore the concentration of OH, and consequently the primary destruction of the HCFCs, is affected, resulting in the determined impact on atmospheric lifetimes. The relatively minor changes in lifetime of the CFCs are primarily a result of increased photolysis rates for the trace gas perturbed atmospheres.

Table 4.3-7. Change in ground level trace gas concentrations assumed in sensitivity studies

Trace Gas	Background Atmosphere	Perturbed Atmosphere
CO ₂	340.0 ppmv	680.0 ppmv
CH ₄	1.6 ppmv	3.2 ppmv
CO	100.0 ppbv	200.0 ppbv
N ₂ O	300.0 ppbv	360.0 ppbv
Br _x	20.0 pptv	40.0 pptv

OZONE DEPLETION POTENTIALS

Table 4.3-8. Sensitivity of calculated lifetimes to changes in trace gas values (based on AER 1-D results)

	Lifetimes (years)			
	CFC-11	CFC-12	HCFC-22	HCFC-123
Present-day atmosphere	60	125	20	2.1
CO ₂ (350 → 680 ppmv)	61	128	20	2.1
CH ₄ (1.6 → 3.2 ppmv)	60	126	23	2.5
CO (100 → 200 ppbv)	60	125	25	2.7
N ₂ O (300 → 360 ppbv)	59	123	20	2.1
CH ₃ Br (20 → 40 pptv)	59	125	20	2.1
All changes combined	60	127	26	2.9

Table 4.3-9 presents ODPs resulting from these calculations. For both the AER 1-D model and the Oslo 2-D model, the largest sensitivity in the ODP for CFC-12 occurs for the assumed concentration change in N₂O. As expected, ODPs for the HCFCs are affected most by change in CH₄ and CO levels.

The calculated sensitivities to background trace gas concentrations can be explained as follows. First, changes in atmospheric lifetimes will affect the ODP in that, as the lifetime increases/decreases, more/less of the CFC or HCFC is accumulated in the atmosphere at steady state for the same mass emitted. Secondly, the response of ozone to increases in chlorine can be different in the future atmosphere. However, this change in response will only affect the ODP estimates if the response of the individual CFCs or HCFCs is different from that of CFC-11. An example of this involves the increased N₂O case: although the absolute changes in ozone for each of the CFCs and HCFCs were determined to be less than half of the ozone changes determined for the present atmosphere calculations, sensitivity of the derived ODPs is much

Table 4.3-9. Sensitivity of ozone potentials to changes in trace gas values

1. AER 1-D Model				
	CFC-12	HCFC-22	HCFC-123	
Present-day atmosphere	0.92	0.057	0.019	
CO ₂ (340 → 680 ppmv)	0.93	0.051	0.018	
CH ₄ (1.6 → 3.2 ppmv)	0.93	0.069	0.023	
CO (100 → 200 ppbv)	0.93	0.070	0.024	
N ₂ O (300 → 360 ppbv)	1.01	0.071	0.019	
CH ₃ Br (20 → 40 pptv)	0.92	0.055	0.019	
All changes combined	0.95	0.076	0.026	
2. Oslo 2-D Model (all calculations with 5.2 ppbv Cl _y)				
	CFC-12	HCFC-22	HCFC-123	HCFC-124
Present-day atmosphere	0.92	0.046	0.013	0.018
CO ₂ (340 → 600 ppmv)	0.94	0.049	0.016	
CH ₄ (1.6 → 3.2 ppmv)	0.93	0.058	0.016	
N ₂ O (300 → 360 ppbv)	0.97	0.042	0.015	
Br _y (18 → 33 pptv)	0.91	0.051	0.016	0.020
All changes combined	0.96	0.062	0.018	

smaller. The increase in NO_y will moderate the impact of increased chlorine by tying up a larger portion of the chlorine in the form of chlorine nitrate, ClNO_3 . This effect is most noticeable in the lower stratosphere where ClNO_3 is more stable. The compensating effect should be more efficient for CFC-11 where more of the odd chlorine is found in the lower stratosphere. This accounts for the high ODP of CFC-22 in the increased N_2O case in the AER model; the Oslo 2-D model does not show this effect.

In conclusion, both lifetimes and derived ODPs are moderately sensitive to significant changes in background trace gas concentrations. However, for the scenarios examined, the range in sensitivity of the ODPs is well within the overall uncertainty range for model-determined ODP values. Possible systematic errors, perhaps due to missing chemistry or other processes, may provide a much more significant impact on the derived ODP values.

4.3.4.3 Variation in ODPs with Latitude and Season

Another manifestation of the effect of differences between species on the chlorine distribution is the variations of the ODP values as a function of latitude and season. Several of the compounds show strong variations in their ODPs as a function of latitude and season.

Figure 4.3-3, based on calculations with the LLNL two-dimensional model (Connell and Wuebbles, 1989; Fisher et al., 1989b), shows the calculated change in total ozone as a function of latitude and season for CFC-11. A constant emission rate of CFC-11 was assumed sufficient to give a steady-state global

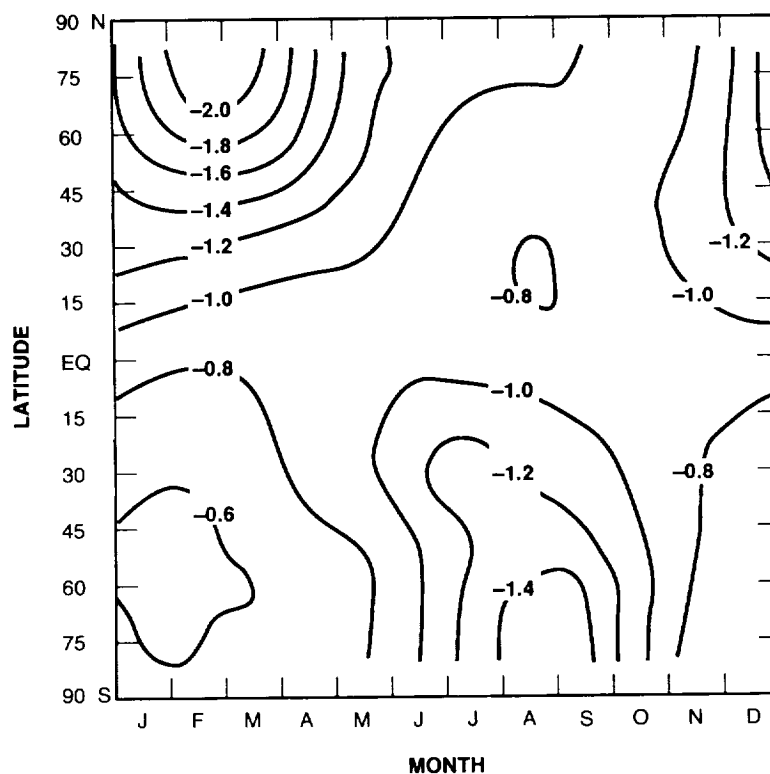


Figure 4.3-3. Calculated latitudinal and seasonal steady-state ozone change from emission of CFC-11 necessary for global 1% change in total ozone (LLNL 2-D model).

OZONE DEPLETION POTENTIALS

decrease in total ozone of about one percent. As expected from previous 2-D analyses of CFC effects on ozone (e.g., WMO, 1985), the largest changes in ozone occur at the poles in late winter to early spring. Once the calculated changes are compared relative to CFC-11 and adjusted for differences in assumed emission rates, the resulting values indicate a generally variable dependency on latitude and generally weaker seasonal variations. In particular, the ODPs for CFC-12, HCFC-22, HCFC-124, and HCFC-142b have strong latitudinal variations, with the ODP increasing from lower tropical values to higher polar values by as much as a factor of three. The changes in total ozone at steady state from the LLNL model, and the derived ODPs from the LLNL, AER, Oslo, and DuPont 2-D models, for CFC-12 and HCFC-22 are shown in Figures 4.3-4 and 4.3-5, respectively. There are significant variations (more than a factor of two) with latitude and season in the ODPs derived for these two compounds. In both cases, the ODPs are smallest in the tropics and largest at the poles in late summer. The results from the models are in good general agreement regarding this pattern, although the LLNL model shows slightly more seasonal response for some species than the other models, particularly at high latitudes in the Southern Hemisphere. Other species, such as HCFC-123, HCFC-141b, and CH_3CCl_3 show little variation with latitude or season (see Fisher et al. (1989b) and Connell and Wuebbles (1989) for figures and further discussion).

The strong latitudinal ODP variation of some species (in contrast to the weak variation determined for others) warrants further discussion. The distinguishing difference between the species categories is based on the difference in the distribution of chlorine atoms which, in turn, depends on the altitudes for destruction of the respective species. Compounds that do not survive transport to the upper stratosphere for dissociation, and are therefore similar to CFC-11, show very little variation in their ODP with latitude

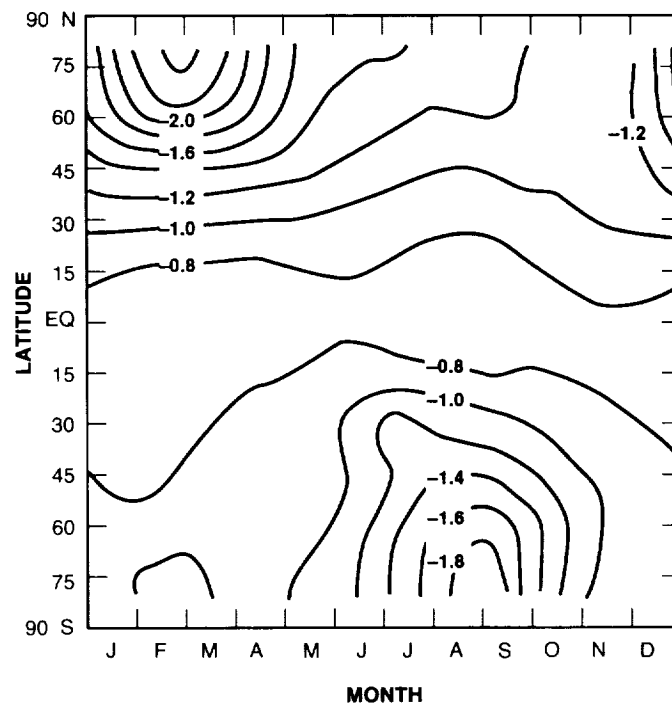


Figure 4.3-4a. Calculated latitudinal and seasonal steady-state ozone change from emission of CFC-12 necessary to give 1% change in total ozone (LLNL 2-D model).

OZONE DEPLETION POTENTIALS

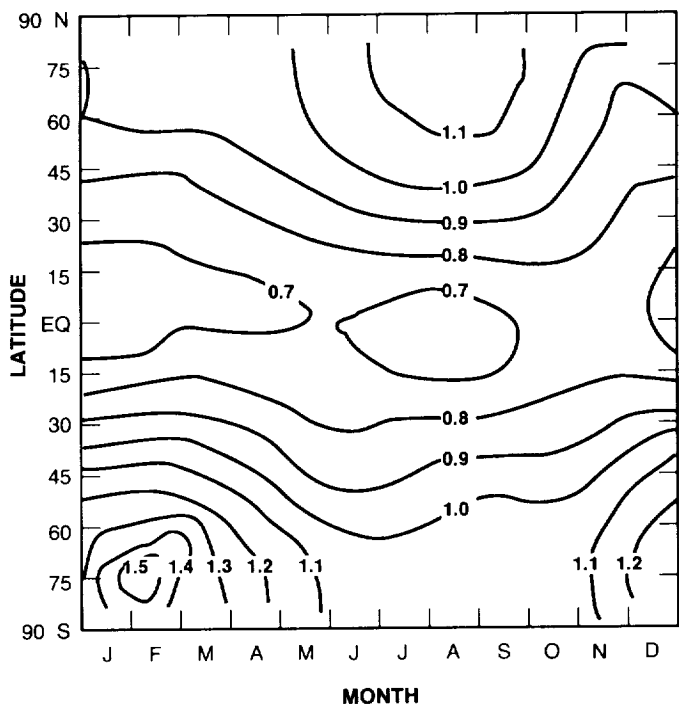


Figure 4.3-4b. Calculated latitudinal and seasonal relative ozone depletion of CFC-12 (LLNL 2-D model).

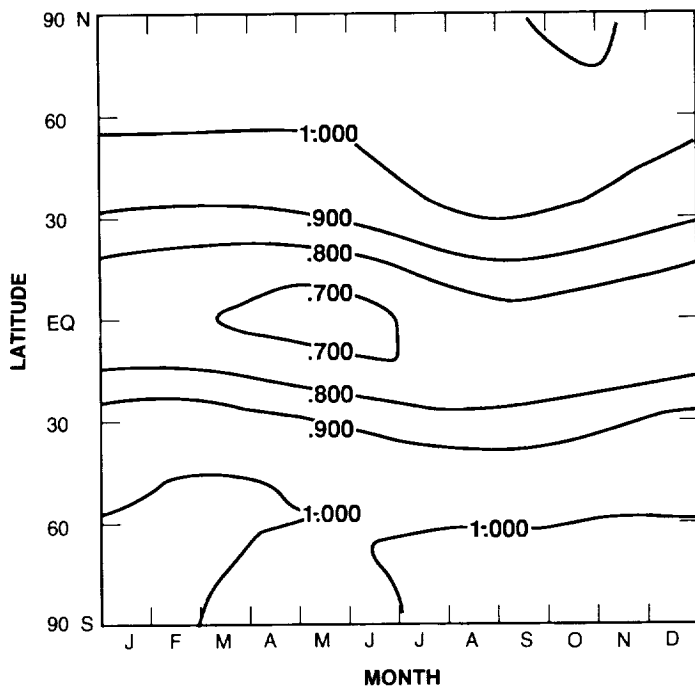


Figure 4.3-4c. Calculated latitudinal and seasonal relative ozone depletion of CFC-12 (AER 2-D model).

OZONE DEPLETION POTENTIALS

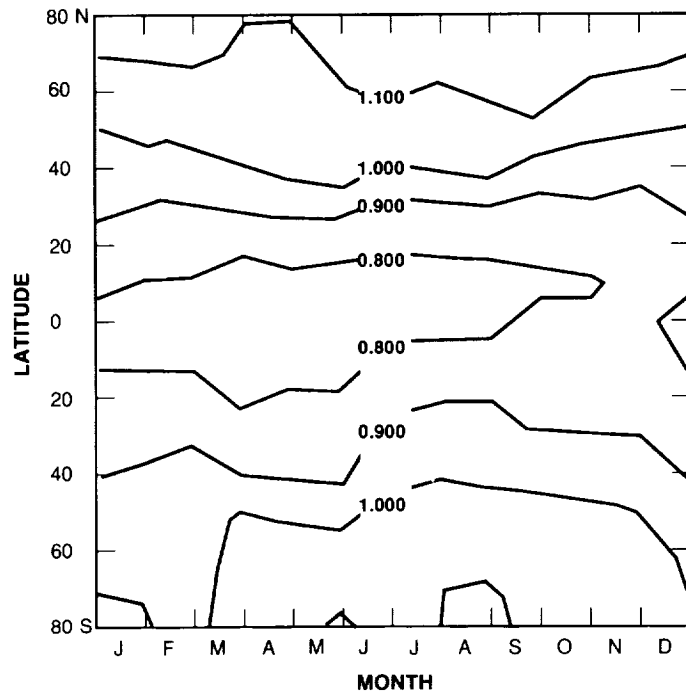


Figure 4.3-4d. Calculated latitudinal and seasonal relative ozone depletion of CFC-12 (Oslo 2-D model).

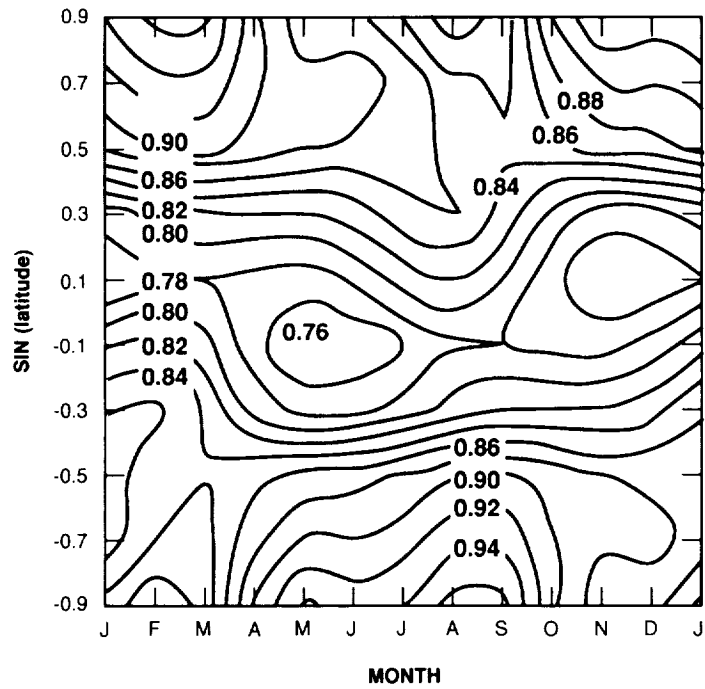


Figure 4.3-4e. Calculated latitudinal and seasonal relative ozone depletion of CFC-12 (DuPont 2-D model).

OZONE DEPLETION POTENTIALS

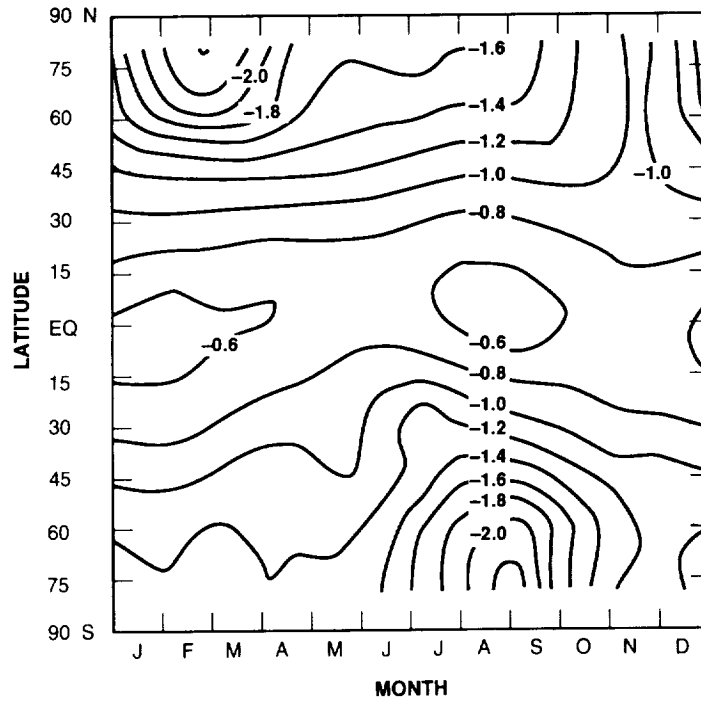


Figure 4.3-5a. Calculated latitudinal and seasonal steady-state ozone change necessary to give 1% change in total ozone from emission of HCFC-22 (LLNL 2-D model).

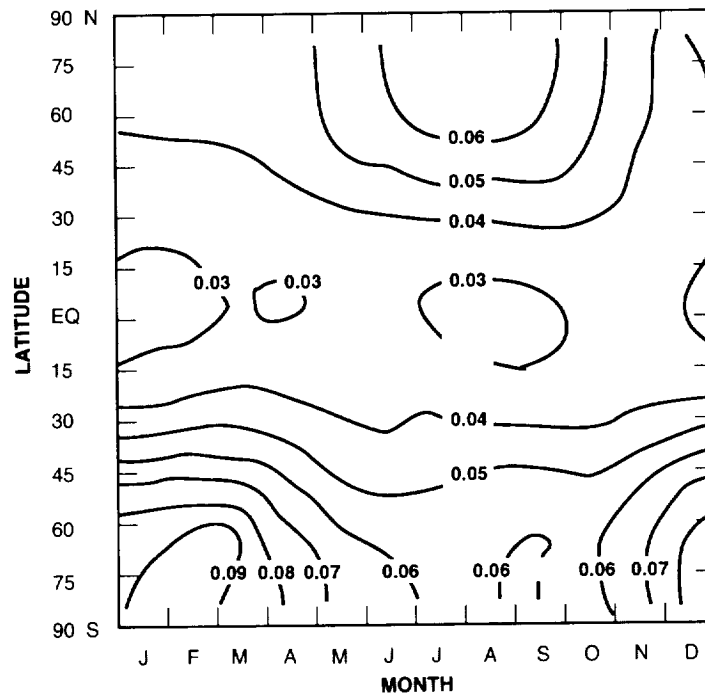


Figure 4.3-5b. Calculated latitudinal and seasonal relative ozone depletion of CFC-22 (LLNL 2-D model).

OZONE DEPLETION POTENTIALS

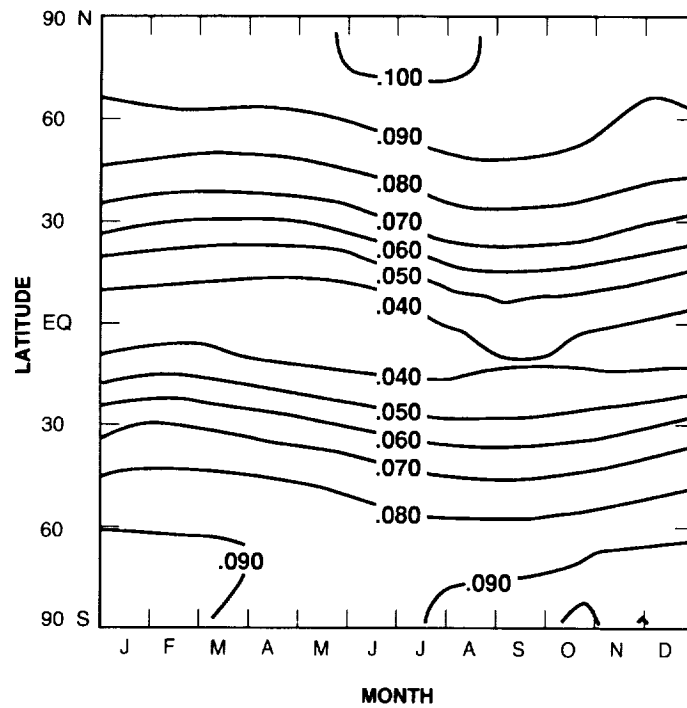


Figure 4.3-5c. Calculated latitudinal and seasonal relative ozone depletion from emission of HCFC-22 (AER 2-D model).

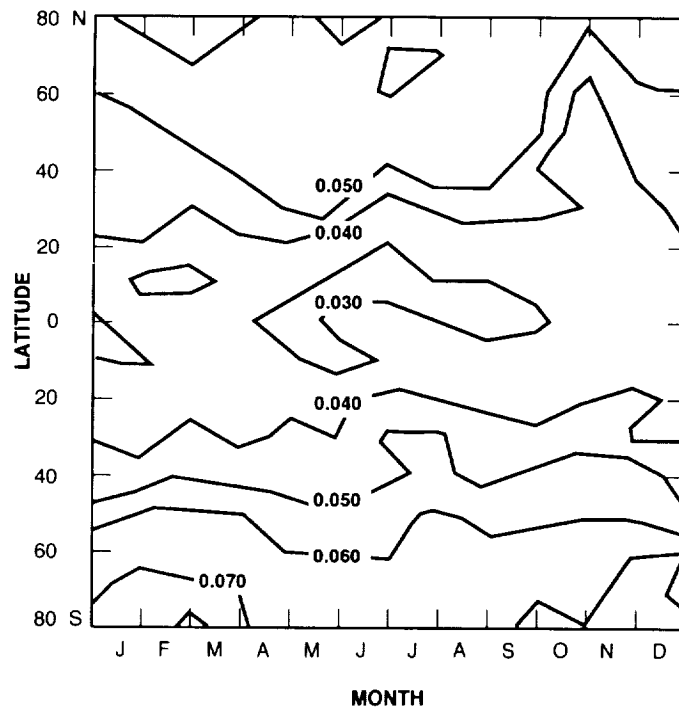


Figure 4.3-5d. Calculated latitudinal and seasonal relative ozone depletion from emission of HCFC-22 (Oslo 2-D model).

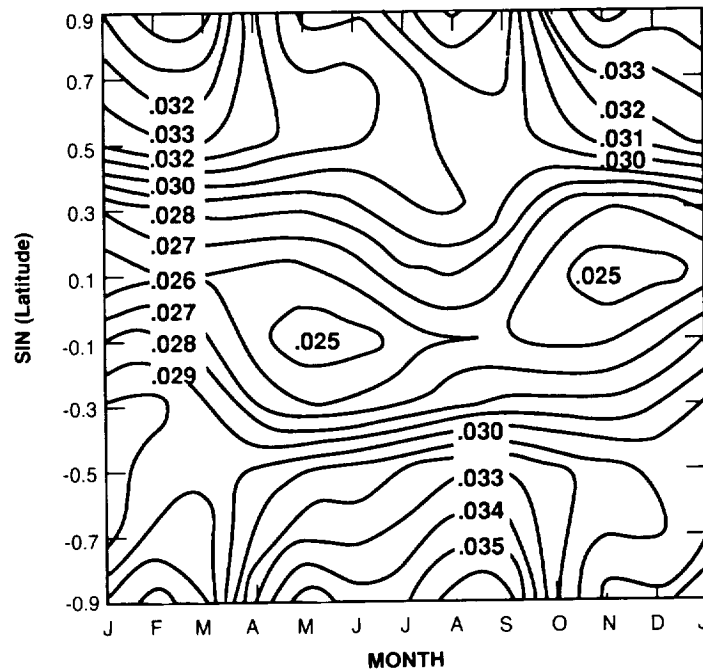


Figure 4.3-5e. Calculated latitudinal and seasonal relative ozone depletion from emission of HCFC-22 (DuPont 2-D model).

and season. HCFC-123 is an example of such a species. On the other hand, species that persist into the upper stratosphere (even if the dominant removal is at lower altitudes) show strong latitudinal dependencies. CFC-12 and HCFC-22 are two examples that show a significant latitudinal dependency. CFC-12 is primarily dissociated at higher altitudes than CFC-11. HCFC-22, on the other hand, is primarily destroyed in the troposphere and lower stratosphere by reaction with OH radical, yet models and observations indicate that a significant fraction survives transport to the upper stratosphere.

The resulting strong variations of ODPs with latitude occur in response to latitudinal differences in upper stratospheric chemistry on ozone destruction and the resultant effects of transport on both the ClO_x produced and on the ozone being destroyed. The extent of these variations depends on the treatment and the strength of the modeled transport. It is not surprising, therefore, to find some differences in the ODP variations with latitude and season between models. The effects of heterogeneous chemistry and polar dynamical effects, not included in the calculations here, would lead to some modifications of these findings but should not qualitatively change the response.

4.3.4.4 Sensitivity of ODP to Modeled Transport

The question can next be raised as to the sensitivity of ODP values to model parameters—primarily transport processes. The treatment of transport processes is a source of significant uncertainty in 2-D models. Changing the model transport parameters would affect the ODP directly in three ways. First, the ODP values can change because of changes in lifetimes. The lifetime for CFC-11 is sensitive to the strength of the circulation in the stratosphere while the lifetime of HCFC-22, which is dominated by removal in the

OZONE DEPLETION POTENTIALS

troposphere, is less sensitive. Second, changing transport parameters would affect the distribution of chlorine atoms in the stratosphere. The responses of each species differ according to where the chlorine atoms are released. Finally, change in transport can also affect the response of ozone to chemical perturbations.

Four sets of calculations were performed using different circulations and K_{yy} (latitudinal eddy diffusivity) values to examine the sensitivity to variations in transport within the AER 2-D model. Calculated effects of CFC-11 and HCFC-22 emissions were determined in each case. These cases are designated by:

Case 1	standard	standard ($3 \times 10^9 \text{ cm}^2 \text{ s}^{-1}$)
Case 2	standard	small ($1 \times 10^8 \text{ cm}^2 \text{ s}^{-1}$)
Case 3	weak	standard ($3 \times 10^9 \text{ cm}^2 \text{ s}^{-1}$)
Case 4	weak	small ($1 \times 10^8 \text{ cm}^2 \text{ s}^{-1}$)

The weak circulation for cases 3 and 4 is chosen to test the response of ODP for HCFC-22 if a larger portion of the HCFC-22 is dissociated in the upper stratosphere. The circulation is adjusted so that the HCFC-22 molecules spend more time in the upper stratosphere, resulting in 90% dissociation of the molecules. Adopting smaller K_{yy} values for cases 2 and 4 represents an attempt to obtain lower concentrations for species such as N_2O , CFC-11, and CFC-12 in the polar lower stratosphere more in line with the observations obtained in the polar vortices during the Antarctic Airborne Ozone Experiment (AAOE) campaign. For simplicity, the smaller value was adopted globally and year round. Clearly, if the smaller values are restricted to the high latitudes and limited to certain seasons, the response could be somewhat different.

Figure 4.3-6 shows calculated profiles of CFC-11 from the four cases for August at 75°S compared to the AAOE measurements. The profiles at equinox for the Equator are shown in Figure 4.3-7. The cases with small K_{yy} predict CFC-11 profiles that are in better agreement with observations at polar latitudes. At the same time, the concentration at the Equator calculated under case 2 is large compared to case 1. Corresponding graphs for HCFC-22 are shown in Figures 4.3-8. Figure 4.3-9 shows the calculated column abundances of O_3 for the four cases. The results from cases 2 and 4 are distinctly different from observations with high columns predicted at high latitudes. Table 4.3-10 summarizes the calculated lifetimes and ODP values from the four cases. The calculated lifetime of CFC-11 is sensitive to the transport field, whereas the lifetime of HCFC-22 is less dependent. The ODP values for HCFC-22 for these cases reflect the impact of transport on the CFC-11 destruction process. Figure 4.3-10a shows that while there is an increase in ODP values at high latitudes for case 2 relative to case 1 (Figure 4.3-5c), the decrease at the tropics more than compensates for it in the global ODP value. Corresponding results for cases 3 and 4 are shown in Figures 4.3-10b and 4.3-10c.

In summary, the analysis presented here represents an attempt to quantify the sensitivity of the calculated ODP to model parameterization of transport. It is difficult to draw a definitive conclusion based on these limited number of simulations. The attempts to increase the ODP at high latitudes by using smaller K_{yy} lead to much smaller ODPs at the tropics because of decreased eddy transport. It is possible that there may be other combinations of circulation and K_{yy} that would change the ODP results significantly. These results did show that the same change in circulation would also have significant effects on the model-simulated ozone and other trace gas profiles. Comparison of these simulated results with available observations would provide a way to validate the ODP values.

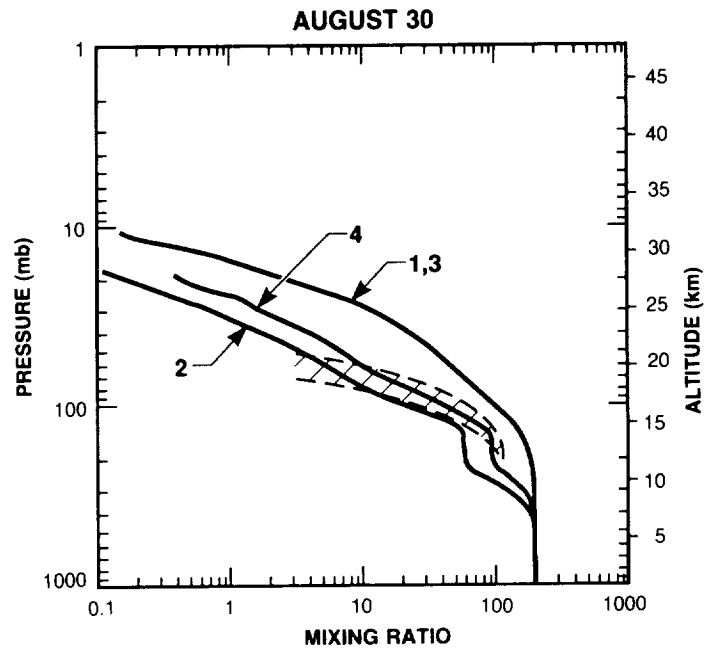


Figure 4.3-6. Calculated CFC-11 profiles from transport sensitivity study at 75° south at equinox (AER 2-D model). AAOE measurements indicated by cross hatch area.

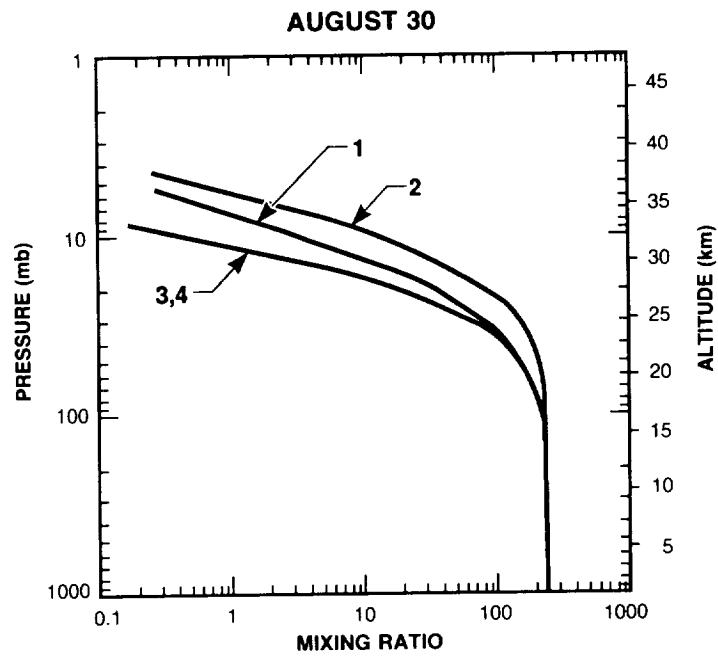


Figure 4.3-7. Calculated CFC-11 profiles from transport sensitivity study at Equator at equinox (AER 2-D model).

OZONE DEPLETION POTENTIALS

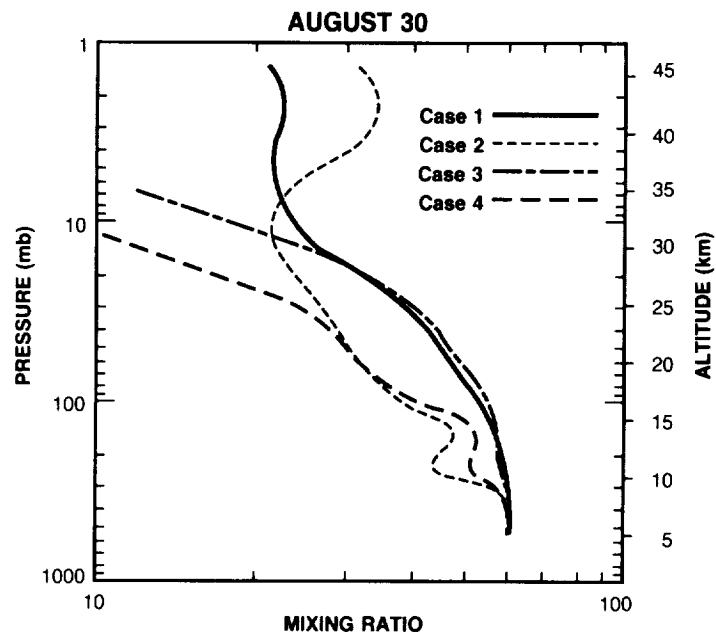


Figure 4.3-8a. Calculated HCFC-22 profiles from transport sensitivity study at 75° south equinox (AER 2-D model).

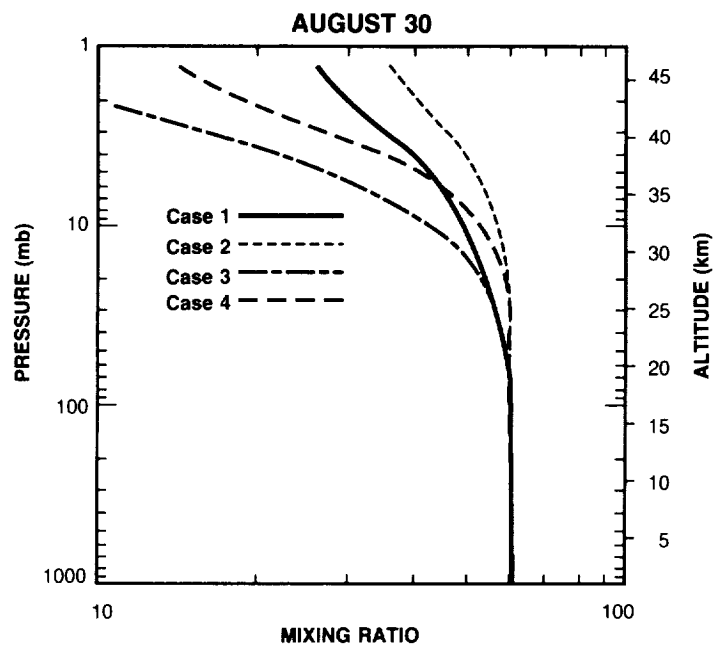


Figure 4.3-8b. Calculated HCFC-22 profiles from transport sensitivity study at the Equator at equinox (AER 2-D model).

OZONE DEPLETION POTENTIALS

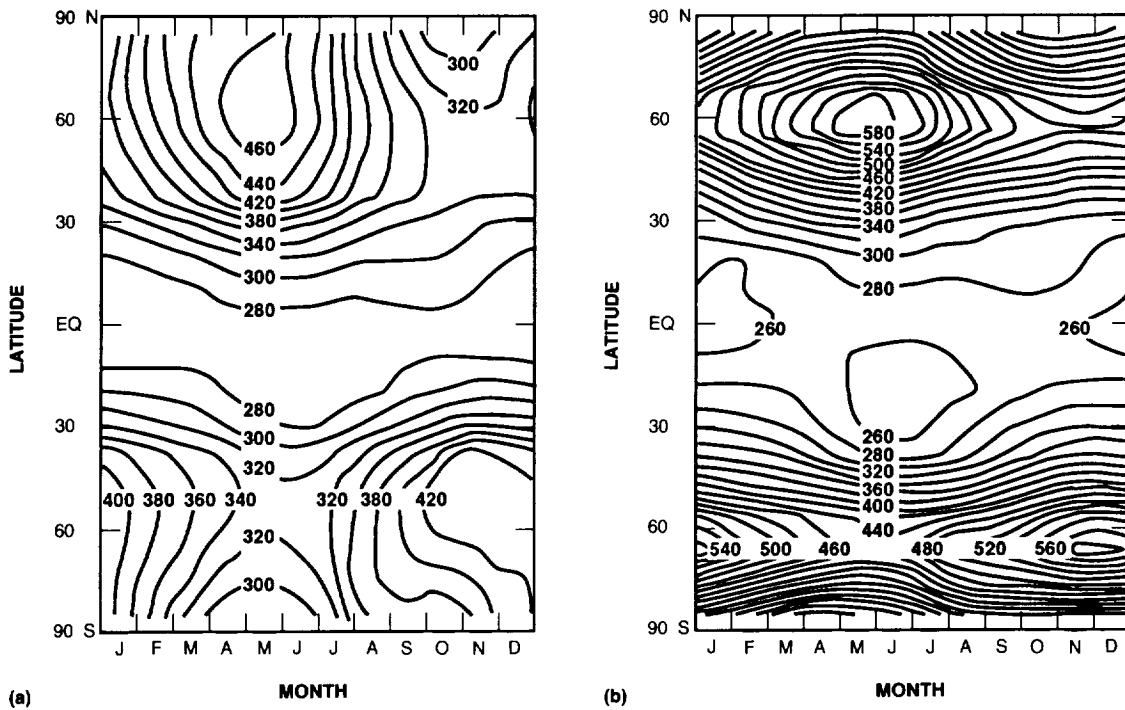


Figure 4.3-9a. i(a) Calculated total ozone abundance (Dobson Units) from transport sensitivity studies [case 1 of transport sensitivity study] (AER 2-D model). (b) Calculated total ozone abundance (Dobson Units) from transport sensitivity studies [case 2 of transport sensitivity study] (AER 2-D model).

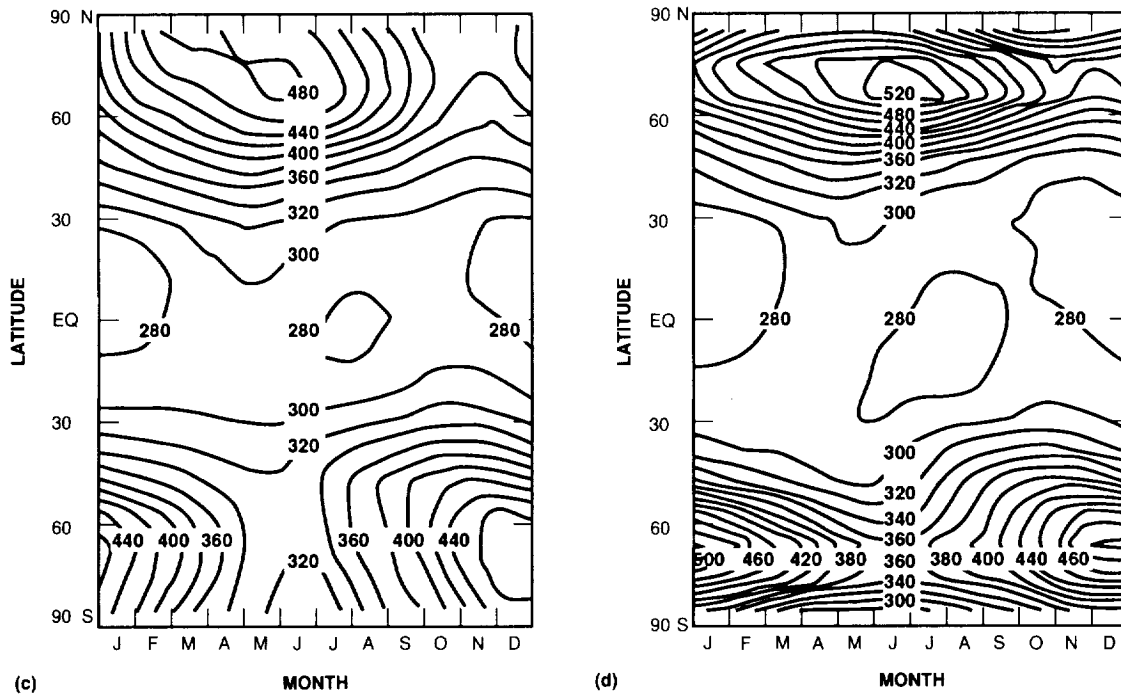


Figure 4.3.9b. ii(c) Calculated total ozone abundance (Dobson Units) from transport sensitivity studies [case 3 of transport sensitivity studies] (AER 2-D model). (d) Calculated total ozone abundance (Dobson Units) from transport sensitivity studies [case 4 of transport sensitivity study] (AER 2-D model).

OZONE DEPLETION POTENTIALS

Table 4.3-10. Results of transport sensitivity study (AER 2-D Model) on ODP and CLP for HCFC-22^a

	Case 1	Case 2	Case 3	Case 4
CFC-11 lifetime	47 years	34 years	51 years	44 years
HCFC-22 lifetime	24 years	22 years	24 years	23 years
ODP	0.07	0.035	0.055	0.034
CLP	0.27	0.35	0.25	0.28

^aThese calculations do not include the CH₃CCl₃ lifetime scaling included in Table 4.3-3.

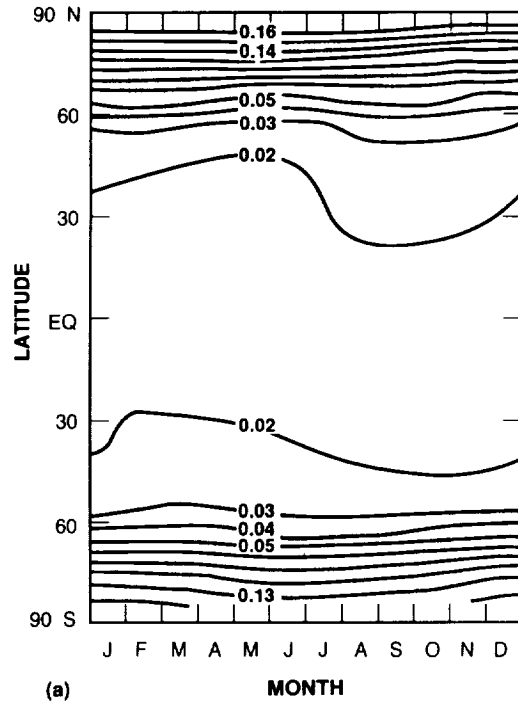


Figure 4.3-10a. Calculated latitudinal and seasonal relative ozone depletion from emission of HCFC-22 [case 2 of transport sensitivity study] (AER 2-D model).

OZONE DEPLETION POTENTIALS

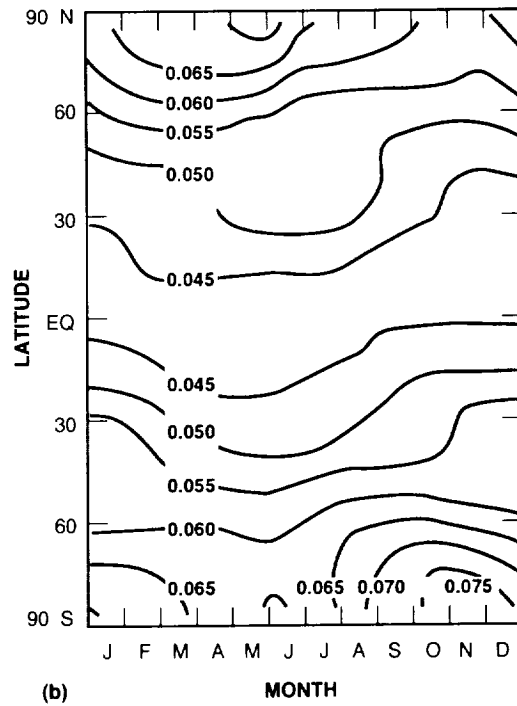


Figure 4.3-10b. Calculated latitudinal and seasonal relative ozone depletion from emission of HCFC-22 [case 3 of transport sensitivity study] (AER 2-D model).

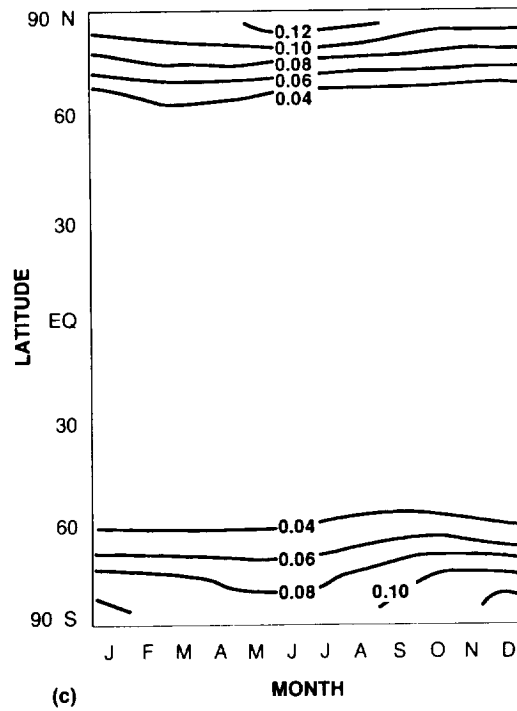


Figure 4.3-10c. Calculated latitudinal and seasonal relative ozone depletion from emission of HCFC-22 [case 4 of the transport sensitivity study] (AER 2-D model).

OZONE DEPLETION POTENTIALS

4.3.4.5 Time-Dependent Relative Ozone Depletion—Transient Effects

One of the limitations associated with the ODP parameter is that it is based on steady-state perturbations; it does not consider the relative time-dependent effects of different constituents on ozone. While we have shown that ODP is equivalently a measure of the cumulative chronic effects of unit-emitted mass of a gas over its life cycle in the atmosphere, we are also interested in the transient response at a constant emission level.

As mentioned earlier, ODP values determined at steady-state may not be representative of the relative transient effects expected for shorter-lived compounds during the early years of emission. During these early years, before one to two equivalent species lifetimes have passed, the ozone depletion per unit mass relative to CFC-11 can be much larger than the steady-state ODP value for some of the short-lived constituents. We note, however, that the changes in ozone occurring during the first few years after emissions are also relatively small compared to the steady-state ozone change. Relative time-dependent ozone depletions for several HCFCs and CFCs from the LLNL 1-D model are shown in Figure 4.3-11 and from the DuPont 1-D model in Figure 4.3-12. Results for the first few years are not shown because the derived changes in ozone were too small to be numerically accurate.

The transient values for relative ozone depletion and the time it takes to approach the steady-state values depend on the time-dependent behavior of the calculated O_3 decrease for the species examined and for the reference gas CFC-11. Since the atmospheric lifetimes of the HCFCs examined in this study are shorter than that of CFC-11, the time constant for exponential decay to the ODP asymptote is determined

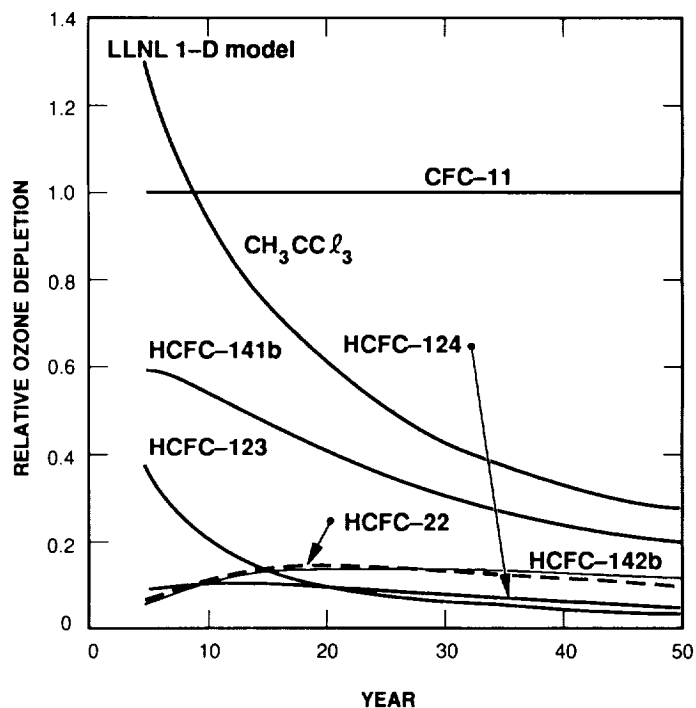


Figure 4.3-11. Calculated time-dependent change in relative ozone column depletion following a step change in emission of the tested halocarbons (LLNL 1-D model).

OZONE DEPLETION POTENTIALS

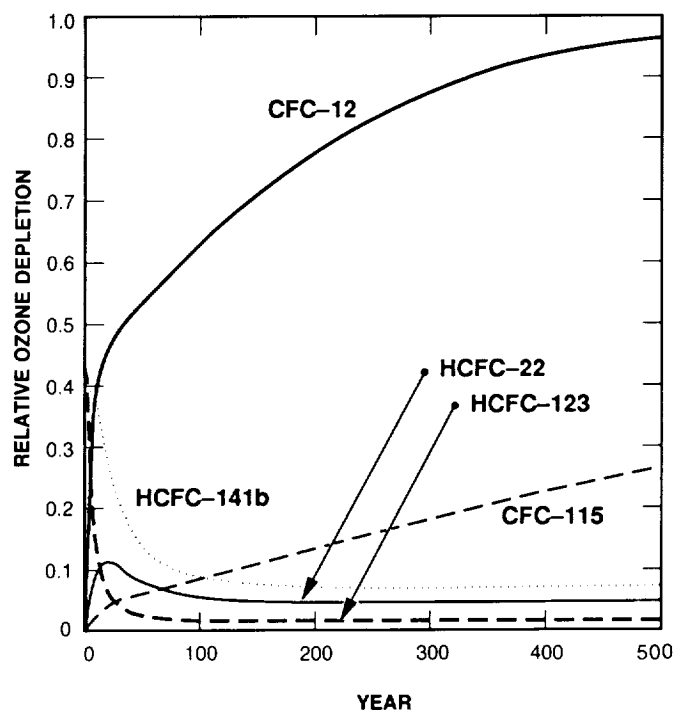


Figure 4.3-12. Calculated time-dependent change in relative ozone column depletion following a step change in emission of the tested halocarbons (DuPont 1-D model).

by the CFC-11 lifetime. The magnitude of the transient relative ozone depletion depends on the stratospheric lifetimes and how rapidly the chlorine atoms are released after transport into the stratosphere.

Several of the HCFCs, namely HCFC-123, HCFC-141b, and CH_3CCl_3 , have much larger relative ozone depletions at early times compared to the ODP values. Each of these gases has relatively short reaction-time constants within the stratosphere—compared to CFC-11. As a result, chlorine atoms are quickly released by these gases and the full effect on ozone is reached much sooner than CFC-11. At longer times, the relative ozone depletions asymptotically approach the ODP value.

Other species, such as HCFC-22, HCFC-124, and HCFC-142b, have long reactive time constants in the stratosphere. The time-dependent relative ozone depletions have much different behavior for these species. The relative ozone depletion builds gradually to a maximum value for these species, reflective of their long stratospheric time constants and the amount of time needed to build up stratospheric concentrations. After the first 20–40 years, the relative ozone depletion for these species gradually decays to the ODP value.

For gases with longer lifetimes than the reference gas, no maximum in relative ozone depletion is noted. This can be seen by examining the results for CFC-12 and CFC-115 in Figure 4.3-12.

Figure 4.3-13 shows the relative time-dependent behavior of chlorine being transported through the tropopause for these same gases (taken relative to CFC-11). In all the cases, the time-dependent strato-

OZONE DEPLETION POTENTIALS

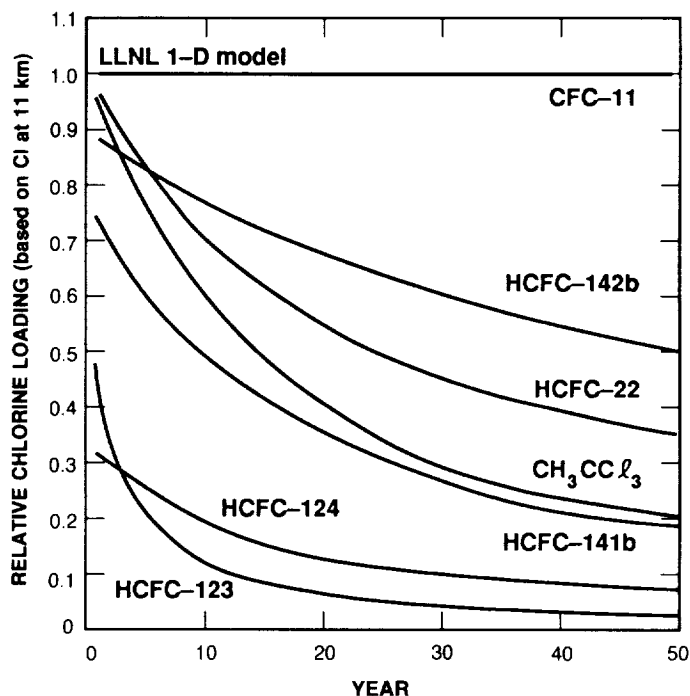


Figure 4.3-13. Calculated time-dependent relative chlorine loading following a step change in emission of the tested halocarbons (LLNL 1-D model).

spheric chlorine loading is much larger initially compared with the eventual steady-state relative Chlorine Loading Potential (CLP) value (given previously in Table 4.3-6) if the lifetime of the species is less than the reference gas.

In summary, time-dependent ozone depletion and chlorine loading values for the HCFCs are generally larger for the first 50 years than the ODP and CLP values defined at steady state. This, in part, arises from the longer atmospheric lifetime of the reference gas (CFC-11). Time-dependent relative ozone depletions for CFCs with lifetimes longer than CFC-11 show a monotonic increase to the steady-state ODP value.

4.3.5 Summary

One-dimensional and two-dimensional global atmospheric models have determined ODPs for a number of halocarbons, including CFCs, other chlorinated compounds, several potential replacement hydrohalocarbons, and several brominated compounds. Although 2-D models have generally a sounder physical basis, there are no real differences between 1-D and 2-D results. In general, the ODPs for fully halogenated compounds, such as the CFCs, are much larger than those for the hydrogenated halocarbons, which include the potential replacement compounds considered.

Brominated compounds should be compared with each other, because of the strong dependence of bromine effects on ozone to background chlorine levels. Bromine Ozone Depletion Potentials (BODPs)

are used for relative comparisons with Halon-1301, which has the longest lifetime and largest ODP, as the reference.

Although the calculated ODPs agree reasonably well among models, many uncertainties still exist. None of the models used for calculating ODPs include the chemical and dynamical processes causing the seasonal ozone losses over Antarctica. Another uncertainty lies in the model-calculated OH, which is a major source of uncertainty for both lifetimes and ODPs of the HCFCs.

Because of the apparent special chlorine processing and dynamics within the winter polar vortex, local Antarctic ODPs are expected to be larger than those derived. Insofar as the observed long-lived tracer distributions, such as CFC-11 in the polar vortex, suggest that much of the total chlorine may be available there, then an upper limit on Antarctic ODPs can be determined by calculating the relative amounts of chlorine transported through the tropopause by the different gases. These CLPs determined using assumed reference lifetimes (which generally agree with those in the models used here) can be as large as a factor of two to three times the derived ODP values. The ramifications of polar ozone depletion for global ODPs are not currently clear.

The time-dependent relative ozone depletion values differ from the steady-state ODP values. The time-dependent values depend on the atmospheric lifetime and the transport time to the region of destruction of the gas. The shorter the stratospheric lifetime, the sooner the gas will impact stratospheric ozone and hence the higher the transient relative ozone depletion. For example, HCFC-123 has a shorter lifetime than CFC-11; its relative ozone depletion is largest soon after emission. Other gases in this category include HCFC-141b and CH_3CCl_3 . Species such as HCFC-22, HCFC-124, and HCFC-142b have somewhat longer time constants in the stratosphere. Their relative ozone depletions build slowly to values (based on their time constants) as large as 0.2 and then decay slowly with time to the derived steady-state ODP value. Relative ozone depletion values for HCFCs are greater than ODP values even after 30 to 50 years. Time-dependent relative ozone depletions for CFCs with lifetimes longer than CFC-11 show a monotonic increase to the ODP value. The ODP is the cumulative response; as discussed above, the transient response of relative ozone depletion may be larger than the ODP value at early times after emission.

Several of the halocarbons indicate a strong latitude dependence in their ODP values and a generally weaker seasonal variation. In particular, ODPs for species such as CFC-12, HCFC-22, HCFC-124, and HCFC-142b, which have stratospheric loss patterns very different from CFC-11, produce strong latitudinal gradients in ODPs, with the largest ODPs near summer poles and smallest values in the tropics. The effects of heterogeneous chemistry and polar dynamical effects could modify these findings.

Sensitivity analyses indicate that ODPs are affected to only a minor degree ($\leq 20\%$) by assumed variations in background levels of N_2O , CH_4 , CO_2 , CO, total stratospheric chlorine, and total stratospheric bromine.

4.4 HALOCARBON GLOBAL WARMING POTENTIALS

4.4.1 Background

The radiative perturbations and potential climatic effects due to the infrared absorption properties of chlorofluorocarbons (CFC-11 and CFC-12) have been assessed in WMO (1985). That assessment and those from accompanying studies (Wang and Molnar, 1985; Owens et al., 1985; Ramanathan et al., 1985, 1987;

OZONE DEPLETION POTENTIALS

Fisher et al., 1989c) demonstrated that the direct radiative forcing (i.e., one in which all parameters are held fixed while the concentration of any CFCs is increased from 0 to 1 ppbv), consists of an increase in the downward longwave flux at the surface (surface radiative forcing) and a decrease in the net upward flux at the tropopause (surface-troposphere net radiative forcing). This imbalance results in a net increase in the amount of longwave radiation trapped within the Earth's atmosphere system, thereby potentially enhancing the greenhouse effect.

Since the 1985 reports, infrared spectral absorption data of several halogenated compounds have become available (Magid, private communication, 1988 and Gehring, private communication, 1988) which not only include CFCs, but also include HFCs and HCFCs. Interest in the latter two classes of compounds stems from their role as potential replacement compounds for CFCs. Laboratory measurements show that all the halogenated compounds possess significant absorption in the $500\text{--}1400\text{ cm}^{-1}$ ("window") region. The absorption spectrum for any of these species typically is one of individual lines spaced very closely together in an arbitrary frequency interval giving the appearance of a continuum structure. The absorption cross sections of the HFCs and HCFCs also occur at similar frequencies in the "window" region and are comparable in magnitude to those for CFCs.

Because the absorption bands of all replacement halogenated compounds fall in the infrared "window" region, the potential greenhouse effects need to be assessed. This need is emphasized by the fact that the clear portions of the Earth's atmosphere have virtually no other constituents (excepting aerosols) with major absorption bands in the "window" region. In overcast conditions, clouds also have absorption bands in this region. Furthermore, the Earth's outward-going radiation is at a maximum near the "window" region for the Earth's surface temperatures. Therefore, the presence of halogenated compounds could play an important part in determining the radiation balance in the clear portion of the atmosphere and a non-negligible role in the overcast portions.

Besides the influence on the infrared radiative fluxes, there is yet another aspect of the perturbations by the halogenated compounds, as pointed out in WMO (1985). This is the heating perturbations induced in the upper troposphere and lower stratosphere which, owing to the large radiative time constant of those regions of the atmosphere, have the potential to increase the temperatures there. Any change in the temperatures near the tropopause region is of potential significance for the tropospheric-stratospheric exchange of water vapor.

The effectiveness of greenhouse gases is accentuated by their lifetimes and in large part by their corresponding atmospheric abundances.

In this report, we consider the most recently available laboratory spectral data of the halogenated compounds and assess the following:

- the direct radiative forcing due to the halogenated compounds, as evaluated by both line-by-line (GFDL) and band models (AER, DuPont),
- the changes in the surface temperature, as evaluated by the one-dimensional radiative-convective models (AER, DuPont), and
- the relative changes in the surface temperatures taking into account the chemical lifetimes of the compounds expressed as Greenhouse Warming Potentials.

The GFDL line-by-line radiative transfer model has been developed from that described in Schwarzkopf and Fels (1989). The band models employed in the AER and DuPont algorithms have been described earlier (Wang and Molnar, 1985; Owens et al., 1985). The absorption cross sections of the halogenated compounds are incorporated in a manner similar to the water vapor continuum. It should be noted that in the absence of a temperature-dependent dataset, none of these algorithms incorporate temperature dependence in calculated radiative effects.

No attempt is made to calculate Greenhouse Warming Potentials for non-halocarbon gases such as carbon dioxide and methane. Due to their current atmospheric concentrations and the spectral locations of their infrared absorption bands, calculated global warming is not proportional to atmospheric concentration changes of these gases. In contrast, calculated warmings are linearly proportional to halocarbon concentrations.

4.4.2 Definition of Halocarbon GWP

Halocarbon Global Warming Potential (Halocarbon GWP) is defined parallel to the Ozone Depletion Potential. It is defined as the ratio of steady-state calculated warming for each unit mass of a gas emitted into the atmosphere (as indicated by the change in infrared flux at the tropopause) relative to the calculated warming for a mass unit of reference gas CFC-11. This definition was chosen as a representative measure of the potential of a compound to effect global warming, since:

1. It provides a measure of the cumulative effect on the radiative balance over its chemical lifetime for each unit released into the atmosphere (see below).
2. The Halocarbon GWP yields a single value for each compound rather than a time-varying multitude of values.
3. It provides a measure of the maximum calculated effect of a compound compared to the maximum calculated effect of CFC-11 on an equal mass basis.

The first reason is perhaps the most important in that it estimates the cumulative effect on potential global warming of each unit released. An illustrative test was performed which quantified the chronic effect from a single pulsed release of test gas into the atmosphere. This particular test used the DuPont model to calculate cumulative global warmings over a 500-year time period following emissions of HCFC-123, HCFC-22, and CFC-11.

The calculated cumulative warmings are shown in Figure 4.4-1. For each case, the modeled warming is maximum very soon after the release and exponentially decays with a time constant equal to the atmospheric lifetime of the species. As seen in the insert table, the time-integrated warmings echo the relative values of the Halocarbon GWP calculated from steady-state figures.

In order to make the definition of Halocarbon GWP consistent between models as well as a conservative estimate of relative effects, the following criteria have been selected:

1. Trace gas levels—Changing the concentration of other trace gases could affect the calculated future equilibrium temperature rise from gases under evaluation here for two reasons. First, if there is overlap of absorption spectra, certain frequency bands would have less effect. Secondly, chemistry and therefore lifetime can be affected by perturbation of these chemicals. Current levels of CO₂, CH₄, N₂O, O₃, and stratospheric H₂O were used in model calculations.

OZONE DEPLETION POTENTIALS

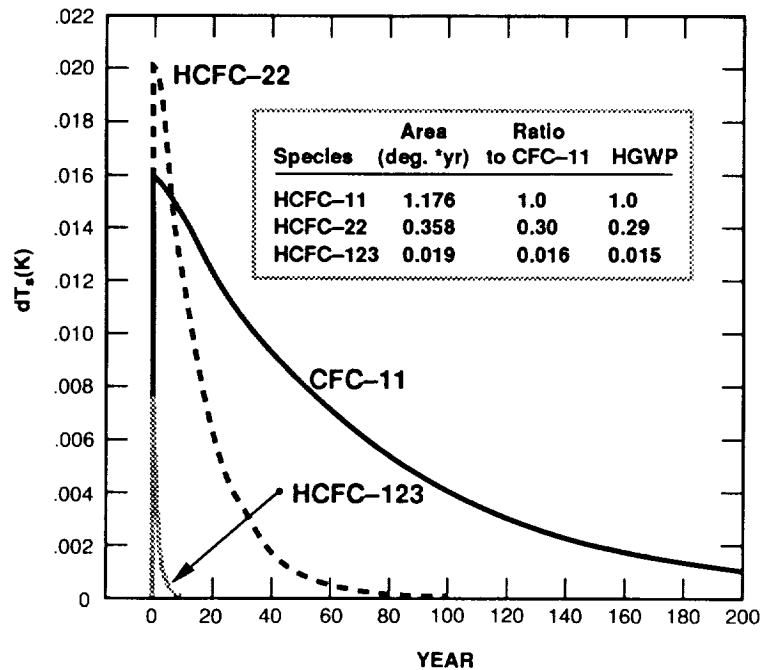


Figure 4.4-1. Calculated change in surface temperature following a pulsed emission of 5×10^9 kg of specified gas.

2. Radiative forcing level—The calculations are based on gas concentrations that yield modeled responses large enough to avoid the “noise levels” of the numerical models, yet small enough to be in the linear response region.
3. Reference gas—CFC-11 has been chosen as the reference compound for Halocarbon GWP calculations in order to have a reference material consistent for both Halocarbon GWP and ODP.

Furthermore, additional parameters are useful in order to facilitate discussion:

4. Net initial IR flux perturbation at the tropopause will be symbolically represented as dF (per unit mixing ratio in the troposphere).
5. Specific Surface Temperature Change—The calculated surface temperature increase for a one part per billion (by volume) surface increase of any gas is defined as the specific surface temperature change, or symbolically dT_s .
6. The climate feedback factor (Dickinson, 1982), represented by λ , is the ratio of the model-calculated surface temperature change to a perturbation in the net radiative forcing (discussion follows).

The response of the Earth’s surface atmosphere to a radiative forcing exerted by the presence of the halogenated compounds involves several feedback mechanisms and can be expressed as:

$$dT_s = \lambda dF$$

where dT_s is a measure of the climate response. The factor λ depends on mechanisms not all of which are quantitatively understood. Nevertheless, as stated in WMO (1985), λ can be expected to be in the range of 0.25–1 K/W m⁻². Studies surveyed by Ramanathan et al. (1985) have two values ranging from 0.47–0.53, while the DuPont and AER models have a λ of 0.64, and 0.81, respectively. It must be realized that the range in λ stated above is not a rigid bracketing. Two important aspects of climate modeling severely restrict our present ability to better quantify λ precisely. One is the lack of understanding of the response of the ocean circulation and the ensuing effects on the atmosphere. The second is the lack of knowledge of the changes in the cloud amounts and cloud properties due to changes in the halocarbon radiative forcing. Our knowledge in both the areas needs to improve substantially in order to better quantify λ .

The Halocarbon GWP definition resembles the ODP definition. For any gas, the general definition is:

$$\text{Halocarbon GWP} = \frac{\text{Calculated IR forcing due to compound X} / \text{Emission rate (steady state) of compound X}}{\text{Calculated IR forcing due to CFC-11} / \text{Emission rate (steady state) of CFC-11}}$$

Note, since lifetimes are proportional to the ratio of atmospheric abundance to (molecular weight * emission rate), an equivalent form of this definition is:

$$\text{Halocarbon GWP} = \frac{[dF(x) * \text{Lifetime}(x) / \text{Molecular weight}(x)]}{[dF(\text{CFC-11}) * \text{Lifetime}(\text{CFC-11}) / \text{Molecular weight}(\text{CFC-11})]}$$

(This formula has been used to calculate Halocarbon GWP from the line-by-line radiative model results.)

Since radiative-convective models calculate a change in surface temperature, it is useful to express an equivalent form of the Halocarbon GWP, assuming the same value of λ for all gases, as:

$$\text{Halocarbon GWP} = \frac{[dT_s(x) * \text{Lifetime}(x) / \text{Molecular weight}(x)]}{[dT_s(\text{CFC-11}) * \text{Lifetime}(\text{CFC-11}) / \text{Molecular weight}(\text{CFC-11})]}$$

Note also, many of these gases have the potential of affecting heating rates indirectly as well, since they can chemically influence the distribution of ozone. Examination of model results indicates that this is a second order effect, at least two orders of magnitude below the IR effect and well below the sensitivity of these calculations (Wang et al., 1989).

4.4.3 Model-Calculated Halocarbon GWPs

A primary input to these radiative calculations are the altitudinal steady-state concentration profiles which are calculated using appropriate chemistry models.

After the concentration profile is determined, the effect of each gas is calculated using a radiative model. This calculation accounts for the amount of energy absorbed by each IR gas over the radiation spectrum and accounts for the spectral overlap with other IR active gases. Quantitative infrared data for this input are available (see Fisher et al., 1989c).

Table 4.4-1 shows the net IR radiative flux at the tropopause (\cong 12 km) for a 1 ppbv tropospheric mixing ratio, as calculated by each of the three models. Note that each of the model's calculations was

OZONE DEPLETION POTENTIALS

Table 4.4-1. Net IR radiative flux at the tropopause (at 12 km) [Wm^{-2}] for 1 ppbv tropospheric mixing ratio of each gas

Species	AER ^a	DuPont ^b	GFDL ^c
CFC-11	0.175	0.133	0.35 (0.22) ^d , (0.30) ^e
CFC-12	0.248	0.158	0.42
CFC-113	0.223	0.163	0.42
CFC-114	0.258	0.181	
CFC-115	0.204	0.164	0.44
HCFC-22	0.151	0.107	0.29
HCFC-123	0.140	0.092	0.28
HCFC-124	0.153	0.108	
HFC-125	0.189	0.119	
HFC-134a	0.135	0.095	0.26
HCFC-141b	0.109	0.076	0.22
HCFC-142b	0.144	0.101	0.27
HFC-143a	0.111	0.087	
HFC-152a	0.092	0.059	0.17
CCl ₄	0.080	0.063	
CH ₃ CCl ₃	0.038	0.033	
[2 × CO ₂]	4.41	3.87	5.68

Note difference in base assumptions:

^aAER calculations based on

—global mean conditions

—48.5% cloud cover

—cloud with spectral optical thickness at 0.55 μm of 8.9. (cloud albedo = 0.54)

^bDuPont calculations based on

—global mean conditions

—50% cloud cover

—cloud albedo = 0.5

^cGFDL calculations based on

—mid-latitude, summer atmosphere

—clear sky conditions

—uniform gas mixing ratio

^dCFC-11 only in troposphere

^eCFC-11 only in troposphere, with 50% black cloud cover at ~4 km

based on different cloud assumptions (GFDL used a clear sky, DuPont used 50% cloud cover [albedo = 0.5], and the AER was based on control climate cloud field with 48.5% cloud cover). Note also that the GFDL model assumed mid-latitude summer radiative conditions, whereas both AER and DuPont models are based on globally and annually averaged radiation.

Specific surface warmings are calculated using the AER and DuPont radiative convective models and are shown in Table 4.4-2 for each of these gases. Again differences in the λ factors between these models yield a systematic difference in the response of surface warming to net radiative flux changes for each compound. Note that HCFCs and HFCs on the average have lower specific surface warming values than

OZONE DEPLETION POTENTIALS

Table 4.4-2. Specific surface temperature (dT_s) increases and lambda (λ) values resulting from 1 ppbv of each gas

Species	dT _s (°K/ppbv)		λ (°K/ppbv/Wm ⁻²)	
	AER	Du Pont	AER	Du Pont
CFC-11	0.135	0.084	0.771	0.632
CFC-12	0.202	0.102	0.815	0.647
CFC-113	0.174	0.103	0.780	0.632
CFC-114	0.208	0.115	0.806	0.635
CFC-115	0.170	0.107	0.833	0.652
HCFC-22	0.124	0.070	0.821	0.650
HCFC-123	0.111	0.059	0.793	0.644
HCFC-124	0.126	0.070	0.824	0.645
HFC-125	0.160	0.078	0.847	0.654
HFC-134a	0.114	0.061	0.844	0.647
HCFC-141b	0.086	0.048	0.789	0.637
HCFC-142b	0.120	0.066	0.833	0.651
HFC-143a	0.092	0.054	0.829	0.625
HFC-152a	0.076	0.038	0.826	0.649
CCl ₄	0.062	0.040	0.775	0.628
CH ₃ CCl ₃	0.027	0.020	0.710	0.618
[2 × CO ₂]	[3.08]	[1.651]		

CFCs by approximately 40%. (Net dF values are also lower by ~40%.) Although total absorptances are about equivalent for each class of compounds, overlap with absorptance bands of other infrared active gases diminishes the efficiencies of these gases as greenhouse gases. Most of the hydrogenated halocarbons have bands that overlap the bands of both CH₄ and N₂O as well as water vapor above 1250 cm⁻¹.

Table 4.4-3 shows the Halocarbon GWP values calculated by each of the three models. Reference lifetimes are based on the estimates used in scenarios developed in Section 3.3.1 for CFCs and from the analysis in Section 4.2 for HCFCs and HFCs.

Halocarbon GWPs for fully halogenated compounds are larger than those for the hydrogenated halocarbons. Fully halogenated CFCs have Halocarbon GWP values ranging from 1.0 to 7.5, whereas HCFCs and HFCs range from 0.02 to 0.7.

Halocarbon GWP values differ between species due to differences in infrared absorbances and differences in lifetimes. The range of absorbances is approximately 4, while the lifetimes range by a factor of 250. Thus, the range of 400 among the Halocarbon GWP values is primarily a result of differences in lifetimes. Additionally, the Halocarbon GWP for halon-1301 has been calculated based on specific surface warmings reported in WMO 1985 and a relative lifetime (to CFC-11) of 1.3 (from LLNL 1-D and Oslo 2-D models). This Halocarbon GWP value is 1.4.

OZONE DEPLETION POTENTIALS

Table 4.4-3. Halocarbon global warming potentials

Species	Reference ^a Lifetime (Yrs)	AER ^b	DuPont ^b	GFDL ^b
CFC-11	60.0	1.0	1.0	1.0
CFC-12	120.0	3.4	2.8	2.7
CFC-113	90.0	1.4	1.4	1.3
CFC-114	200.0	4.1	3.7	
CFC-115	400.0	7.5	7.6	7.5
HCFC-22	15.3	0.37	0.34	0.34
HCFC-123	1.6	0.02	0.017	0.019
HCFC-124	6.6	0.10	0.092	
HFC-125	28.1	0.65	0.51	
HFC-134a	15.5	0.29	0.25	0.26
HCFC-141b	7.8	0.097	0.087	0.096
HCFC-142b	19.1	0.39	0.34	0.34
HFC-143a	41.0	0.76	0.72	
HFC-152a	1.7	0.033	0.026	0.029
CCl ₄	50.0	0.34	0.35	
CH ₂ Cl ₂	6.3	0.022	0.026	

^aLifetimes are based on estimates used in scenario development (Chapter 3, Section 3.2.1) for CFCs and from the analysis in Section 4.2 for HCFCs and HFCs.

^bAER and DuPont results are based on surface temperature perturbations calculated using radiative-convective models; GFDL results are based on line-by-line determined radiative forcing.

4.4.3.1 Sensitivity to Trace Gas Levels

The Halocarbon GWP values have all been based on calculations that assume present-day values for concentrations of trace gases of CO₂, CH₄, CO, N₂O, and CFCs. Because the Halocarbon GWP values are for consideration with future atmospheres different from today, we have examined the sensitivity of these parameters to changes in CO₂ and CH₄ at levels that might be achieved if current trends continue.

Trace gas changes and the resulting calculated changes in lifetimes, surface temperature rises, and Halocarbon GWP values (from the AER model) are shown in Table 4.4-4. Calculated changes in surface temperature for tested CFCs and HCFCs were compared to a reference atmosphere including the assumed gas perturbation (note the Halocarbon GWP values are different than listed above, since they are based on model-calculated lifetimes rather than reference lifetime values).

As seen in Table 4.4-4, trace gas changes have little effect on Halocarbon GWP values. CO₂ has the greatest effect on CFC radiative forcing because the albedo feedback is weaker in the warmer atmosphere. As a result, the radiative forcing for CFC-11 and -12 is somewhat weakened. Methane affects the chemical lifetimes of the HCFCs, resulting in slightly greater Halocarbon GWP values for these compounds. Nevertheless, these relatively major perturbations in trace gas levels have only minor effect on calculated Halocarbon GWP values, indicating that the GWP formalism is robust over the range of trace gases projected for the next century.

OZONE DEPLETION POTENTIALS

Table 4.4-4. Sensitivity study—variation in trace gas levels and impact on halocarbon GWP values (AER 1-D model)

	Atmosphere	Species			
		CFC-11	CFC-12	HCFC-22	HCFC-123
Lifetime (yrs)	Present Day	60	125	20	2.1
	CH ₄ (1.6 → 3.2 ppbv)	60	126	23	2.5
	CO ₂ (340 → 680 ppm)	61	128	20	2.1
dT, (°K/ppbv)	Present Day	0.14	0.20	0.12	0.11
	CH ₄ (1.6 → 3.2 ppbv)	0.14	0.20	0.12	0.11
	CO ₂ (340 → 680 ppm)	0.12	0.17	0.12	0.11
GWP	Present Day	1.0	3.5	0.49	0.026
	CH ₄ (1.6 → 3.2 ppbv)	1.0	3.5	0.56	0.031
	CO ₂ (340 → 680 ppm)	1.0	3.4	0.49	0.027

4.4.3.2 Time Dependency of Relative Global Warming

Since the Halocarbon GWP parameter is based on steady-state effects, it does not describe the relative time-dependent effects of constituents on warming. Even though the Halocarbon GWP is an equivalent measure of the cumulative warming during its lifetime for each unit mass emitted, the transient response to a constant emission level is also of interest.

The calculated warmings for a number of halocarbons are shown in Figure 4.4-2. As seen, the calculated warming reaches an asymptote rapidly for the HCFCs, but requires longer periods to approach steady-state for CFCs. These response patterns echo the respective patterns for increases in atmospheric abundances for each species, seen in Figure 4.4-3.

Relative warmings are shown in Figure 4.4-4. For HCFCs, the relative effects are at a maximum at very short times. One can easily show (using L'Hospital's rule) that the initial relative value is the ratio of the value of the specific surface temperature increase (°K/ppbv) / molecular weight—relative to the same ratio for CFC-11). Thus initially, while the individual effects are small, the relative effects are on the order unity. However, as atmospheric concentrations build and chemistry differences affect the relative amount in the atmosphere, the relative effects either grow or decrease depending on whether the lifetimes are longer or shorter than that of CFC-11. As seen in Figure 4.4-4, the HCFCs have lifetimes shorter than the lifetime of the reference gas and have relative effects that asymptotically approach the Halocarbon GWP value with a time constant equal to the lifetime of CFC-11. Longer-lived species have relative effects that grow with time, asymptotically approaching their Halocarbon GWP value with time constant for their own lifetime.

4.4.4 Uncertainties

Uncertainties in the effectiveness of gases to produce global warming fall into two general classes—those that are generalized for the entire greenhouse effect and those that are specific to individual species.

OZONE DEPLETION POTENTIALS

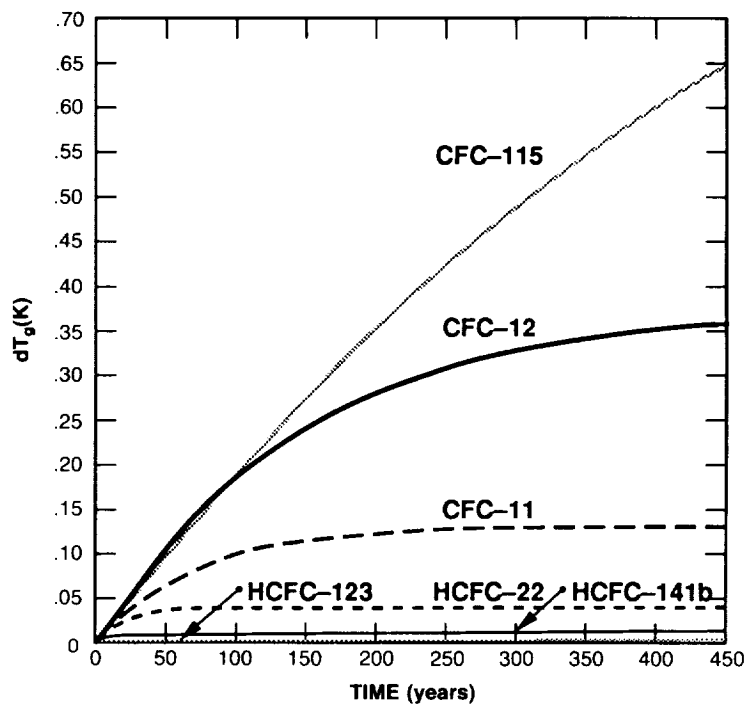


Figure 4.4-2. Change of calculated warming following a step change of emission of specified gas at 5×10^8 kg/yr (DuPont 1-D model).

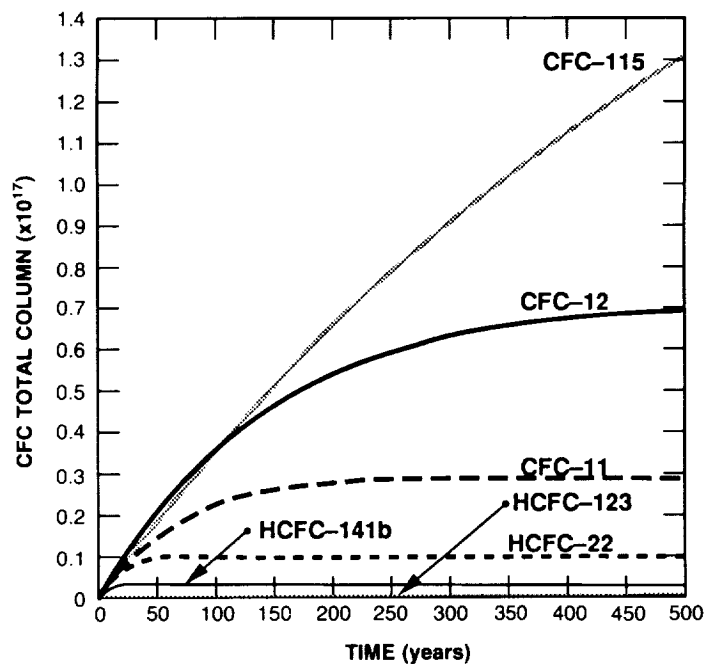


Figure 4.4-3. Column of (hydro) chlorofluorocarbons following a step change of emission of specified gas at 5×10^8 kg/yr (DuPont 1-D model).

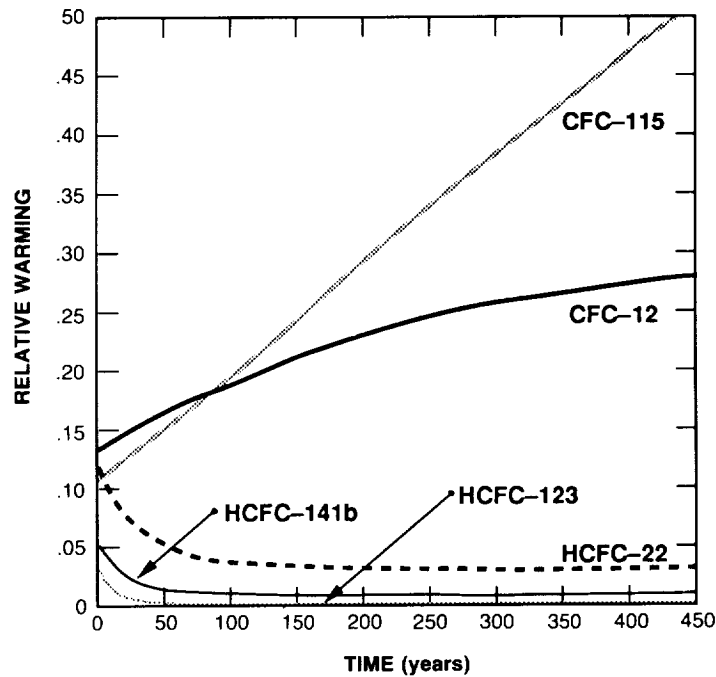


Figure 4.4-4. Calculated relative warmings following a step change of emission of specified gas [CFC-11 reference] (DuPont 1-D model).

There are a number of uncertainties in the modeling of greenhouse warming. These concern the radiative properties of the Earth's surface-atmosphere system, such as changes in the surface and ice cover albedos, and changes in cloud cover and composition. Changes in the temperature structure of the atmosphere will affect the convective patterns and chemistry of the stratosphere. The coupling of oceans (as heat reservoirs) and ocean currents to surface temperature changes will also affect the timing and location of the warming. Research is being carried out to understand these questions, which apply to all gases that affect the future radiative balance of the Earth.

Uncertainties also exist regarding the individual species and their influence on the radiative balance. Temperature dependence of the absorptances of individual species need to be resolved and modeled. The chemical processes affecting both lifetimes and atmospheric profiles are also the subject of continuing research. Resolution of questions related to the general greenhouse warming modeling will directly affect timing and magnitude of global warming, whereas resolution of the radiative and chemical parameterizations for halocarbons will have a direct impact on the Halocarbon GWP values for these species.

4.4.5 Summary

Halocarbon Global Warming Potentials have been defined and calculated in order to allow estimates of the relative environmental effects of halocarbons. The results presented here indicate that the Halocarbon GWPs depend primarily on the atmospheric lifetime of the compounds and to a lesser degree on the molecular IR absorption characteristics.

OZONE DEPLETION POTENTIALS

The reduction in Halocarbon GWP that might be expected due to use replacement of a CFC by a hydrohalocarbon can be estimated by taking the ratio of the Halocarbon GWP of the hydrohalocarbon to the Halocarbon GWP of the CFC it would replace. For example, the reduction in Halocarbon GWP in replacing uses of CFC-12 by HCFC-134a is $(0.26 \pm 0.030)/(3.07) = 0.085 \pm 0.01$. Of course, the relative quantities of the compound required in the use application must also be taken into account.

Although the Halocarbon GWP values reported here agree reasonably well among models, uncertainties in the values still exist because of the uncertainties in modeled chemistry and dynamics and their direct effect on the chemical lifetimes of these compounds.

Halocarbon GWP values appear to be reasonably robust parameters since their calculated values are nearly insensitive to assumed concentrations of other radiative gases. The minor shifting of the Halocarbon GWP values is primarily influenced by the changes in calculated lifetimes and therefore the abundance in the atmosphere.

Calculated time-dependent relative global warmings for Halocarbons are initially on order unity but decrease or increase depending on whether their lifetimes are shorter or longer than that of the reference gas. At longer times, the relative global warmings asymptotically approach the Halocarbon GWP values.

REFERENCES

- Blake, D. R., and F. S. Rowland, Continuing worldwide increase in tropospheric methane, 1978 to 1987, *Science*, 239, 1129–1131, 1988.
- Bojkov, R. D., Surface ozone during the second half of the nineteenth century, *J. Climate and Appl. Meteor.*, 25, 343–352, 1986.
- Chameides, W. L., and J. C. G. Walker, A photochemical theory of tropospheric ozone, *J. Geophys. Res.*, 78, 8751–8760, 1973.
- Chameides, W. L., S. C. Liu, and R. C. Cicerone, Possible variations in atmospheric methane, *J. Geophys. Res.*, 82, 1795–1798, 1977.
- Connell, P. S., and D. J. Wuebbles, "Evaluating CFC Alternatives From the Atmospheric Viewpoint," Air and Waste Management Association paper 89-5.7, 1989; also Lawrence Livermore National Laboratory report UCRL-99927 Rev.1, 1989.
- Cox, R. A., and R. G. Derwent, Gas phase chemistry of the minor constituents of the troposphere, in *Specialist Periodic Report Gas Kinetics and Energy Transfer*, Vol. 4, The Royal Society of Chemistry, London, pp. 189–232, 1981.
- Crutzen, P. J., A discussion of the chemistry of some minor constituents of the stratosphere and troposphere, *Pure and Applied Geophys.*, 106–108, 1385–1399, 1973.
- Crutzen, P. J., Photochemical reactions initiated by and influencing ozone in unpolluted tropospheric air, *Tellus*, 26, 47–57, 1974.
- Crutzen, P. J., Tropospheric ozone: An overview, in *Tropospheric Ozone: Regional and Global Scale Interactions*, edited by I. S. A. Isaksen, NATO ASI Series C, D. Reidel, Dordrecht, 1988.
- Crutzen, P. J., and C. Bruhl, The impact of observed changes in atmospheric chemistry and climate, in *The Environmental Record in Glaciers and Ice Sheets*, edited by H. Oeschger and C. C. Langway, Jr., Wiley, New York, pp. 249–266, 1989.
- Crutzen, P. J., and J. Fishman, Average concentrations of OH in the troposphere, and the budgets of CH₄, CO, CH₃CCl₃, *Geophys. Res. Lett.*, 4, 321–324, 1977.

OZONE DEPLETION POTENTIALS

- Cunnold, D. M., R. G. Prinn, R. A. Rasmussen, P. G. Simmonds, F. N. Alyea, C. A. Cardelino, A. J. Crawford, P. J. Fraser, and R. D. Rosen, Atmospheric lifetime and annual release estimates for CCl_3F and CCl_2F_2 from five years of ALE data, *J. Geophys. Res.*, *91*, 10797–10817, 1986.
- Davidson, J. A., H. I. Schiff, T. J. Brown, and C. J. Howard, Temperature dependence of the rate constants for reactions of $\text{O}(^1\text{D})$ atoms with a number of halocarbons, *J. Chem. Phys.*, *69*, 4277–4279, 1978.
- DeMore, W. B., M. J. Molina, S. P. Sander, D. M. Golden, R. F. Hampson, M. J. Kurylo, C. J. Howard, and A. R. Ravishankara, *Chemical Kinetics and Photochemical Data for Use in Stratospheric Modeling*, JPL Publication 87–41, pp. 196, Jet Propulsion Laboratory, Pasadena, CA, 1987.
- Derwent, R. G., and A. R. Curtis, "Two-Dimensional Model Studies of Some Trace Gases and Free Radicals in the Troposphere," AERE report R8853, H.M. Stationery Office, London, 1977.
- Derwent, R. G., and A. E. J. Eggleton, Two-dimensional model studies of methyl chloroform in the troposphere, *Quart. J. Roy. Met. Soc.*, *107*, 231–242, 1981.
- Derwent, R., and A. Volz-Thomas, The tropospheric lifetime of halocarbons and their reactions with OH radicals: an assessment based on the concentration of ^{14}CO , in *Alternative Fluorocarbons Environmental Acceptability Study (AFEAS)*, Vol. II, Appendix, this report (1990), 1989.
- Dickinson, R. E., Modeling climatic changes due to carbon dioxide increases, in *Carbon Dioxide Review*, edited by W.C. Clark, pp. 101–133, Clarendon Press, New York, 1982.
- Dorn, H. P., J. Callies, U. Platt, and D. H. Ehhalt, Measurement of tropospheric OH concentrations by laser long-path absorption spectroscopy, *Tellus*, *40B*, 437–445, 1988.
- Ehhalt, D. H., How has the atmospheric concentration of CH_4 changed? in *The Changing Atmosphere*, edited by F. S. Rowland and I. S. A. Isaksen, Wiley-Interscience, New York, pp. 25–32, 1988.
- Ehhalt, D. H., and J. Rudolph, On the importance of light hydrocarbons in multiphase atmospheric systems, Ber. Kernforschungsanlage, Julich, West Germany, JUL-1942, pp. 1–43, 1984.
- Fahey, D. W., G. Hubler, D. D. Parrish, E. J. Williams, R. B. Norton, B. A. Ridley, H. C. Singh, S. C. Liu, and F. C. Fehsenfeld, Reactive nitrogen species in the troposphere: Measurements of NO , NO_2 , HNO_3 , particulate nitrate, peroxyacetyl nitrate (PAN), O_3 , and total reactive odd nitrogen (NO_x) at Niwot Ridge, Colorado, *J. Geophys. Res.*, *91*, 9781–9793, 1986.
- Fehsenfeld, F. C., D. D. Parrish, and D. W. Fahey, The measurement of NO_x in the non-urban troposphere, in *Tropospheric Ozone: Regional and Global Scale Interactions*, edited by I. S. A. Isaksen, NATO ASI Series C, D. Reidel, Dordrecht, 1988.
- Fisher, D. A., C. H. Hales, D. L. Filkin, M. K. W. Ko, D. N. Sze, P. S. Connell, D. J. Wuebbles, I. S. A. Isaksen, and F. Stordal, Ozone depletion potentials for CFCs and possible replacements, submitted to *Nature*, 1989a.
- Fisher, D. A., C. H. Hales, D. L. Filkin, M. K. W. Ko, N. D. Sze, P. S. Connell, D. J. Wuebbles, I. S. A. Isaksen, and F. Stordal, Relative effects on stratospheric ozone of halogenated methanes and ethanes of social and industrial interest, in *Alternative Fluorocarbons Environmental Acceptability Study (AFEAS)*, Vol. II, Appendix, this report (1990), 1989b.
- Fisher, D. A., C. H. Hales, W. C. Wang, K. W. Ko, and N. D. Sze, Relative effects of global warming of halogenated methanes and ethanes of social and industrial interest, in *Alternative Fluorocarbons Environmental Acceptability Study (AFEAS)*, Vol. II, Appendix, this report (1990), 1989c.
- Fishman, J., and P. J. Crutzen, The origin of ozone in the troposphere, *Nature*, *274*, 855–858, 1978.
- Fraser, P. J., P. Hyson, R. A. Rasmussen, A. J. Crawford, and M. A. K. Khalil, Methane, carbon monoxide and methyl chloroform in the southern hemisphere, *J. Atmos. Chem.*, *4*, 3–42, 1986.
- Gillotay, G., P. C. Simon, and G. Brasseur, Absorption cross section of alternative chlorofluoroethanes and potential effects on the ozone layer, *Plant Space Sci.*, in press 1989.
- Golombek, A., and R. G. Prinn, A global three-dimensional model of the circulation and chemistry of CFCl_3 , CF_3Cl_2 , CH_3CCl_3 , CCl_4 and N_2O , *J. Geophys. Res.*, *91*, 3985–4001, 1986.

OZONE DEPLETION POTENTIALS

- Hampson, R. F., Kurylo, M. J., and Sander, S. P., Evaluated rate constants for selected HCFC's and HFC's with OH and O(¹D), in *Alternative Fluorocarbons Environmental Acceptability Study (AFEAS)*, Vol. II, Appendix, this report (1990), 1989.
- Hammitt, J. K., F. Camm, P. S. Connell, W. E. Mooz, K. A. Wolf, D. J. Wuebbles, and A. Bemazai, Future emission scenarios for chemicals that may deplete stratospheric ozone, *Nature*, *330*, 711–716, 1987.
- Hubrich, C., and F. Stuhl, The ultraviolet absorption of some halogenated methanes and ethanes for atmospheric interest, *J. Photochem.*, *12*, 93–107, 1980.
- Isaksen, I. S. A., Tropospheric ozone budget and possible man-made effects, in *Quadrennial International Ozone Symposium*, Vol. II, edited by J. London, pp. 845–852, IAMAP, NCAR, Boulder, Colorado, 1981.
- Isaksen, I. S. A., and O. Hov, Calculation of trends in the tropospheric concentrations of O₃, OH, CO, CH₄ and NO, *Tellus*, *39B*, 271–285, 1987.
- IUPAC:R. Atkinson, D. L. Baulch, R. A. Cox, R. F. Hampson Jr., J. A. Kerr, and J. Troe, Evaluated kinetic and photochemical data for atmospheric chemistry, Suppl. III, *J. Phys. Chem. Ref. Data*, 1989.
- Khalil, M. A. K., and R. A. Rasmussen, The atmospheric lifetime of methyl chloroform, *Tellus*, *36B*, 317–332, 1984.
- Levy II, H., Normal atmosphere: Large radical and formaldehyde concentrations predicted, *Science*, *173*, 141–143, 1971.
- Levy II, H., J. D. Mahlman, and W. J. Moxim, A stratospheric source of reactive nitrogen in the unpolluted troposphere, *Geophys. Res. Lett.*, *7*, 441–444, 1980.
- Levy II, H., J. D. Mahlman, W. J. Moxim, and S. C. Liu, Tropospheric ozone: The role of transport., *J. Geophys. Res.*, *90*, 3753–3772, 1985.
- Liu, S. C., Group report on oxidizing capacity of the atmosphere, in *The Changing Atmosphere*, edited by F. S. Rowland and I. S. A. Isaksen, Wiley Interscience, New York, pp. 219–232, 1988.
- Liu, S. C., and M. Trainer, Tropospheric ozone response to column ozone change, *J. Atmos. Chem.*, *6*, 221–223, 1987.
- Logan, J. A., Tropospheric ozone: Seasonal behavior, trends and anthropogenic influence. *J. Geophys. Res.*, *90*, 10463–10482, 1985.
- Logan, J. A., M. J. Prather, S. C. Wofsy, and M. B. McElroy, Tropospheric chemistry: A global perspective, *J. Geophys. Res.*, *86*, 7210–7254, 1981.
- Lovelock, J. E., Methyl chloroform in the troposphere as an indicator of OH radical abundance, *Nature*, *267*, 32–33, 1977.
- Makide, Y., and F. S. Rowland, Tropospheric concentrations of methyl chloroform, CH₃CCl₃, in January 1978 and estimates of atmospheric residence times for hydrocarbons, *Proc. Natl. Acad. Sci., USA*, 5933–5937, 1981.
- McConnell, J. C., and H. I. Schiff, Methyl chloroform: Impact on stratospheric ozone, *Science*, *199*, 174–177, 1978.
- McKay, C., M. Pandow, and R. Wolfgang, On the chemistry of natural radio-carbon, *J. Geophys. Res.*, *68*, 3829–3931, 1963.
- Midgeley, P. N., The production and release to the atmosphere of 1,1,1-trichloroethane (methyl chloroform), *Atm. Env.*, in press, 1989.
- Molina, M. J., Review of ultraviolet absorption cross sections of a series of alternative fluorocarbons, in *Alternative Fluorocarbons Environmental Acceptability Study (AFEAS)*, Vol. II, Appendix, this report (1990), 1989.
- Molina, L. T., M. J. Molina, and F. S. Rowland, Ultraviolet absorption cross sections of several brominated methanes and ethanes of atmospheric interest, *J. Phys. Chem.*, *86*, 2672–2675, 1982.

- Morel, O., R. Simonaitis, and J. Heicklen, Ultraviolet absorption spectra of HO_2NO_2 , $\text{CCl}_3\text{O}_2\text{NO}_2$, $\text{CCl}_2\text{FO}_2\text{NO}_2$ and $\text{CH}_3\text{O}_2\text{NO}_2$, *Chem. Phys. Lett.*, 73, 38–42, 1980.
- NASA: W. B. DeMore, S. P. Sander, M. J. Molina, D. M. Golden, R. F. Hampson, M. J. Kurylo, C. J. Howard, and A. R. Ravishankara, *Chemical Kinetics and Photochemical Data for Use in Stratospheric Modeling*, NASA Panel for Data Evaluation, Evaluation No. 8, JPL, Publication 87–41, Jet Propulsion Laboratory, Pasadena, CA, 1987.
- Neely, W., and J. Plonka, Estimation of time-averaged hydroxyl radical concentrations in the troposphere, *Environ. Sci. Tech.*, 12, 317–321, 1978.
- Neftel, A., J. Beer, H. Oeschger, and F. Zurcher, Sulphate and nitrate concentrations in snow from south Greenland, *Nature*, 314, 611–613, 1985.
- Niki, H., An assessment of potential impact of alternative fluorocarbons on tropospheric ozone, in *Alternative Fluorocarbons Environmental Acceptability Study (AFEAS)*, Vol. II, Appendix, this report (1990), 1989.
- Owens, A. J., C. H. Hales, D. L. Filkin, C. Miller, J. M. Steed, and J. P. Jesson, A coupled one-dimensional radiative-convective, chemistry transport model of the atmosphere, *J. Geophys. Res.*, 90, 2283–2311, 1985.
- Perner, D., U. Platt, M. Trainer, G. Huebler, J. W. Drummond, W. Junkermann, J. Rudolph, B. Schubert, A. Volz, D. H. Ehhalt, K. J. Rumpel, and G. Helas, Tropospheric OH concentrations: A comparison of field data with model predictions, *J. Atmos. Chem.*, 5, 185–216, 1987.
- Platt, U., M. Rateike, W. Junkermann, J. Rudolph, and D. H. Ehhalt, New tropospheric OH measurements, *J. Geophys. Res.*, 93, 5159–5166, 1988.
- Prather, M. J., Tropospheric hydroxyl concentrations and the lifetimes of hydrochlorofluorocarbons (HCFCs), in *Alternative Fluorocarbons Environmental Acceptability Study (AFEAS)*, Vol. II, Appendix, this report (1990), 1989.
- Prinn, R. G., R. A. Rasmussen, P. G. Simmonds, F. N. Alyea, D. M. Cunnold, B. C. Lane, C. A. Cardelino, and A. J. Crawford, The atmospheric lifetime experiments, 5, results for CH_3CCl_3 based on three years of data, *J. Geophys. Res.*, 88, 8415–8426, 1983.
- Prinn, R. G., D. Cunnold, R. A. Rasmussen, P. Simmonds, F. Alyea, A. J. Crawford, P. Fraser, and R. Rosen, Atmospheric trends in methyl chloroform and the global average for the hydroxyl radical, *Science*, 238, 945–950, 1987.
- Ramanathan, V., R. J. Cicerone, H. B. Singh, and J. T. Kiehl, Trace gas trends and their potential role in climate change, *J. Geophys. Res.*, 90, 5547–5566, 1985.
- Ramanathan, V., L. Callis, R. Cess, J. Hansen, I. Isaksen, W. Huhn, A. Lacis, F. Luther, J. Mahlman, R. Reck, and M. Schlesinger, Climate-chemical interactions and effects of changing atmospheric trace gases, *Rev. Geophys.*, 25, 1441–1482, 1987.
- Rasmussen, R. A., and M. A. K. Khalil, Isoprene over the Amazon basin, *J. Geophys. Res.*, 93, 1417–1421, 1988.
- Rognerud, B., I. S. A. Isaksen, and F. Stordal, Model studies of stratospheric ozone depletion, *Proceedings of the Quadrennial Ozone Symposium*, Gottingen, F.R.G., edited by R. D. Bojkov and P. Fabian, Deepak Publications, Hampton, VA., 1988.
- Rudolph, J., Two-dimensional distribution of light hydrocarbons: Results from the STRATOZ III experiment, *J. Geophys. Res.*, 93, 8367–8377, 1988.
- Schwarzkopf, M. D., and S. B. Fels, The simplified exchange method revised: An accurate rapid method for computation of IR cooling rates, *J. Geophys. Res.*, in press, 1989.
- Singh, H. B., Atmospheric halocarbons: Evidence in favour of reducing average hydroxyl radical concentration in the troposphere, *Geophys. Res. Lett.*, 4, 101–104, 1977a.
- Singh, H. B., Preliminary estimates of average tropospheric OH concentrations in the northern and southern hemispheres, *Geophys. Res. Lett.*, 4, 453–456, 1977b.

OZONE DEPLETION POTENTIALS

- Singh, H. B., and J. F. Kasting, Chlorine-hydrocarbon photochemistry in the marine troposphere and lower stratosphere, *J. Atmos. Chem.*, 7, 261–285, 1988.
- Singh, H. B., L. J. Salas, and R. E. Stiles, Selected man-made halogenated chemicals in the air and oceanic environment, *J. Geophys. Res.*, 88, 3675–3683, 1983.
- Singh, H. B., L. J. Salas, and W. Viezee, The global distribution of peroxyacetyl nitrate, *Nature*, 321, 588–591, 1986.
- Sze, N. D., Anthropogenic CO emissions: Implications for the atmospheric CO-OH-CH₄ cycle, *Science*, 195, 673, 1977.
- Thompson A. M., R. W. Stewart, M. A. Owens, and J. A. Heruche, Sensitivity of tropospheric oxidants to global chemical and climate change, *Atmos. Environ.*, 23, 519–532, 1989.
- United Nations Environment Programme., *Montreal Protocol on Substances that Deplete the Ozone Layer—Final Act.*, UNEP, Nairobi, Kenya, 1987.
- Volz, A., D. H. Ehhalt, and R. G. Derwent, Seasonal and latitudinal variation in ¹⁴CO and the tropospheric concentration of hydroxyl radicals, *J. Geophys. Res.*, 86, 5163–5171, 1981.
- Wang, W.-C., and G. Molnar, A model study of the greenhouse effects due to increasing CH₄, N₂O, CF₂Cl₂ and CFC_{1,2}, *J. Geophys. Res.*, 90, 12971–12980, 1985.
- Wang, W.-C., G. Molnar, M. K. W. Ko, S. Goldenberg, and N. D. Sze, Atmospheric trace gas and global climate: A seasonal study, *Tellus*, in press, 1989.
- Warneck, P., On the role of OH and HO₂ radicals in the troposphere, *Tellus*, 26, 39–46, 1974.
- Warneck, P., Production rates of OH in the troposphere, *Planet. Space Sci.*, 23, 1507–1518, 1975.
- Watson, R. T. and Ozone Trends Panel, Prather, M. J. and Ad Hoc Theory Panel, and Kurylo, M. J. and NASA Panel for Data Evaluation, *Present State of Knowledge of the Upper Atmosphere 1988: An Assessment Report*, NASA Reference Publication 1208, U.S. Govt. Print. Off., Washington D.C., 1988.
- Weinstock, B. The residence time of carbon monoxide in the atmosphere, *Science*, 166, 224–225, 1969.
- Weinstock, B., and H. Niki, Carbon monoxide balance in nature, *Science*, 176, 290–292, 1972.
- Wilson, S. R., P. J. Crutzen, G. Schuster, D. W. T. Griffith, and G. Helas, Phosgene measurements in the upper troposphere and lower stratosphere, *Nature*, 334, 689–691, 1988.
- WMO, *Atmospheric Ozone 1985*, WMO Global Ozone Research and Monitoring Project, WMO Report No. 16, Sponsored by WMO, NASA, NOAA, FAA, UNEP, CEC, and BMFT, Washington, D.C., 1986.
- Wuebbles, D. J., "The Relative Efficiency of a Number of Halocarbons for Destroying Stratospheric Ozone," Rep. UCID-18924, Lawrence Livermore National Laboratory, Livermore, CA, 1981.
- Wuebbles, D. J., Chlorocarbon emission scenarios: Potential impact on stratospheric ozone, *J. Geophys. Res.*, 88, 1433–1443, 1983.
- Zimmerman, P. R., J. P. Greenberg, and C. E. Westberg, Measurements of atmospheric hydrocarbons and biogenic emissions fluxes in the Amazon boundary layer, *J. Geophys. Res.* 93, 1407–1416, 1988.

Appendix A
Contributors and Reviewers

Appendix B
List of Figures and Tables

APPENDIX A

CONTRIBUTORS AND REVIEWERS

STEERING COMMITTEE

Chairmen

R.T. Watson	NASA Headquarters	USA
D.L. Albritton	NOAA Aeronomy Laboratory	USA

Members

F. Arnold	Max-Planck-Institut fur Kernphysik	FRG
R.D. Bojkov	World Meteorological Organization	Switzerland
D. Ehhalt	Kernforschungsanlage Julich	FRG
P. Fraser	CSIRO	Australia
I. Isaksen	University of Oslo	Norway
V. Khattatov	State Committee for Hydrometeorology	USSR
C. Mateer	Atmospheric Environment Service (Retired)	Canada
T. Matsuno	University of Tokyo	Japan
M. Prendez	Universidad de Chile	Chile
J.A. Pyle	University of Cambridge	UK
B.H. Subbaraya	Physical Research Laboratory	India
P. Usher	United Nations Environment Programme	Kenya

AUTHORS

Chapter 1. Polar Ozone

Coordinator

S. Solomon	NOAA Aeronomy Laboratory	USA
------------	--------------------------	-----

Principal Authors

W.L. Grose	NASA Langley Research Center	USA
R.L. Jones	Meteorological Office	UK
M.P. McCormick	NASA Langley Research Center	USA
M.J. Molina*	Jet Propulsion Laboratory	USA
A. O'Neill	Meteorological Office	UK
L.R. Poole	NASA Langley Research Center	USA
K.P. Shine	University of Reading	UK
S. Solomon	NOAA Aeronomy Laboratory	USA

*Dr. Molina has been at MIT since Fall 1989.

CONTRIBUTORS

Other Contributors

R.A. Plumb	Massachusetts Institute of Technology	USA
U. Schmidt	Kernforschungsanlage Julich	FRG
V. Pope	Meteorological Office	UK

Chapter 2. Global Trends

Coordinator

G. Megie	Service d'Aeronomie du CNRS	France
----------	-----------------------------	--------

Principal Authors

M.-L. Chanin	Service d'Aeronomie du CNRS	France
D. Ehhalt	Kernforschungsanlage Julich	FRG
P. Fraser	CSIRO	Australia
J.F. Frederick	University of Chicago	USA
J.C. Gille	National Center for Atmospheric Research	USA
M.P. McCormick	NASA Langley Research Center	USA
G. Megie	Service d'Aeronomie du CNRS	France
M. Schoeberl	NASA Goddard Space Flight Center	USA

Other Contributors

L. Bishop	Allied-Signal, Inc.	USA
R.D. Bojkov	World Meteorological Organization	Switzerland
W. Chu	NASA Langley Research Center	USA
J.J. DeLuisi	NOAA Air Resources Laboratory	USA
J.F. Frederick	University of Chicago	USA
M. Geller*	NASA Goddard Space Flight Center	USA
S. Godin	Service d'Aeronomie du CNRS	France
N.R.P. Harris	University of California, Irvine	USA
W.J. Hill	Allied-Signal, Inc.	USA
R.D. Hudson	NASA Goddard Space Flight Center	USA
J.B. Kerr	Atmospheric Environment Service	Canada
W.D. Komhyr	NOAA Air Resources Laboratory	USA
K. Kunzi	University of Bremen	FRG
K. Labitzke	Freie Universitat, Berlin	FRG
C. Mateer	Atmospheric Environment Service (Retired)	Canada
R.D. McPeters	NASA Goddard Space Flight Center	USA
A.J. Miller	NOAA Climate Analysis Center	USA
R.M. Nagatani	NOAA Climate Analysis Center	USA
G.C. Reinsel	University of Wisconsin, Madison	USA
G.C. Tiao	University of Chicago	USA

*Dr. Geller is now with SUNY Stony Brook.

Chapter 3. Theoretical Predictions

Coordinator

G. Brasseur	National Center for Atmospheric Research	Belgium
-------------	--	---------

Principal Authors and Contributors

B.A. Boville	National Center for Atmospheric Research	USA
G. Brasseur	National Center for Atmospheric Research	Belgium
C. Bruhl	Max-Planck-Institut fur Chemie	FRG
M. Caldwell	Utah State University	USA
P. Connell	Lawrence Livermore National Laboratory	USA
A. De Rudder	Belgium Institute for Space Aeronomy	Belgium
A. Douglass	NASA Goddard Space Flight Center	USA
I. Dyominov	Novosibirsk State University	USSR
D. Fisher	E.I. DuPont de Nemours and Co., Inc.	USA
J.F. Frederick	University of Chicago	USA
R. Garcia	National Center for Atmospheric Research	USA
C. Granier	Service d'Aeronomie du CNRS	France
R. Hennig	Max-Planck-Institut fur Chemie	FRG
M. Hitchman	University of Wisconsin	USA
I. Isaksen	University of Oslo	Norway
C. Jackman	NASA Goddard Space Flight Center	USA
M. Ko	Atmospheric and Environmental Research, Inc.	USA
S. Madronich	National Center for Atmospheric Research	USA
M. Prather	NASA Goddard Institute for Space Studies	USA
R. Rood	NASA Goddard Space Flight Center	USA
S. Solomon	NOAA Aeronomy Laboratory	USA
F. Stordal	University of Oslo	Norway
T. Sasaki	Meteorological Research Institute	Japan
G. Visconti	University de l'Aquila	Italy
S. Walters	National Center for Atmospheric Research	USA
D. Wuebbles	Lawrence Livermore National Laboratory	USA
A. Zadarozhny	Novosibirsk State University	USSR
E. Zhadin	Central Aerological Observatory	USSR

Chapter 4. Halocarbon Ozone Depletion and Global Warming Potentials

Coordinators

R.A. Cox	Harwell Laboratory	UK
D.J. Wuebbles	Lawrence Livermore National Laboratory	USA

CONTRIBUTORS

Principal Authors and Contributors

R. Atkinson	California Statewide Air Pollution Center	USA
P. Connell	Lawrence Livermore National Laboratory	USA
H.P. Dorn	Kernforschungsanlage Julich	FRG
A. De Rudder	Belgium Institute for Space Aeronomy	Belgium
R.G. Derwent	Harwell Laboratory	UK
F.C. Fehsenfeld	NOAA Aeronomy Laboratory	USA
D. Fisher	E. I. DuPont de Nemours and Co., Inc.	USA
I. Isaksen	University of Oslo	Norway
M. Ko	Atmospheric and Environmental Research, Inc.	USA
R. Lesclaux	Universite de Bordeaux	France
S.C. Liu	NOAA Aeronomy Laboratory	USA
S.A. Penkett	University of East Anglia	UK
V. Ramaswamy	NOAA Geophysical Fluid Dynamics Laboratory	USA
J. Rudolph	Kernforschungsanlage Julich	FRG
H.B. Singh	NASA Ames Research Center	USA
W.-C. Wang	Atmospheric and Environmental Research, Inc.	USA

Reviewers

Attendees: Review Meeting, 10-14 July 1989,
Les Diablerets, Switzerland

D.L. Albritton	NOAA Aeronomy Laboratory	USA
R.D. Bojkov	World Meteorological Organization	Switzerland
G. Brasseur	National Center for Atmospheric Research	Belgium
D. Cariolle	Meteorologie Nationale EERM/CNRM	France
G.D. Cartwright	NOAA National Weather Service/WMO	USA
M.-L. Chanin	Service d'Aeronomie du CNRS	France
A. Charnikov	Central Aerological Observatory	USSR
R.A. Cox	Harwell Laboratory	UK
D.H. Ehhalt	Kernforschungsanlage Julich	FRG
J.C. Farman	British Antarctic Survey	UK
D. Fisher	E.I. DuPont de Nemours and Co., Inc.	USA
P.J. Fraser	CSIRO	Australia
J.F. Frederick	University of Chicago	USA
J.C. Gille	National Center for Atmospheric Research	USA
W.J. Hill	Allied-Signal, Inc.	USA
M. Hitchman	University of Wisconsin	USA
A.M.A. Ibrahim	Egyptian Meteorological Authority	Egypt
M. Ilyas	University of Science of Malaysia	Malaysia
J.B. Kerr	Atmospheric Environment Service	Canada
M.J. Kurylo	NASA Headquarters	USA
C. Mateer	Atmospheric Environment Service (Retired)	Canada
T. Matsuno	University of Tokyo	Japan

CONTRIBUTORS

M.P. McCormick	NASA Langley Research Center	USA
M. McFarland	E. I. DuPont de Nemours and Co., Inc.	USA
G. Megie	Service d'Aeronomie du CNRS	France
M.J. Molina	Jet Propulsion Laboratory	USA
A. O'Neill	Meteorological Office	UK
A. Owino	Kenya Meteorological Department	Kenya
S.A. Penkett	University of East Anglia	UK
M. Prather	NASA Goddard Institute for Space Studies	USA
M. Prendez	Universidad de Chile	Chile
J.A. Pyle	University of Cambridge	UK
V. Ramaswamy	NOAA Geophysical Fluid Dynamics Laboratory	USA
J.M. Rodriguez	Atmospheric and Environment Research, Inc.	USA
J.M. Russell	NASA Langley Research Center	USA
S. Solomon	NOAA Aeronomy Laboratory	USA
R. Stolarski	NASA Goddard Space Flight Center	USA
B.H. Subbaraya	Physical Research Laboratory	India
A.F. Tuck	NOAA Aeronomy Laboratory	USA
P. Usher	United Nations Environment Programme	Kenya
R.T. Watson	NASA Headquarters	USA
D.J. Wuebbles	Lawrence Livermore National Laboratory	USA

Mail Reviewers

J.G. Anderson	Harvard University	USA
J.K. Angell	NOAA Air Resources Laboratory	USA
R. Atkinson	Bureau of Meteorology	Australia
G. Betteridge	Physics and Engineering Laboratory, DSIR	New Zealand
J.P. Burrows	Max-Planck-Institut fur Chemie	FRG
B. Carli	IROF-CNR	Italy
S. Chubachi	Meteorological Research Laboratory	Japan
T.S. Clarkson	Meteorological Service	New Zealand
P. Crutzen	Max-Planck-Institut fur Chemie	FRG
D.W. Fahey	NOAA Aeronomy Laboratory	USA
G. Fiocco	University la Sapieuza	Italy
A. Ghazi	Commission of the European Communities	Belgium
L. Gray	Rutherford - Appleton Laboratories	UK
J.S. Hoffman	Environmental Protection Agency	USA
Y. Iwasaka	Nagoya University	Japan
P. Johnson	Physics and Engineering Laboratory, DSIR	New Zealand
P. S. Jovanovic	Association of Scientific Unions	Yugoslavia
J.G. Keys	Physics and Engineering Laboratory, DSIR	New Zealand
V. Kirchoff	INPE	Brazil
D. Kley	Kernforschungsanlage Julich	FRG
Y.-P. Lee	National Tsing Hua University	Taiwan
W.A. Matthews	Physics and Engineering Laboratory, DSIR	New Zealand
R. McKenzie	Physics and Engineering Laboratory, DSIR	New Zealand
A.P. Mitra	Department of Science and Industrial Research	India

CONTRIBUTORS

J. L. Moyers	National Science Foundation	USA
L.P. Prahm	Danish Meteorological Institute	Denmark
M. H. Proffitt	NOAA Aeronomy Laboratory	USA
L. X. Qui	Academia Sinica	PRC
F. S. Rowland	University of California, Irvine	USA
P. C. Simon	Institut d'Aeronomie Spatiale	Belgium
Y. Sasano	National Institute for Environmental Studies	Japan
J. Swager	Air Directorate	Netherlands
D.W. Wei	Institute of Atmospheric Physics, NEPA	PRC
R. Zellner	University of Gottingen	FRG
C.S. Zerefos	University of Thessaloniki	Greece

Logistical Support

R. D. Bojkov	World Meteorological Organization	Switzerland
M. -C. Charrierts	World Meteorological Organization	Switzerland
F. M. Ormond	ARC Professional Services Group	USA
J. Waters	NOAA Aeronomy Laboratory	USA

APPENDIX B

LIST OF FIGURES and TABLES*

FIGURES

		Page
Introduction		
Figure 1.1	Calculated time-dependent change in relative ozone depletion following a step change in emission of halocarbons	xxx
Figure 1.2	Calculated column ozone change following a pulsed input of 5×10^9	xxxix
Chapter 1—Polar Ozone		
Figure 1.1.2-1	Logarithm of the computed lifetime of the odd oxygen family in Northern Hemisphere winter versus latitude and height	3
Figure 1.1.2-2	The first three years of ozone data from the Dobson instrument at Halley Bay, Antarctica compared to Spitzbergen	4
Figure 1.1.2-3	Observed global variation of total ozone with latitude and season	5
Figure 1.1.2-4	Seasonal cycles of total ozone and 50 mb temperatures at 60°N (Jan.-Dec.) and 60°S (July-June)	6
Figure 1.1.2-5	As in Figure 1.1.2-4, but for 80°N (Jan.-Dec.) and 80°S (July-June)	6
Figure 1.1.3-1	Observed long-term trends in total ozone from the ground-based Antarctic stations at Syowa, Halley Bay, and the South Pole	8
Figure 1.1.3-2	TOMS October monthly mean minimum total ozone measurements along with equatorial zonal wind speed	9
Figure 1.1.3-3	Seasonal decline in total ozone above McMurdo Station in 1986 as deduced by visible, UV, and IR spectroscopy, as well as from ozonesonde observations	10
Figure 1.1.3-4	(A) Same as Figure 1.1.3-3, but for 1987; (B) Seasonal decline in the daily TOMS ozone minimum during 1987	11
Figure 1.1.3-5	Contour plot of the ozone decrease obtained from 1978-1988; derived from a TOMS linear trend analysis	12
Figure 1.1.3-6	SAGE II total column ozone above 100 mb for all measurement events from day 270 through 293 (Sept. 27- Oct., 20 1985, 1986, and 1987; September 26- October 19, 1988)	13
Figure 1.1.3-7	False color images of SAGE II total column ozone above 100 mb for 1985 through 1988	14
Figure 1.1.5-1	Observations of the change in the vertical profile of ozone as measured by ozonesondes. At Syowa, the South Pole, Halley Bay, McMurdo, Molodezhnaya, and Dakshin Gangotri	18
Figure 1.1.5-2	(A) Average vertical profiles of summertime ozone from February 1-10 (SAGE II). (B) The most severely depleted profiles observed (SAGE I [1981] and SAGE II [1985-1988])	19

*Titles have been shortened to economize on space.

FIGURES

	Page
Figure 1.1.5-3	Trend in total ozone at 18 km observed from ozonesondes at McMurdo Station in 1986 and 1987 20
Figure 1.2.1-1	(Left) Vertical profiles of cloud particles observed during balloon soundings at McMurdo Station in September, 1988. (Right) Particle size distributions at various altitudes 25
Figure 1.2.2-1	Observations of PSC sightings (per week) from SAM II during 1979, 1980, 1981, 1982, and 1984 for May through October in the Southern Hemisphere vortex ... 28
Figure 1.2.2-2	As in Figure 1.2.2-1, but for 20, 22, and 24 km 29
Figure 1.2.2-3	As in Figure 1.2.2-1, but for 1985 through 1988 29
Figure 1.2.2-4	As in Figure 1.2.2-3, but for 20, 22, and 24 km 30
Figure 1.2.2-5	As in Figure 1.2.2-1, but for November through April in the Northern Hemisphere vortex for the 1978-1979 through 1983-1984 winter seasons 31
Figure 1.2.2-6	As in Figure 1.2.2-5, but for 20, 22, and 24 km 31
Figure 1.2.2-7	As in Figure 1.2.2-5, but for 1984-1985 through 1988-1989 32
Figure 1.2.2-8	As in Figure 1.2.2-7, but for 20, 22, and 24 km 32
Figure 1.2.3-1	SAM II optical depth integrated from 2 km above the tropopause to 30 km, for the Northern and Southern Hemispheres 33
Figure 1.2.3-2	Observations of SAM II PSC sightings for Antarctica from 1979 through 1988 at 14, 16, and 18 km, during the month of October 34
Figure 1.2.3-3	As in Figure 1.2.3-2, but for September 35
Figure 1.2.4-1	Changes in net heating caused by mountain PSCs with and without cirrus 38
Figure 1.3.2-1	Plot of the flight track data for the encounter with a PSC event on August 17, 1987 41
Figure 1.3.2-2	Observations of the percent of total observed nitrate in the particulate phase as a function of time for September 4, 1987 42
Figure 1.5.1-1	ClO dimer thermal decomposition and photolysis rates 47
Figure 1.5.1-2	Calculated time behavior of ClO and ClONO ₂ during Arctic spring for three different cases 50
Figure 1.5.2-1	Absorption cross sections of ClOOCl 51
Figure 1.5.2-2	Rate constants for the ClO + ClO + M → Cl ₂ O ₂ + M reaction, with N ₂ as the third body M 52
Figure 1.5.2-3	Photolysis rates for Cl ₂ O ₂ , HOCl, Cl ₂ , HNO ₃ , and O ₂ at 70°S at noon as a function of day, at the 50 mb level 53
Figure 1.6.1-1	Observed ClO mixing ratio latitude gradients on the 425 and 450 K potential temperature surfaces averaged over the AAOE mission period 56
Figure 1.6.1-2	The vertical profile of ClO mixing ratio within the southern polar vortex, from ground-based microwave measurements and in situ measurements 56
Figure 1.6.1-3	Diurnal variation of the column abundance of ClO below about 25 km at McMurdo Station, Antarctica 57
Figure 1.6.1-4	Diurnal variation of the column abundance of OClO above McMurdo Station September 18-19, 1986 58
Figure 1.6.1-5	Daily measurements of the sunset OClO column abundances above McMurdo Station in 1986 and 1987 59
Figure 1.6.1-6	Observed distribution of the ClONO ₂ column abundance, a function of latitude relative to the edge of the vortex in August and September, 1987 60
Figure 1.6.1-7	Observed latitude gradients of HCl and HF on the 24th of September and 2nd of October, 1987 61

FIGURES

	Page
Figure 1.6.2-1	Observations of the latitude gradient of column NO ₂ in the Southern Hemisphere 63
Figure 1.6.2-2	Observations of the seasonal trend in morning and evening twilight slant column NO ₂ abundances from three Antarctic sites 64
Figure 1.6.2-3	Total NO ₂ (a), total O ₃ (b), and 50 mb temperature (c) at Molodezhnaya in 1987 and Mirny in 1988 65
Figure 1.6.2-4	Cross section of NO ₂ vs. latitude and pressure for the period September 27 to October 7, 1987, from SAGE II observations 66
Figure 1.6.2-5	Observed column of HNO ₃ plotted as a function of latitude relative to the edge of the polar vortex in August and September, 1987 66
Figure 1.6.2-6	Measurements of total reactive nitrogen (NO _x) versus N ₂ O obtained from aircraft observations 67
Figure 1.6.2-7	Observed total reactive nitrogen profile as a function of potential temperature .. 69
Figure 1.6.2-8	Observed NO mixing ratios versus latitude relative to the chemically perturbed region 70
Figure 1.6.3-1	Observed latitude gradient of H ₂ O on September 22, 1987 near 450 K surface ... 70
Figure 1.6.3-2	Cross section of H ₂ O vs. latitude and pressure for the period September 27 to October 7, 1987, measured by SAGE II 71
Figure 1.6.3-3	BrO mixing ratios versus latitude for nine flights from about 54° and 72°S, taken between August 28 and September 22, 1987 72
Figure 1.6.3-4	Variation of the BrO mixing ratio with potential temperature 73
Figure 1.6.3-5	Diurnal variation of the BrO slant column at McMurdo Station 74
Figure 1.6.4-1	Calculated and observed ClO mixing ratios on the 428 K surface, 4-12 September, 1987 76
Figure 1.6.4-2	Calculated and observed ClO mixing ratio profiles at 72°S, 4th/9th September, 1987 77
Figure 1.6.4-3	Observed NO and ClO mixing ratios from an aircraft flight on August 28, 1987 78
Figure 1.6.4-4	Observed and calculated rates of ozone decline for different ClO dimer formation rates as a function of potential temperature 79
Figure 1.6.4-5	Observed October mean total ozone abundance over Halley Bay, Antarctica ... 81
Figure 1.7.1-1	The range, near 90 mb, of minimum brightness temperatures poleward of latitude 20, computed daily for winter and spring from 1980 to 1988 83
Figure 1.7.1-2	Comparison of N ₂ O vertical profiles during austral winter-spring, austral summer, and austral winter 84
Figure 1.7.1-3	Vertical distributions of the total amount of chlorine bonded in the five most abundant anthropogenic halocarbons 85
Figure 1.7.1-4	(i) Monthly mean perspectives during June 1982 of the three-dimensional structure of the westerly vortex in the Southern Hemisphere 86
Figure 1.7.1-4	(ii) As for Figure 1.7.1(i), but for September 87
Figure 1.7.1-4	(iii) As for Figure 1.7.1(i), but for October 87
Figure 1.7.1-5	Time of the reversal of the zonal wind at latitude 60°, and of the temperature difference between 60° and 85° for the Northern and Southern Hemispheres 88
Figure 1.7.1-6	Evolution of zonal-mean total ozone (Dobson units) derived from the TOMS instruments, 1987 and 1988 90
Figure 1.7.1-7	Minimum brightness temperature near 90 mb (Channel 24 of the MSU) in the Southern Hemisphere during 1987 91

FIGURES

	Page
Figure 1.7.1-8	The fractional area of the Southern Hemisphere over which minimum temperatures near 90 mb in 1987 fell below 193 K 91
Figure 1.7.1-9	As for Figure 1.7.1-7 but for 1988 92
Figure 1.7.1-10	As for Figure 1.7.1-8 but for 1988 92
Figure 1.7.1-11	Isentropic maps of Ertel's potential vorticity and winds on the 500 K isentropic surface in the Southern Hemisphere on 1 August 1987 93
Figure 1.7.1-12	As for Figure 1.7.1-11, but for 31 October 1987 94
Figure 1.7.1-13	As for Figure 1.7.1-11, but on 1 August 1988 94
Figure 1.7.1-14	As for Figure 1.7.1-11, but on 20 October 1988 95
Figure 1.7.1-15	As for Figure 1.7.1-11, but for the Northern Hemisphere on 18 January 1989 96
Figure 1.7.1-16	As for Figure 1.7.1-11, but for the Northern Hemisphere on 20 February 1989 .. 97
Figure 1.7.1-17	Minimum brightness temperature derived from channel 24 of the MSU in the Northern Hemisphere for December through May 98
Figure 1.7.1-18	The total ozone fields (in Dobson units) from November 1978 to October 1987 with annual cycle removed 99
Figure 1.7.1-19	As for Figure 1.7.1-18, but after application of a broad-band filter 100
Figure 1.7.1-20	Variation in October mean total ozone and 70 mb temperature over the South Pole 101
Figure 1.7.1-21	As for Figure 1.7.1-20, but for the April mean in the Northern Hemisphere 101
Figure 1.7.1-22	Correlation of August-September winds over Singapore at 30 mb with the total ozone decline rate in September 102
Figure 1.7.1-23	Ozone mixing ratio variation at the maximum of the 11-year solar cycle 103
Figure 1.7.2-1	An example of a mini-hole over the Antarctic Peninsula on 5 September 1987 ... 105
Figure 1.7.2-2	(i) Longitude/pressure cross sections on 5 September 1987 at latitude 65°S from 90°W to 30°W, and from 250 to 30 mb 106
Figure 1.7.2-2	(ii) As for Figure 1.7.2-2 (i) 107
Figure 1.7.2-3	A sequence of potential vorticity distributions on the 428 K surface of potential temperature 108
Figure 1.7.4-1	Ertel's potential vorticity on the 600 K isentropic surface 111
Figure 1.7.4-2	TOMS total ozone. Monthly variation of difference between 1987-1988 average and 1979-1980 average as a function of latitude 112
Figure 1.7.4-3	Percent change in the simulated steady-state seasonal and latitudinal distribution of zonal-mean column ozone 113
Figure 1.7.4-4	Percent difference in zonal-mean column ozone for Antarctic ozone hole 114
Figure 1.7.4-5	Percent difference in the integrated global and hemispheric column ozone for Antarctic ozone hole 116
Figure 1.7.4-6	TOMS total ozone for the Southern Hemisphere 117
Figure 1.7.4-7	Difference between Ertel's potential vorticity (500 K isentropic surface) for 8 December and 14 December 1987 118
Figure 1.8.1-1	Linear trends calculated from NMC data for the period 1979-1986, for August, September, November, and December 119
Figure 1.8.2-1	Deviations of temperatures 1958-1988 (°C) for Angell's (1988b) six south polar stations 120
Figure 1.8.2-2	Monthly mean temperatures at 100 mbar for Halley Bay, 1958-1988 121
Figure 1.8.2-3	Temperatures at 100 mbar as a function of month from Halley Bay 122
Figure 1.8.2-4	Deviation of NMC zonal mean temperatures for 1987 from the 1979-1986 mean for September to December 123

	Page
Figure 1.8.3-1	2-D model temperatures at 39 mb and 76°S with and without an imposed ozone hole 125
Figure 1.8.3-2	Deviation of zonal mean temperature for a calculation with an imposed ozone hole from a control run without the hole, using the NCAR Community Climate Model 126
Figure 1.9-1	Ratio of biologically effective downward radiation computed for a range of ozone values at McMurdo 127
Figure 1.9-2	Computed time history of erythemal irradiance for local noon and clear skies over Palmer Station 129
Figure 1.9-3	Spectra of UV solar irradiance measured from Palmer Station at local noon 130
Figure 1.9-4	Ratio of noontime irradiance for 295-305 nm to that for 335-345 nm, for the period 19 September and 21 December 1988 131
Figure 1.10.1-1	Observation of the Noxon cliff 131
Figure 1.10.1-2	The mean annual cycle of NO ₂ at 71°N (Point Barrow, Alaska) 132
Figure 1.10.1-3	Variation of total NO ₂ column abundance over Point Barrow, Alaska (71°N) in three different winter-spring seasons 133
Figure 1.10.1-4	NO _x (NO + NO ₂) mixing ratio profiles observed on balloon flights using a chemiluminescent detector 134
Figure 1.10.1-5	Zonally and monthly averaged HNO ₃ mixing ratio distributions for November, December, and January from LIMS observations 136
Figure 1.10.1-6	Latitude gradients of HCl and HF in the Northern Hemisphere 137
Figure 1.10.1-7	Observations of the nighttime abundance of OClO versus lunar zenith angle at various locations 138
Figure 1.10.2-1	Ozone partial pressure and mixing ratio profiles measured at Kiruna, Sweden, on 23 January, 1989 140
Figure 1.10.2-2	NMC temperatures at 30 mb for the 1988-1989 Northern Hemisphere winter-spring season 141
Figure 1.10.2-3	NMC temperatures at 30 mb for the 1975-1976 Northern Hemisphere winter-spring season 142

Chapter 2—Global Trends

Figure 2.1-1	Time-lines of measurements available for use in ozone trend analyses at the present time 164
Figure 2.1-2	Location of Dobson and M-83 stations 166
Figure 2.1-3	Time-lines for ozone-measuring systems that are projected to be operating over the next decade 175
Figure 2.1-4a	Comparison between archived TOMS total ozone data and Dobson data 182
Figure 2.1-4b	Comparison between TOMS total ozone data where diffuser plate degradation was corrected by the “pair justification” method and Dobson data 183
Figure 2.1-5	Samples of profile pairs measured by ozonesondes and the SAGE I instrument and the mean percentage difference between the ozonesondes and the SAGE I ozone 186
Figure 2.1-6	Samples of profile pairs measured by ozonesondes and the SAGE II instrument and the mean percentage difference between the ozonesondes and the SAGE II ozone 187
Figure 2.1-7	Mean differences between SAGE I and ozonesondes and SAGE II and ozonesondes 188

FIGURES

	Page
Figure 2.2-1	Monthly and zonally averaged Dobson total ozone values versus time after removal of seasonal, QBO, solar cycle, and nuclear test effects 197
Figure 2.2-2a	Regional plots of Dobson total ozone after removal of seasonal, solar, QBO, and nuclear test effects for North America, Europe, and Japan 198
Figure 2.2-2b	Same as 2.2-2a for winter months (December-March) 199
Figure 2.2-2c	Same as 2.2-2a for summer months (May-August) 200
Figure 2.2-3	Plots of Dobson total ozone monthly averages combined into time series for each latitudinal zone 201
Figure 2.2-4	Individual trend estimates for the period 1970-1986 using the AS2 model 203
Figure 2.2-5	Same as Figure 2.2-4 except trends are fitted only through October 1982 205
Figure 2.2-6	Same as Figure 2.2-4 except trends are fitted using updated data into 1988 208
Figure 2.2-7	Differences between estimated trends into 1988 versus trends through 1986 210
Figure 2.2-8	Solar coefficient computed for 25 Northern Hemisphere stations from the AS2 model 211
Figure 2.2-9a	Geographic structure in total ozone changes based on TOMS 212
Figure 2.2-9b	Same as Figure 2.2-9a for Southern Hemisphere 213
Figure 2.2-10	Geographic pattern of change in total ozone derived from SBUV for the Northern Hemisphere winter and summer 215
Figure 2.2-11	Geographic pattern of change in total ozone derived from SBUV for the Southern Hemisphere winter and summer 215
Figure 2.2-12	Changes in total ozone based on eight-year data sets from the SBUV and TOMS instruments 217
Figure 2.2-13	Changes in total ozone derived from Dobson data for the eight-year period over which SBUV measurements are available 218
Figure 2.3-1	Latitudes of the SAGE I and SAGE II sampling locations for sunset 222
Figure 2.3-2	Zonal mean ozone number density at 30 km for SAGE I during the period 2/79-11/81 and SAGE II during the period 10/84-11/87 for five latitude bands 223
Figure 2.3-3	Daily mean ozone number density at 35 km for SAGE II for twelve latitude bands 224
Figure 2.3-4	Mean percentage difference between SAGE II and SAGE I versus altitude computed from the intersection of SAGE I with SAGE II 225
Figure 2.3-5	Deseasonalized Umkehr data at Arosa for layers 4-9, unadjusted for aerosols, for the period January 1977 through December 1987 227
Figure 2.3-6	Stratospheric aerosol optical thickness derived from lidar data for the period 1977-1987 228
Figure 2.3-7	Umkehr data trend estimates from 10 individual Umkehr stations for layers 4-9, for the period January 1977 through December 1987 229
Figure 2.3-8	Trend estimates derived from ozonesondes measurements at 9 stations for 15 fractional Umkehr layers 233
Figure 2.4-1a	Seasonal temperatures with the long-term seasonal averages removed and smoothed 1-2-1 in time for Angell, Berlin, NMC, MSU, SSU 238
Figure 2.4-1b	Seasonal temperatures with the long-term seasonal averages removed and smoothed 1-2-1 in time: NMC; SSU Channels 25 and 26 × 239
Figure 2.4-1c	Seasonal temperatures with the long-term seasonal averages removed and smoothed 1-2-1 in time: NMC; SSU Channel 26 240
Figure 2.4-1d	Seasonal temperatures with the long-term seasonal averages removed and smoothed 1-2-1 in time: NMC 5-1 mb; SSU Channels 27 and 36 X 241

FIGURES

		Page
Figure 2.4-2	Lidar temperature and SSU channel 27 brightness temperature from 1981 to 1987	242
Figure 2.4-3	Lidar and NMC temperature at 42 km	242
Figure 2.4-4	Comparison of the 10.7 cm solar flux, in 10^{-22} W/(m ² Hz), and the 30-mb temperature, in °C, at the North Pole	243
Figure 2.4-5	Summary of global stratospheric temperature differences (1985 and 1986 minus the average of 1979 and 1980)	244
Figure 2.4-6	As in Figure 2.4-4, except for Tropics and including rocket stations	245
Figure 2.5-1	Halocarbon (pptv) and nitrous oxide (ppbv) observations at Cape Grim, Tasmania, as part of the GAGE program	248
Figure 2.5-2	CHClF ₂ (pptv) observations at Cape Grim, Tasmania, from the Oregon Graduate Center flask sampling program	249
Figure 2.5-3	CH ₂ Cl (pptv) observations at Cape Grim, Tasmania, from the Oregon Graduate Center flask sampling program	249
Figure 2.5-4	CHCl ₃ (pptv) observations at Cape Grim, Tasmania, from the Oregon Graduate Center flask sampling program	250
Figure 2.5-5	Long-term trends of N ₂ O from the GMCC program, the SIO program, the OGC-ALE program, the FIAER-CSIR program, and CSIRO-GAGE data	252
Figure 2.5-6	Long-term trends of CH ₄ from the CSIRO global program and the FIAER-CSIR program at Cape Point, South Africa	254
Figure 2.5-7	The global distribution, seasonality, and trend of CH ₄ from the GMCC network	255
Figure 2.5-8	Long-term trends of CO from the CSIRO network and from Cape Point, South Africa	257
Figure 2.5-9	The temporal behavior of the CO ₂ trends observed at the GMCC stations	258
Figure 2.5-10	Surface ozone measurements at the GMCC stations, at Cape Point, South Africa, and at Cape Grim, Tasmania	260
Figure 2.6-1	Aerosol integrated backscatter coefficient over the period 1974-88	262
Figure 2.7-1	Solar spectral irradiance incident on the Earth's surface computer for January and July at latitudes 34.5°, 46.0°, and 58.5°N	264
Figure 2.7-2	Percent changes in solar spectral irradiance between 1970 and 1986 computed for January, March, and July at latitudes 34.5°, 46.0°, and 58.5°N	266

Chapter 3—Theoretical Predictions

Figure 3.1-1	Schematic diagram showing an algorithm for determining the coupled set of transport parameters with prescribed T as input	287
Figure 3.1-2	Total ozone field on 28 February 1989 as measured by TOMS and as modeled from a January 1 initial condition	291
Figure 3.1-3	Two-dimensional distribution of tropospheric source gas X from nine models for the month of December	295
Figure 3.1-4	Two-dimensional distribution of the ClO/HCl ratio from nine models	298
Figure 3.1-5	Zonally and monthly averaged distribution of nitrous oxide observed in January 1979 by SAMS and calculated by GSFC model	301
Figure 3.1-6	Same as in Figure 3.1-5 but for methane	302
Figure 3.1-7	Zonally and monthly averaged distribution of nighttime NO ₂ observed in January 1979 by LLMS	303

FIGURES

	Page
Figure 3.1-8	Same as in Figure 3.1-7 but for nitric acid 304
Figure 3.1-9	Zonally and monthly averaged distribution of ozone for January based on data obtained by SBUV and distribution by different two-dimensional models 307
Figure 3.1-10	Latitudinal and seasonal variation of the ozone column abundance based on satellite observations (TOMS) and different model calculations 312
Figure 3.1-11	Comparison between one-dimensional mixing ratio profiles of chemically active trace gases measured by ATMOS 316
Figure 3.2-1	Time history, 1960-2060, of mean tropospheric concentrations of the trace gases assumed for the different scenarios 319
Figure 3.2-2	Time history, 1980-2060, of total atmospheric chlorine and total atmospheric bromine from the different scenarios 321
Figure 3.2-3	Dobson map of percent change in column ozone from 1960 to 1980 using the specified trace-gas scenario 329
Figure 3.2-4	Latitude-by-altitude contour map of the percent change in local ozone concentration from 1960 to 1980 for the specified trace-gas scenario 333
Figure 3.2-5	Time-line of the percent change in column ozone as a function of latitude for the months of March from 1980 through 2060 for scenario A1 338
Figure 3.2-6	Dobson map of percent change in column ozone from 1980 to 2020 using scenario A1 340
Figure 3.2-7	Dobson map of percent change in column ozone from 1980 to 2060 using scenario A1 342
Figure 3.2-8	Latitude-by-altitude contour map of the percent change in local ozone concentration from 1980 to 2060 for scenario A1 347
Figure 3.2-9	Time-line vs. latitude of the percent change in column ozone during March from 1980 to 2060 for scenario A2 351
Figure 3.2-10	Dobson map of percent change in column ozone from 1980 to 2060 using scenario A2 352
Figure 3.2-11	Latitude-by-altitude map of the percent change in local ozone concentration from 1980 to 2060 for scenario A2 353
Figure 3.2-12	Temperature change (K) for December (scenario A1: 1980-2060) from the AER and WisCAR models 354
Figure 3.2-13	Zonal wind and zonal wind change from December 1980 to December 2060 for the WisCAR model (scenario A1) 355
Figure 3.2-14	Net radiative heating (K/day) for December 1980 in the AER and WisCAR models 356
Figure 3.2-15	Change in net radiative heating (K/day) from December 1980 to December 2060 (scenario A1) in the AER and WisCAR models 357
Figure 3.2-16	Time-line vs. latitude of the percent change in column ozone during March from 1980 to 2060 for scenario A1 359
Figure 3.2-17	Dobson map of percent change in column ozone from 1980 to 2060 using scenario B1 360
Figure 3.2-18	Latitude-by-altitude map of the percent change in local ozone concentration from 1980 to 2060 for scenario B1 361
Figure 3.2-19	Time-line vs. latitude of the percent change in column ozone during March from 1980 to 2060 for scenario C1 363
Figure 3.2-20	Dobson map of percent change in column ozone from 1980 to 2060 using scenario C1 364

	Page
Figure 3.2-21	Latitude-by-altitude map of the percent change in local ozone concentration from 1980 to 2060 for scenario C1 364
Figure 3.2-22	Time-line vs. latitude of the percent change in column ozone during March from 1980 to 2060 for scenario D1 365
Figure 3.2-23	Dobson map of percent change in column ozone from 1980 to 2060 using scenario D1 366
Figure 3.2-24	Latitude-by-altitude map of the percent change in local ozone concentration from 1980 to 2060 for scenario D1 368
Figure 3.2-25	Time-line vs. latitude of the percent change in column ozone during March from 1980 to 2060 for scenario D2 371
Figure 3.2-26	Dobson map of percent change in column ozone from 1980 to 2060 using scenario D2 371
Figure 3.2-27	Latitude-by-altitude map of the percent change in local ozone concentration from 1980 to 2060 for scenario D2 372
Figure 3.2-28	Time-line vs. latitude of the percent change in column ozone during March from 1980 to 2060 for scenario D3 372
Figure 3.2-29	Dobson map of percent change in column ozone from 1980 to 2060 using scenario D3 373
Figure 3.2-30	Latitude-by-altitude map of the percent change in local ozone concentration from 1980 to 2060 for scenario D3 373
Figure 3.2-31	Time-line vs. latitude of the percent change in column ozone during March from 1980 to 2060 for scenario D4 374
Figure 3.2-32	Dobson map of percent change in column ozone from 1980 to 2060 using scenario D4 375
Figure 3.2-33	Latitude-by-altitude map of the percent change in local ozone concentration from 1980 to 2060 for scenario D4 375
Figure 3.2-34	Two-year sequence of percent change in column ozone from the Cambridge model with PSC chemistry in the Northern Hemisphere 376
Figure 3.2-35	Dobson maps of percent change in column ozone from 1960 to 2060 from the WisCAR model with and without heterogeneous chemistry on PSCs for scenario A1 377
Figure 3.2-36	Dobson maps of percent change in column ozone from 1960 to 1985 and from 1985 to 2060 from the AER model using scenario B1 378
Figure 3.2-37	Dobson maps of percent change in column ozone from 1985 to 2050 from the Oslo model with and without heterogeneous chemistry on the natural sulfate layer 380
Figure 3.2-38	Dobson maps of percent change in column ozone from 1985 to 2060 from the AER model using scenario B1 381
Figure 3.2-39	Action spectra used as weighting functions to calculate biologically effective radiation 381
Figure 3.2-40	Daily doses for 1979/80 based on ozone column from TOMS measurements normalized to Dobson 386
Figure 3.2-41	Daily dose changes from 1960 to 1980, GSFC2 model 388
Figure 3.2-42	Daily dose changes from 1960 to 2060, GSFC2 model, scenario A1 389
Figure 3.2-43	Daily dose changes from 1960 to 2060, GSFC2 model, scenario D1 390
Figure 3.2-44	Daily DNA damage dose changes from 1980 to 2060, WisCAR model, scenarios A1, A2, and D1 391

FIGURES

	Page
Figure 3.2-45	Transformed Eulerian mean vertical velocity for a 240-day average simulation performed with the NCAR Community Climate Model 394
Figure 3.2-46	As in Figure 3.3-40 but for the ozone reduction scenario shown in Figure 3.3.41b; percentage change in ozone from the two-dimensional model of Ko et al., 1985 394
 Chapter 4—Halocarbon Ozone Depletion Potentials and Global Warming Potentials	
Figure 4.2-1	Reactions governing concentrations of OH and HO ₂ 411
Figure 4.2-2	Schematic presentation of the measured vertical distribution of NO and NO _y over midlatitude oceanic and coastal regions 419
Figure 4.3-1	Calculated column ozone change in the DuPont 1-D model following a pulsed input of 5.0×10^9 kg of specified gas 425
Figure 4.3-2	Atmospheric concentrations of halocarbons with 5- and 100-year lifetimes following onset of a constant emission of each compound 426
Figure 4.3-3	Calculated latitudinal and seasonal steady-state ozone change from emission of CFC-11 necessary for global 1% change in total ozone (LLNL 2-D model) 435
Figure 4.3-4a	Calculated latitudinal and seasonal steady-state ozone change from emission of CFC-12 necessary to give 1% change in total ozone (LLNL 2-D model) 436
Figure 4.3-4b	Calculated latitudinal and seasonal relative ozone depletion of CFC-12 (LLNL 2-D model) 437
Figure 4.3-4c	Calculated latitudinal and seasonal relative ozone depletion of CFC-12 (AER 2-D model) 437
Figure 4.3-4d	Calculated latitudinal and seasonal relative ozone depletion of CFC-12 (Oslo 2-D model) 438
Figure 4.3-4e	Calculated latitudinal and seasonal relative ozone depletion of CFC-12 (DuPont 2-D model) 438
Figure 4.3-5a	Calculated latitudinal and seasonal steady-state ozone change necessary to give 1% change in total ozone from emission of HCFC-22 (LLNL 2-D model) 439
Figure 4.3-5b	Calculated latitudinal and seasonal relative ozone depletion of CFC-22 (LLNL 2-D model) 439
Figure 4.3-5c	Calculated latitudinal and seasonal relative ozone depletion from emission of HCFC-22 (AER 2-D model) 440
Figure 4.3-5d	Calculated latitudinal and seasonal relative ozone depletion from emission of HCFC-22 (Oslo 2-D model) 440
Figure 4.3-5e	Calculated latitudinal and seasonal relative ozone depletion from emission of HCFC-22 (DuPont 2-D model) 441
Figure 4.3-6	Calculated CFC-11 profiles from transport sensitivity study at 75°S at equinox (AER 2-D model) 443
Figure 4.3-7	Calculated CFC-11 profiles from transport sensitivity study at Equator at equinox (AER 2-D model) 443
Figure 4.3-8a	Calculated HCFC-22 profiles from transport sensitivity study at 75°S at equinox (AER 2-D model) 444
Figure 4.3-8b	Calculated HCFC-22 profiles from transport sensitivity study at Equator at equinox (AER 2-D model) 444
Figure 4.3-9a	Calculated total ozone abundance (Dobson units) from transport sensitivity studies (case 1 and case 2) 445

FIGURES

	Page
Figure 4.3-9b	Calculated total ozone abundance (Dobson units) from transport sensitivity studies (case 3 and case 4) 445
Figure 4.3-10a	Calculated latitudinal and seasonal relative ozone depletion from emission of HCFC-22 (case 2) 446
Figure 4.3-10b	Calculated latitudinal and seasonal relative ozone depletion from emission of HCFC-22 (case 3) 447
Figure 4.3-10c	Calculated latitudinal and seasonal relative ozone depletion from emission of HCFC-22 (case 4) 447
Figure 4.3-11	Calculated time-dependent change in relative ozone column depletion following a step change in emission of the tested halocarbons (LLNL 1-D model) 448
Figure 4.3-12	Calculated time-dependent change in relative ozone column depletion following a step change in emission of the tested halocarbons (DuPont 1-D model) 449
Figure 4.3-13	Calculated time-dependent relative chlorine loading following a step change in emission of the tested halocarbons (LLNL 1-D model) 450
Figure 4.4-1	Calculated change in surface temperature following a pulsed emission of 5×10^9 kg of specified gas 454
Figure 4.4-2	Change of calculated warming following a step change of emission of specified gas at 5×10^8 kg/yr 460
Figure 4.4-3	Column of chlorofluorocarbons following step change of emission of specified gas at 5×10^8 kg/yr 460
Figure 4.4-4	Calculated relative warmings following a step change of emission of specified gas (CFC-11 reference) 461

TABLES

		Page
Introduction		
Table 1	Range of Ozone Depletion Potentials (ODPs) and halocarbon Global Warming Potentials (GWPs) determined by one-dimensional and two-dimensional models	xi
Table 2	Scenarios for halocarbon abundances	xxiv
Table 3	Range of Ozone Depletion Potentials (ODPs) determined by one-dimensional and two-dimensional models	xxviii
Table 4	Ozone Depletion Potentials for brominated compounds as calculated in the LLNL one-dimensional model and the University of Oslo two-dimensional model	xxix
Table 5	Maximum relative Chlorine Loading Potential (CLP) for examined CFCs, HCFCs, HFCs	xxix
Table 6	Halocarbon Global Warming Potentials (Halocarbon GWPs) scaled relative to reference set of halocarbon lifetimes	xxxii
 Chapter 1—Polar Ozone		
Table 1.1.6-1	Changes in average total ozone abundances, as measured at individual Dobson stations over the 22-year period, 1965-1986	21
Table 1.1.6-2	Coefficients of multiple regression statistical analysis of re-analyzed Dobson measurements of total ozone concentrations collected into latitudinal band averages	22
Table 1.1.6-3	Percentage changes in total column ozone	23
Table 1.4-1	Reaction probabilities on water-ice	44
Table 1.6-1	Potential temperatures and approximate geometric altitude and pressure equivalents for late winter and early spring for the Antarctic region	55
Table 1.6.4-1	Assumed chlorine tracer concentrations and inorganic chlorine content as a function of potential temperature at 72°S	75
Table 1.9-1	Comparison of noontime irradiances computed for McMurdo during October with values for the summer solstice	128
 Chapter 2—Global Trends		
Table 2.1-1	Estimated overall percentage differences of the calculated zonal mean ozone layer amount of SBUV, SAGE, and LIMS with respect to the average of these three instruments	184
Table 2.1-2	Summary of Ozone Trend Estimates (in % per year) in total ozone and associated standard error	191
Table 2.2-1	Comparison of trend results by season and latitude	195
Table 2.2-2	List of Dobson total ozone stations at latitudes between 26°N and 64°N	202
Table 2.2-3	Summary of sensitivity analysis (% per decade effect on trends)	204
Table 2.2-4	Regional sensitivity analysis comparing trends from the “provisionally revised” Dobson data set with the original published data	206
Table 2.2-5	Trends in total ozone derived from Dobson data updated into 1988 compared with trends derived through 1986	209

TABLES

	Page
Table 2.2-6	Trends in total ozone derived by region based on data through 1986 and data updated through October 1988 211
Table 2.2-7	Latitudes and longitudes of the 14 grid points selected for comparison of changes in ozone derived from SBUV and TOMS 216
Table 2.2-8	Changes in total ozone derived from the Dobson network for periods coincident with the SBUV and TOMS data sets 219
Table 2.3-1	Overall trend estimates (in % per year) from 10 Umkehr stations for the period 1977-1987 with associated standard errors ($\pm 2\sigma$) 230
Table 2.3-2	Ozonesonde stations, data spans, and measurement methods 231
Table 2.3-3	Fractional Umkehr layers 231
Table 2.3-4	Trend estimates for nine stations (in % per year; data through December 1986 when available) 232
Table 2.3-5	Summary of averages of trend estimates (% per year) and standard errors (S.E. $\pm 2\sigma$) 234
Table 2.5-1	Concentrations and global trends of tropospheric gases for 1987 246
Table 2.5-2	N ₂ O mixing ratios and rates of increase observed in the troposphere 251
Table 2.5-3	Global average methane mixing ratios and rates of increase observed in the troposphere by various laboratories 253
Table 2.5-4	Surface carbon monoxide concentrations and trends 256
Table 2.5-5	Surface ozone concentrations and trends deduced from ground-based and balloon-borne instruments 259
Table 2.7-1	Percent changes in total column ozone, 1970-1986, used in the radiative transfer calculations 265

Chapter 3—Theoretical Predictions

Table 3.1-1	Capabilities of an international group of 2-D assessment models 285
Table 3.1-2	Comparison of ten rates and species at 3 mb, Equator, in March from five modeling groups 300
Table 3.2-1	UNEP Scenarios: 1960 through 2060 318
Table 3.2-2a	Assumed history of trace gas concentrations: Halocarbons and other gases 322
Table 3.2-2b	Assumed history of trace gas concentrations: Montreal products and replacements 322
Table 3.2-3a	Projected surface mixing ratios for Scenario A: Montreal products and replacements 323
Table 3.2-3b	Projected surface mixing ratios for Scenario B: Montreal products and replacements 323
Table 3.2-3c	Projected surface mixing ratios for Scenario C: Montreal products and replacements 324
Table 3.2-3d	Projected surface mixing ratios for Scenario D: Montreal products and replacements 324
Table 3.2-4	Chlorine and bromine loading of the atmosphere for the UNEP scenarios 327
Table 3.2-5	Participating assessment models 332
Table 3.2-6	Global mean lifetimes (yr.) of the trace gases 332
Table 3.2-7	Extended scenarios for halocarbon abundances 337
Table 3.2-8	Stratopause changes from 1980 to 2060 382
Table 3.2-9	Surface UV irradiance ^a : Comparison of model predictions 385
Table 3.2-10	Environmental effects on DNA radiation amplification factor (RAF) 392

TABLES

	Page
Chapter 4—Halocarbon Ozone Depletion Potentials and Global Warming Potentials	
Table 4.2-1	404
Table 4.2-2	408
Table 4.2-3	414
Table 4.2-4	416
Table 4.2-5	420
Table 4.3-1	428
Table 4.3-2	429
Table 4.3-3	429
Table 4.3-4	430
Table 4.3-5	432
Table 4.3-6	432
Table 4.3-7	433
Table 4.3-8	434
Table 4.3-9	434
Table 4.3-10	446
Table 4.4-1	456
Table 4.4-2	457
Table 4.4-3	458
Table 4.4-4	459